

Aus der Kinderchirurgischen Klinik und Poliklinik  
im Dr. von Haunerschen Kinderspital  
Klinik der Universität München  
Direktor: Professor Dr. med. Dietrich von Schweinitz

## **“BCORL1 regulates stemness in hepatoblastoma cells through inhibition of *KRT19* expression”**

Dissertation  
zum Erwerb des Doktorgrades der Naturwissenschaften  
an der Medizinischen Fakultät der  
Ludwig-Maximilians-Universität zu München

vorgelegt von

Tamara Manuela Krause  
aus  
Wangen im Allgäu  
2019

**Mit Genehmigung der Medizinischen Fakultät  
der Universität München**

Betreuer: Prof. Dr. rer. nat. Roland Kappler

Zweitgutachter: Prof. Dr. rer. nat. Aloys Schepers

Dekan: Prof. Dr. med. dent. Reinhard Hickel

Tag der mündlichen Prüfung: 15.10.2020

## **Eidesstattliche Erklärung**

**Tamara Manuela Krause**

Ich erkläre hiermit an Eides statt,  
dass ich die vorliegende Dissertation mit dem Thema,

**BCORL1 regulates stemness in hepatoblastoma cells through inhibition of KRT19 expression**

selbstständig verfasst, mich außer der angegebenen keiner weiteren Hilfsmittel bedient und alle Erkenntnisse, die aus dem Schrifttum ganz oder annähernd übernommen sind, als solche kenntlich gemacht und nach ihrer Herkunft unter Beziehung der Fundstelle einzeln nachgewiesen habe.

Ich erkläre des Weiteren, dass die hier vorliegende Dissertation nicht in gleicher oder in ähnlicher Form bei einer anderen Stelle zur Erlangung eines akademischen Grades eingereicht wurde.

München, 22.10.2020

Tamara Krause

## TABLE OF CONTENT

---

Table of content .....	1
List of abbreviations.....	4
1. Introduction .....	7
1.1. Hepatoblastoma .....	7
1.1.1. Epidemiology .....	7
1.1.2. Histology.....	7
1.1.3. Symptoms and diagnosis/clinical presentation .....	8
1.1.4. Staging .....	8
1.1.5. Long-term and side effects of chemotherapeutical treatment .....	10
1.1.6. Cytogenetics of hepatoblastoma.....	10
1.1.7. Genetics of hepatoblastoma .....	11
1.1.8. Other signaling pathways .....	14
1.1.9. Epigenetics of hepatoblastoma .....	15
1.2. BCL6 Corepressor Like 1.....	17
1.3. Hepatocellular carcinoma .....	19
1.4. Transitional liver cell tumor .....	19
1.5. Aim .....	19
2. Materials .....	20
2.1. Cell culture .....	20
2.1.1. Cell lines.....	20
2.1.2. Cell Culture Reagents .....	20
2.1.3. Cell Culture Material.....	20
2.1.4. Cell Culture Transfection Reagents .....	21
2.2. Prokaryotic Cultures .....	21
2.2.1. Bacteria.....	21
2.2.2. Culture Media.....	21
2.3. Primers.....	22
2.4. Antibiotics .....	23
2.5. Plasmids .....	23
2.6. Short-hairpin RNAs (shRNAs) .....	23
2.7. Guide RNAs (gRNAs) .....	23
2.8. Antibodies .....	23
2.8.1. Primary Antibodies .....	23
2.8.2. Secondary Antibodies.....	24
2.9. Chemicals/Reagents.....	24
2.10. Buffers and Solutions .....	26
2.10.1. Cloning.....	26
2.10.2. Proliferation assay .....	26
2.10.3. Western Blot.....	27
2.10.4. Immunoprecipitation.....	27

## TABLE OF CONTENT

2.10.5. ChIP.....	28
2.10.6. Immunocytochemistry.....	29
2.11. Molecular Size Markers .....	29
2.12. Enzymes .....	29
2.13. Kits .....	29
2.14. Consumables.....	30
2.15. Equipment.....	30
2.16. Software.....	32
3. Methods .....	33
3.1. Patients .....	33
3.2. Polymerase chain reaction (PCR).....	33
3.3. RNA extraction.....	33
3.4. Reverse Transcription .....	34
3.5. Quantitative real-time PCR (qRT-PCR) .....	34
3.6. Knockdown/knockout of BCORL1 .....	34
3.6.1. Generation of a short-hairpin RNA vector.....	34
3.6.2. Generation of a CRISPR-Cas9 vector.....	35
3.7. Plasmid propagation .....	36
3.7.1. Transformation of DH5 $\alpha$ .....	36
3.7.2. Colony picking and MiniPrep.....	36
3.8. Cell culture .....	36
3.8.1. Thawing of cells .....	36
3.8.2. Passaging of cells .....	36
3.8.3. Freezing of cells .....	36
3.8.4. Transient/stable transfection of cells.....	36
3.9. Phenol-Chloroform extraction of DNA.....	37
3.10. Proliferation assay .....	37
3.11. Clonogenicity assay.....	37
3.12. Immunocytochemistry.....	37
3.13. Immunodetection of proteins/Western Blot.....	38
3.13.1. Protein extraction.....	38
3.13.2. SDS-PAGE and Western blot.....	39
3.13.3. Antibody establishment .....	39
3.14. Immunoprecipitation (IP).....	39
3.15. Chromatin Immunoprecipitation (ChIP) .....	40
3.15.1. Chromatin preparation.....	40
3.15.2. Chromatin shearing .....	40
3.15.3. Chromatin quality check.....	40
3.15.4. Immunoprecipitation.....	41
3.15.5. Evaluation of ChIP.....	41
3.16. Sequencing.....	41

## TABLE OF CONTENT

3.16.1. Sanger sequencing.....	41
3.16.2. RNA sequencing.....	41
3.16.3. ChIP sequencing .....	41
4. Results .....	42
4.1. Genetic investigation .....	42
4.2. Protein level.....	43
4.2.1. Improvement of protein extraction.....	44
4.2.2. BCORL1 antibody screening.....	45
4.3. Creation of BCORL1 knockout cells.....	50
4.3.1. CRISPR efficiency .....	50
4.3.2. Mutation analysis of knockout clones .....	51
4.3.3. Effects of genome editing on protein level .....	52
4.4. Effect of BCORL1 knockout on tumor biology.....	52
4.4.1. Morphology .....	52
4.4.2. Cell proliferation.....	54
4.4.3. Clonogenicity .....	55
4.5. Effect of BCORL1 knockout on gene regulation .....	56
4.5.1. Establishment of ChIP .....	56
4.5.2. Establishment of ChIP-seq .....	58
4.5.3. Target genes of BCORL1 regulation .....	59
4.6. BCORL1 rescue .....	67
4.6.1. Effect of BCORL1 rescue on morphology.....	67
4.6.2. Effect of BCORL1 rescue on proliferation .....	68
4.6.3. Effect of BCORL1 rescue on clonogenicity .....	69
4.6.4. Effect of BCORL1 rescue on gene regulation .....	70
5. Discussion.....	73
5.1. Mutations.....	73
5.2. Target genes of BCORL1.....	75
5.3. Perspectives and future plans.....	77
6. Summary/Zusammenfassung .....	79
6.1. Summary.....	79
6.2. Zusammenfassung .....	80
7. APPENDIX .....	82
8. ACKNOWLEDGEMENTS .....	86
9. References.....	87

## LIST OF ABBREVIATIONS

---

°C	Degree Celsius
CRISPR	Clustered Regularly Interspaced Short Palindromic Repeats
ACTB	Beta-actin
AFP	Alpha-fetoprotein
AKT	Protein kinase B
ALAS1	Delta-aminolevulinate synthase 1
ALDH2	Aldehyde dehydrogenase 2
APC	Adenomatous polyposis coli
ATCC	American Type Culture Collection
bp	Base pair
BSA	Bovine Serum Albumin
BWS	Beckwith-Wiedemann syndrome
C1	Cluster 1
C2	Cluster 2
ChIP	Chromatin immunoprecipitation
CK1	Casein kinase 1
CO <sub>2</sub>	Carbon dioxide
COG	Children's Oncology Group
Ct	Cycle of threshold
CTNNB1	Beta-catenin
d	Day
DAPI	4',6-diamidino-2-phenylindole
DAVID	Database for Annotation, Visualization and Integrated Discovery
DMSO	Dimethyl sulfoxide
dNTPs	Deoxy-nucleoside triphosphate
DTT	Dithiothreitol
<i>E.coli</i>	Lat: <i>Escherichia coli</i>
ECL	Electrochemiluminescence
EDTA	Ethylenediaminetetraacetic acid
EPCAM	Epithelial cell adhesion molecule
EtOH	Ethanol
FAP	Familial adenomatous polyposis
FCS	Fetal Calf Serum
FWD	Forward
FZD	Frizzled
GADPH	Glyceraldehyde-3-phosphate dehydrogenase
GPC3	Glypican 3
GSK3β	Glycogen synthase kinase 3 beta
h	Hour
H3K27me3	Histone H3 lysine 27 tri-methylation

## LIST OF ABBREVIATIONS

H3K4me3	Histone H3 lysine 4 tri-methylation
HBV	Hepatitis B virus
HCC	Hepatocellular carcinoma
HDAC	Histone deacetylase
HHIP	Hedgehog-interacting protein
IGF2	Insulin-like growth factor 2
IGFBP3	Insulin-like growth factor binding protein 3
IGF1R	Insulin-like growth factor 1 receptor
IgG	Immunoglobulin G
INI1	Integrase Interactor 1 Protein
KRT19	Keratin 19
kDa	Kilo Dalton
l	Liter
LB	Lysogeny Broth
LOH	Loss of heterozygosity
LRP	Low density lipoprotein receptor-related protein
M	Molar
MeOH	Methanol
MgCl <sub>2</sub>	Magnesium chloride
min	Minute
ml	Milliliter
mM	Millimolar
n	Nano
NaCl	Sodium chloride
NSD1	Nuclear receptor binding SET Domain Protein 1
ng	Nanogram
nm	Nanometer
O <sub>2</sub>	Oxygen
PBS	Phosphate buffered saline
PCR	Polymerase chain reaction
PcG	Polycomb Group
PCGF	Polycomb Group Ring Finger
PI3K	Phosphoinositide 3-kinase
PRC	Polycomb repressive complex
PRETEXT	Pre-treatment EXTend of disease
POSTEXT	POST-Treatment EXTend of Tumor
PTCH1	Patched1
PTEN	Phosphatase and tensin homolog
qRT-PCR	Quantitative real time polymerase chain reaction
RV	Reverse
RING	Ring Finger Protein
RNA	Ribonucleic acid

## LIST OF ABBREVIATIONS

rpm	Rounds per minute
RPMI	Roswell Park Memorial Institute Medium
RT	Room temperature
SDS	Sodium dodecyl sulfate
sec	Second
SEM	Standard error of the mean
SFRP1	Secreted frizzled-related protein 1
SHH	Sonic hedgehog
SIOPEL	International Childhood Liver Tumor Strategy Group
SMO	Smoothened
STE	Sodium Chloride-Tris-EDTA
TBE	Tris/Borate/EDTA
TBP	TATA-Box-binding-Protein
TE	Tris-EDTA Buffer
TLCT	Transitional liver cell tumor
Tris	Tris (hydroxymethyl) aminomethane
TSG	Tumor suppressor gene
U	Unit
UV	Ultraviolet
V	Volt
WIF	Wnt Inhibitory Factor
$\beta$	Beta
$\mu$ g	Microgram
$\mu$ l	Microliter
$\mu$ M	Micromolar

## 1. INTRODUCTION

---

The term cancer describes different diseases associated with uncontrolled cell growth. These malignant neoplasms or tumors can potentially spread to other parts of the body and invade them [1]. Benign tumors do not spread and therefore do not count as cancer [2]. While there are over 100 types of cancer that may affect human beings [1], there are common unspecific signs and symptoms like fever, weight loss, fatigue or skin changes. Most symptoms are more locally observed, like masses or lumps.

Pediatric cancer is a relatively rare disease compared to adult cancer, but nonetheless one of 600 children with an age below 15 years is affected. The 5 year survival is about 80 % [3] but the development of pediatric cancers is still mostly unidentified [4]. Whereas adult cancers originate from acquired mutations, pediatric cancers are suspected to arise from mistakes in embryogenesis. Subtypes and tumor localization also differ from adult cancers [5]. One of the subclasses of pediatric cancers is hepatobiliary cancer, which includes hepatoblastoma, transitional liver cell tumors (TLCTs) and hepatocellular liver carcinoma (HCC).

### 1.1. Hepatoblastoma

---

#### 1.1.1. Epidemiology

---

Hepatoblastoma makes up 1 % of all pediatric cancers and thus, is classified a rare disease. With 1 child per million children per year affected, hepatoblastoma is still the most common childhood liver tumor below the age of 15 years [6, 7]. In 80 % of patients, the manifestation age is between 6 to 36 months [8]. Occurrence is more frequently in boys [9-11], as well as children with low birth weight and premature births [12, 13]. Even though the origin of hepatoblastoma is still unknown, the prominent theory of tumorigenesis is based on derailed developmental processes of the immature hepatocyte precursors, which are normally supposed to differentiate into cells like hepatocytes, biliary, mesenchymal, and epithelial cells.

#### 1.1.2. Histology

---

The histology of hepatoblastoma is heterogenic with different phenotypes. The epithelial phenotype makes up 56 % of cases, with 31 % being fetal, 19 % embryonal, 3 % small-cell undifferentiated, and 3 % macrotrabecular. The mixed epithelial-mesenchymal phenotype makes up 44 % [14-16]. Mesenchymal elements like spindle cells, fibrous tissue, and osteoid are most frequent. In advanced disease, these elements also promise better prognosis. Fetal elements on the other hand show better results with resected tumors. Undifferentiated cells are generally more aggressive and have a worse prognosis [17].

## INTRODUCTION

### 1.1.3. Symptoms and diagnosis/clinical presentation

Usually hepatoblastoma occurs associated with unspecific symptoms varying with tumor size and presence of metastases. These symptoms include weight loss, swollen abdomen, fever, pain, and nausea. Blood tests for kidney function, liver vitality, blood count, and alpha-fetoprotein (AFP) levels are used for diagnosis. Low AFP levels are associated with high risk [18-21]. Metastases are present in 20 % of hepatoblastoma cases in the lung, but are also possible in brain and bone [22]. Magnetic resonance imaging as well as computed tomography or ultrasound can help in staging the hepatoblastoma.

### 1.1.4. Staging

Based on tumor localization and presence of metastases, hepatoblastoma cases are staged according to one of the following systems.

#### 1.1.4.1. PRE-Treatment tumor EXTension (PRETEXT)

The radiologic PRETEXT staging system depends on the tumor extent identified prior to any therapy [23]. Stage I involves the right posterior or left lateral liver section. With two adjoining tumor-free sections, the tumor is defined as stage II. In stage III cases, one or two sections are free of tumor. The tumor defines as stage IV, when all four liver sections are involved [23]. Besides the primary tumor extent, other factors are included in the PRETEXT system. These include caudate lobe involvement (C), extrahepatic abdominal disease (E), multifocality of the liver tumor (F), and the existence of distant (M) or lymph node metastases (N). Other important factors are the involvement of the portal vein (P), tumor rupture at the time of diagnosis (R), and hepatic vein or inferior vena cava involvement (V) [24].

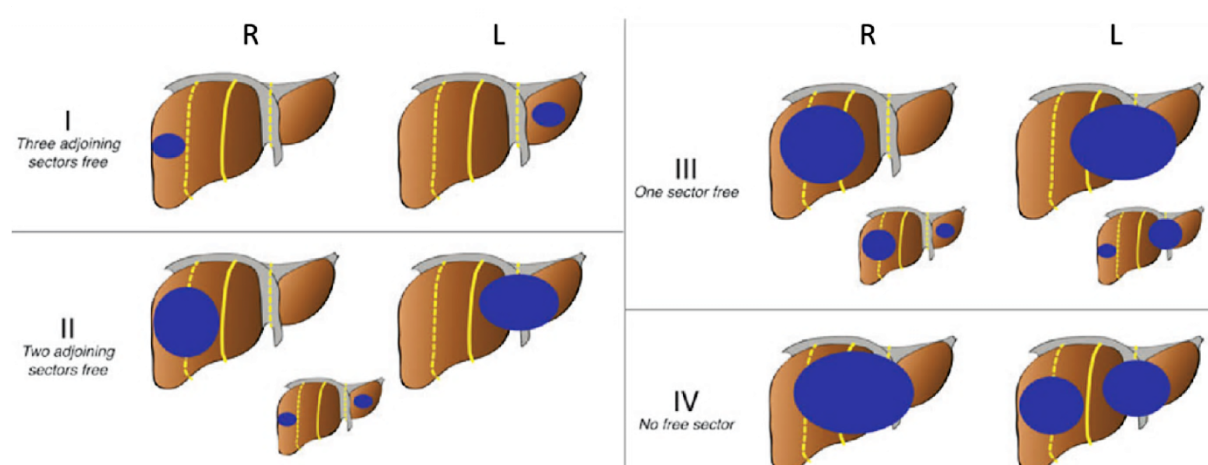


Figure 1: PRETEXT staging system, Emre *et al.*, 2012 [25].

## INTRODUCTION

### **1.1.4.2. Childhood Liver Tumors Strategy Group (SIOPEL)**

---

SIOPEL started with its first clinical study in 1990 with 154 hepatoblastoma cases and 40 pediatric HCCs. Since then, more SIOPEL studies have been done and led to a SIOPEL staging system that divides into high-risk and standard risk patients [26]. With the SIOPEL 1 study, a combination of doxorubicin and cisplatin was tested [10]. SIOPEL 2 focused on the efficacy and toxicity of cisplatin monotherapy in standard risk hepatoblastoma. Moreover, alternating cycles of cisplatin, carboplatin and doxorubicin were tested in high-risk patients [11]. SIOPEL 3 then compared cisplatin with multiagent chemotherapy and aggressive surgery in standard risk patients [27, 28]. The SIOPEL 4 study focused on high-risk hepatoblastoma cases by using radical surgery and cisplatin therapy [27].

Collectively, these studies allowed staging and led to a therapy scheme for hepatoblastoma patients. Patients with standard risk tumors present with PRETEXT I, II or III tumors and no additional adverse features [29]. The standard treatment is four cycles preoperative cisplatin therapy followed by surgical resection and two post-operative cycles of therapy [28, 30]. Patients of the high-risk group present with PRETEXT IV tumors and/or factors like extrahepatic abdominal disease (E), metastases (M), portal (P) or hepatic vein or inferior vena cava involvement (V) and/or AFP levels less than 100 ng/ml [26]. Treatment recommendation is seven preoperative alternating cisplatin and carboplatin cycles with addition of doxorubicin and three cycles postoperatively [31]. Patients in this group are likely to have challenging surgical disease and are recommended to consult with a specialist liver surgery/transplant service [30].

### **1.1.4.3. German Society for Pediatric Oncology and Hematology (GPOH)**

---

GPOH groups patients not only into standard risk and high-risk, but also has a category for very high-risk cases. Hepatoblastoma cases with PRETEXT I, II and III are ranked as standard risk. High-risk hepatoblastoma cases are staged PRETEXT IV and show additional features like multifocality (F), vascular involvement (P, V) or invasion of extrahepatic structures (E). GPOH differentiates very high-risk patients, as any hepatoblastoma with distant metastases (M) and/or AFP <100 ng/ml [32]. Standard risk patients are treated with two or three cycles of cisplatin and doxorubicin presurgically with one postsurgical cycle [10] or four cycles cisplatin presurgically and two cycles postsurgically [28, 32]. For high-risk hepatoblastoma, GPOH recommends four cycles of cisplatin alternating with carboplatin and doxorubicin presurgically and two cycles of carboplatin and doxorubicin alternating with cisplatin postsurgically [31, 32]. Patients that rank into the very high-risk group are treated with three cycles of cisplatin and doxorubicin and one cycle carboplatin and doxorubicin before resection and one cycle of carboplatin and doxorubicin postsurgically [27, 32].

## INTRODUCTION

### 1.1.4.4. 16-gene signature of hepatoblastoma

---

In 2008, Cairo *et al.*, discriminated tumor samples through a microarray expression analysis approach into two clusters and showed that the 16-gene classifier discriminates aggressive from more favorable tumors. The 16-gene classifier is very precise at prediction of survival. When compared to clinical criteria, multiple analyses exhibited a strong correlation with the 16-gene signature [33]. Cluster 1 (C1) tumors are mostly of fetal phenotype, whereas C2 tumors present with immature pattern and embryonal or crowded fetal histology. C2 tumors have a high proliferation rate and exhibit upregulation of hepatic progenitor and proliferation markers like Alpha Fetoprotein (AFP), Keratin 19 (KRT19), and Epithelial cell adhesion molecule (EPCAM) compared to C1 tumors. Furthermore, markers for mature hepatocytes are downregulated in C2 tumors. These include 5'-Aminolevulinate Synthase 1 (ALAS1) and Aldehyde Dehydrogenase 2 Family Member (ALDH2), as well as UDP Glucuronosyltransferase Family 2 Member B4 (UGT2B4) [33].

### 1.1.5. Long-term and side effects of chemotherapeutical treatment

---

Chemotherapeutic agents have a range of side effects, not specific to the type of hepatoblastoma, but the type of therapy and dosage. It can cause nausea, hair loss, bruising, bleeding, fatigue, and diarrhea. Moreover, patients suffer from increased infection risk. Doxorubicin and cisplatin can also have long-term consequences. These include ototoxicity as well as nephrotoxicity in case of carboplatin or cisplatin. Moreover, doxorubicin can lead to cardiac toxicity [34]. Other long-term effects include secondary cancers, infertility, lung defects, cognitive impairment and growth deficiencies due to treatment related developmental changes [35]. Because of treatment and hospitalization, psychological difficulties like depression, learning difficulties, and social behavior problems concerning same age are also known to affect children suffering from hepatoblastoma [36, 37]. Thus, it is necessary to improve treatment and diagnostics in order to reduce toxicity, side effects, and late treatment effects.

### 1.1.6. Cytogenetics of hepatoblastoma

---

Cytogenetic changes are rare in hepatoblastoma. Besides genetic or overgrowth syndromes, hepatoblastoma occurs sporadically. One genetic syndrome associated with hepatoblastoma is familial adenomatous polyposis (FAP) [38].

FAP is an autosomal recessive disease, which presents with polyps in the colon and is associated with germline mutations of the tumor suppressor gene adenomatous polyposis coli (APC). These mutations can cause multiple colon polyps or even colon cancer [39]. In about 0.42 % of FAP cases, patients also develop hepatoblastoma [40].

## INTRODUCTION

The most commonly known overgrowth syndrome is the Beckwith-Wiedemann syndrome (BWS). BWS patients have a 2,280-fold increased risk of developing hepatoblastoma compared to healthy children [41, 42]. Besides macroglossia and macrosomia, BWS can cause neonatal hypoglycemia, ear pits/creases, and midline abdominal defects. This is due to variations of chromosome 11p like uniparental isodisomy of 11p.15.5. This variation correlates with occurrence of embryonal tumors like hepatoblastoma through paternal duplication and maternal loss of heterozygosity (LOH) [43]. Aside from BWS, there are other overgrowth syndromes that are associated with hepatoblastoma, like the Sotos syndrome or the Simpson-Golabi-Behmel syndrome. These are caused by mutations or deletions in different genes. In case of the Sotos syndrome, the Nuclear receptor binding SET Domain Protein 1 (*NSD1*) gene is affected, while the Simpson-Golabi-Behmel syndrome revealed changes of the Glypican 3 (*GPC3*) gene on chromosome Xq26 [44-46].

The most frequent cytogenetic alteration of hepatoblastoma is trisomy of chromosome 2, 8, and 20. Besides an individual occurrence, these trisomies can occur alongside with structural changes of the DNA. In contrast, the loss of chromosomes is relatively rare [47, 48]. The most likely to be lost is chromosome 18. Furthermore, unbalanced translocations of the chromosomal arm 1p and 4q occur in hepatoblastoma. One of the first recurrent translocations described, was identified as der(4)t(1;4)(q12;q34) [49]. This typical breakpoint at the chromosomal arm 1p always leads to 1q duplication. Hepatoblastoma was reported to be associated with translocations at breakpoints on chromosome 1q12 and 1q24 [48, 50].

### **1.1.7. Genetics of hepatoblastoma**

---

In contrast to adult tumors, pediatric tumors are characterized by a low mutation rate [51]. With a remarkable low mutation rate of 2.9 mutations per tumor genome [52], hepatoblastoma reveals the lowest mutation rate of all tumors (Figure 2). This indicates that hepatoblastoma is a rather simple tumor from a genetic perspective [51].

## INTRODUCTION

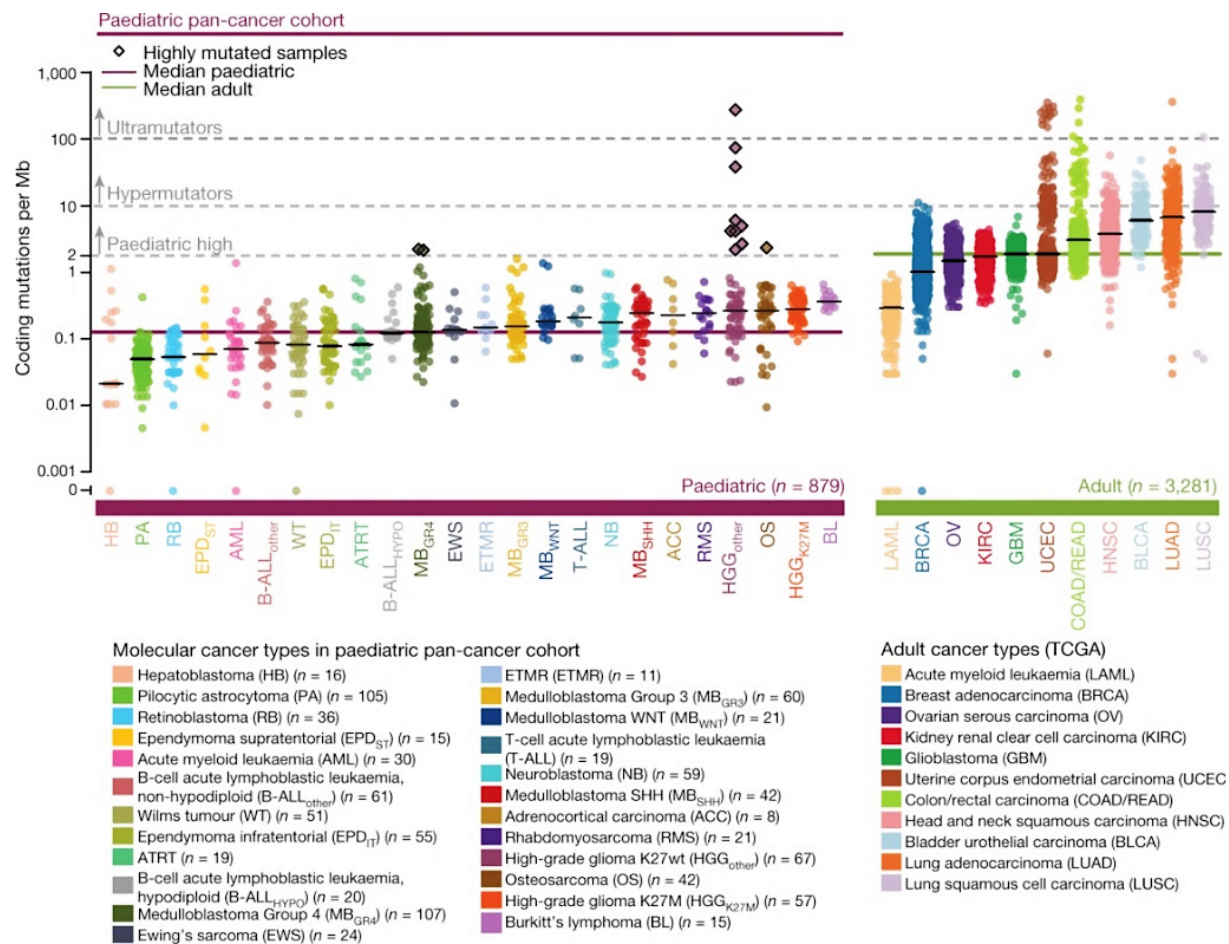


Figure 2: Mutation rate of different cancer types in children and adults, Gröbner *et al.*, 2018 [51].

Very few recurrent mutations have been identified so far. The best investigated gene is the  $\beta$ -catenin (*CTNNB1*) gene and the connected Wnt pathway. Our lab previously showed that *CTNNB1* is mutated in 72.5 % of hepatoblastoma cases [52]. Other genes with recurrent mutations are the Nuclear Factor, Erythroid 2 Like 2 (*NFE2L2*) gene, which demonstrated a mutation rate of 9.8 % and the telomerase reverse-transcriptase (*TERT*) gene with a mutation rate of 5.9 % [52].

### 1.1.7.1. *CTNNB1* and the Wnt pathway

The *CTNNB1* mutations are mostly point mutations or deletions in exon 3 [53]. *CTNNB1* is involved in the canonical Wnt signaling pathway, which plays an important role in organogenesis and processes like differentiation, proliferation, morphology, cell motility, apoptosis, and cell survival [54, 55]. Moreover, it has a crucial function in development, metabolism, and regeneration of the liver. Furthermore, it strongly supports the maintenance of the normal adult liver function. Wnt was first identified in fruit flies missing wings as Wingless (Wg). The combination with the later identified mouse homologue Integrin 1 (Int1) [56, 57] led to the name fusion Wnt [58].

## INTRODUCTION

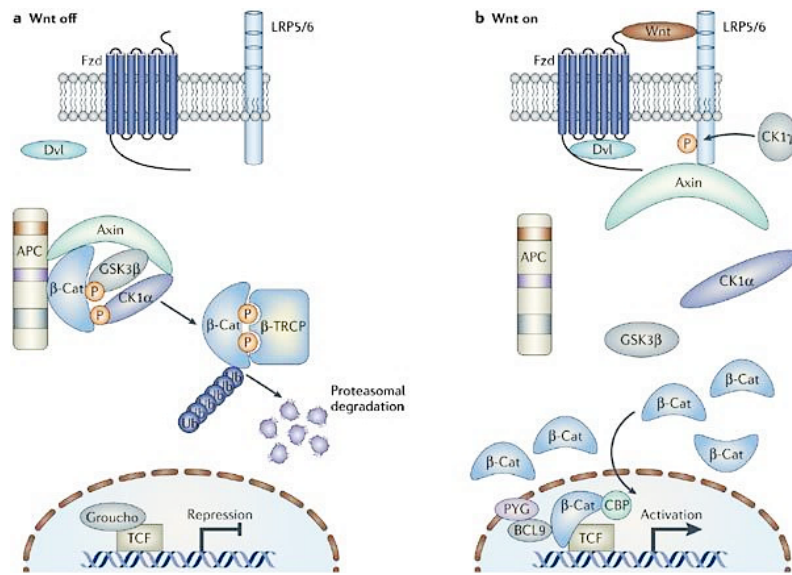


Figure 3: **Canonical Wnt signaling pathway, Barker et al., 2006 [59].** A) Without Wnt-binding,  $\beta$ -catenin is marked through phosphorylation and ubiquitination by the destruction complex (APC, AXIN, GSK3 $\beta$ , CK1 $\alpha$ ) leading to proteasomal degradation. B) Wnt binding causes dissociation of AXIN and inactivation of the destruction complex. Thus, cytoplasmatic  $\beta$ -catenin levels increase and lead to translocation of  $\beta$ -catenin to the nucleus, activating Wnt target gene expression by binding to TCF [59].

In quiescent cells, CTNNB1 is part of adherens junctions located at the plasma membrane. These consist of cadherin 1 (CDH1) and  $\alpha$ -catenin besides CTNNB1. As part of the destruction complex, the Glycogen Synthase Kinase 3 Beta (GSK3 $\beta$ ) phosphorylates excess cytoplasmic CTNNB1 and thereby marks it for degradation. Other proteins belonging to this complex are Adenomatous Polyposis Coli (APC), Axis Inhibition protein (AXIN), and Casein Kinase 1  $\alpha$  (CK1 $\alpha$ ) [60-62]. Activation of the Wnt pathway takes place when Wnt or other ligands are bound by Frizzled (FZD). Recruitment of the low density lipoprotein receptor-related protein (LRP) 5/6, is followed by Dishevelled and AXIN recruitment to the membrane [63]. As a consequence, the destruction complex is inactivated and CTNNB1 not phosphorylated. Hence, CTNNB1 is stabilized in the cytosol and can replace the repressor Groucho in a TCF/LEF-complex in the nucleus and induce the expression of Wnt target genes like the proto-oncogene *MYC*, the cell cycle regulating cyclin D1 (*CCND1*), and Paired Like Homeodomain 2 (*PITX2*) [64-69]. Other target genes are proteins of the Wnt signaling pathway like FZD, LRP5/6, AXIN and TCF/LEF leading to auto-regulation of the pathway [58]. Wnt signaling is also negatively regulated by inhibitors of the Dickkopf (DKK) family, which mediate inactivation by LRP-binding. Other inhibitors of the Wnt signaling pathway are the Wnt inhibitory factor 1 (WIF1) and the secreted Frizzled-related protein 1 (SFRP1) [70, 71]. These two proteins can either form an inactive complex with the FZD or directly bind Wnt [72].

When CTNNB1 is mutated, it cannot be degraded by the ubiquitin-proteasome pathway. Thus, CTNNB1 translocates to the nucleus to activate target genes [64-68]. Somatic APC and AXIN mutations

## INTRODUCTION

are associated with hepatoblastoma but with a low frequency of less than 10 % [33, 73-75]. *CTNNB1* and *AXIN* are both also found to be mutated in HCC. The co-occurrence of these mutations in hepatoblastoma and HCC suggest that the Wnt signaling pathway possesses a crucial role in liver tumor development [74, 76, 77]. *CTNNB1* mutations can induce hepatomegaly or even induce tumors in bipotential fetal liver cells of mice [78].

### 1.1.7.2. Nuclear Factor, Erythroid 2 Like 2

---

Mutations of the *NFE2L2* gene are missense mutations [52]. *NFE2L2* is a transcription factor, regulating the counteraction of xenobiotics and oxidative stress by activating the cellular antioxidant response. In normal cells, cytoplasmic *NFE2L2* is ubiquitinated by a Cullin 3 (CUL3)-dependent E3 ubiquitin ligase and thus marked for proteasomal degradation. The Kelch-like erythroid cell-derived protein 1 (KEAP1) facilitates this reaction. *NFE2L2* is not degraded when the cell is under oxidative stress. After translocation to the nucleus and heterodimerization with musculoaponeurotic fibrosarcoma (Maf) family proteins, *NFE2L2* induces expression of genes involved in cytoprotection and metabolism [79-81]. Mutations in the *NFE2L2* gene in tumor cells prevent the proteasomal degradation and create protection from anti-oxidative stress, chemotherapy [82-84], and radiotherapy [85].

### 1.1.7.3. Telomerase reverse-transcriptase

---

Previous studies identified point mutations associated with increased *TERT* expression. The Mutations were located in the *TERT* promoter upstream of the transcriptions start site [52]. *TERT* is part of the telomerase complex [86], which adds telomeric repeats to the ends of chromosomal DNA, allowing cells to escape senescence and even become immortal [87]. Upregulation of *TERT* is found in stem cells and cancerous cells [88-91]. *TERT* expression is regulated by activating transcription factors like MYC, specificity protein 1 (SP1), hypoxia-inducible factor-1 (HIF-1), adipocyte protein 2 (AP2), and suppressing genes such as p53 and the Wilms tumor protein (WT1) [91-94].

## 1.1.8. Other signaling pathways

---

### 1.1.8.1. Hedgehog signaling pathway

---

The HH signaling pathway is involved in liver regeneration after injury in adults [95-98] and developmental processes [99-107]. HH signaling is induced through autocatalytic processing of an HH ligand [108], leading to interaction of Patched 1 (PTCH1) and Smoothened (SMO) [109-115]. This interaction induces GLI transcription factor family-mediated expression of target genes like *MYCN*, *IGF2* and *CCND1* [116-118]. Hedgehog interacting protein (HHIP) alters HH signaling by binding HH to prevent complex formation with PTCH1 [119].

## INTRODUCTION

Deregulation of the HH pathway was found in solid tumors like cholangiocarcinoma, HCC, and hepatoblastoma [52, 98, 120, 121]. In hepatoblastoma, overexpression of Sonic Hedgehog (*SHH*), *PTCH1*, *SMO*, and *GLI1* [52, 122] and silencing of *HHIP* [52] was observed.

### 1.1.8.2. IGF2/PI3K/AKT

---

Another important signaling pathway concerning hepatoblastoma is the insulin-like growth factor 2 (IGF2) pathway. This pathway takes regulates normal liver development and liver cell growth. Insulin-like growth factor binding-protein-3 (IGFBP3) binds IGF2 in normal cells, hence reduces its availability for insulin-like growth factor 1 receptor (IGF1R). As a consequence, IGF-independent apoptosis is induced in order to prevent abnormal cell growth [123]. When IGF2 binds to IGF1R, diverse signaling pathways are activated. These include the PI3K/AKT and RAS/RAF/MEK/ERK pathways, which stimulate transcription as well as cell cycle progression. As a result, proliferation and cell growth increase [123].

*IGF2* upregulation [124, 125] and *IGFBP3* silencing [122] were reported in hepatoblastoma. Both result in a constant activation of the IGF2 signaling pathway and hence inadequate activation of proliferation [126]. Amplifications of the IGF2 activator Pleomorphic adenoma gene 1 (*PLAG1*) [127] could contribute to this deregulation.

Hepatoblastoma also shows a small variety of frequently occurring mutations in genes of the PI3K signaling pathway, like Phosphatidylinositol-4-Phosphate 3-Kinase Catalytic Subunit Type 2 Beta (*PIK3C2B*) or Phosphatidylinositol-4,5-Bisphosphate 3-Kinase Catalytic Subunit Alpha (*PIK3CA*) [128, 129]. Moreover, the downstream target *AKT* and Phosphatase and Tensin Homolog (*PTEN*) were found to be mutated [130], and AKT activation in hepatoblastoma due to phosphorylation was reported [128].

Taking together these findings, an active IGF signaling pathway seems to be characteristic for liver pathogenesis.

### 1.1.9. Epigenetics of hepatoblastoma

---

Epigenetics study phenotypic alterations, which do not stem from changes in certain gene sequences, but a specific transcriptional program. This program is started by a triggering signal and uphold until a new input signal triggers an alternative program [131]. Criteria for epigenetic information are quite simple. They have to regulate gene transcription and self-propagate across cell divisions until the signal is replaced. This is true for chemical or post-translational modifications of DNA or histones [131]. In general, a nucleosome consists of an octamer of histones (H2A, H3, H2B and H4) wrapped in DNA, RNAs and non-histonic proteins. These nucleosomes build up chromatin loops, stabilized by effector proteins, non-coding RNAs (ncRNAs), and histone modifications [132, 133]. These histone modifications can be arranged by histone (de)acetylases, histone methyltransferases, and

## INTRODUCTION

other proteins [134-136]. Acetylation leads to relaxation of chromatin and induction of transcription, whereas the effects of methylation depend on the histone residue. Trimethylation of lysine 4 of histone 3 (H3K4me3) is known to be a histone modification on active genes in contrast to H3K27me3, which is a silencing mark [136]. Due to relaxation of the chromatin, the DNA is more accessible for the RNA polymerase II (RNAP) and cofactors, which upon transcriptional activation elongates the DNA and produces mRNA [137].

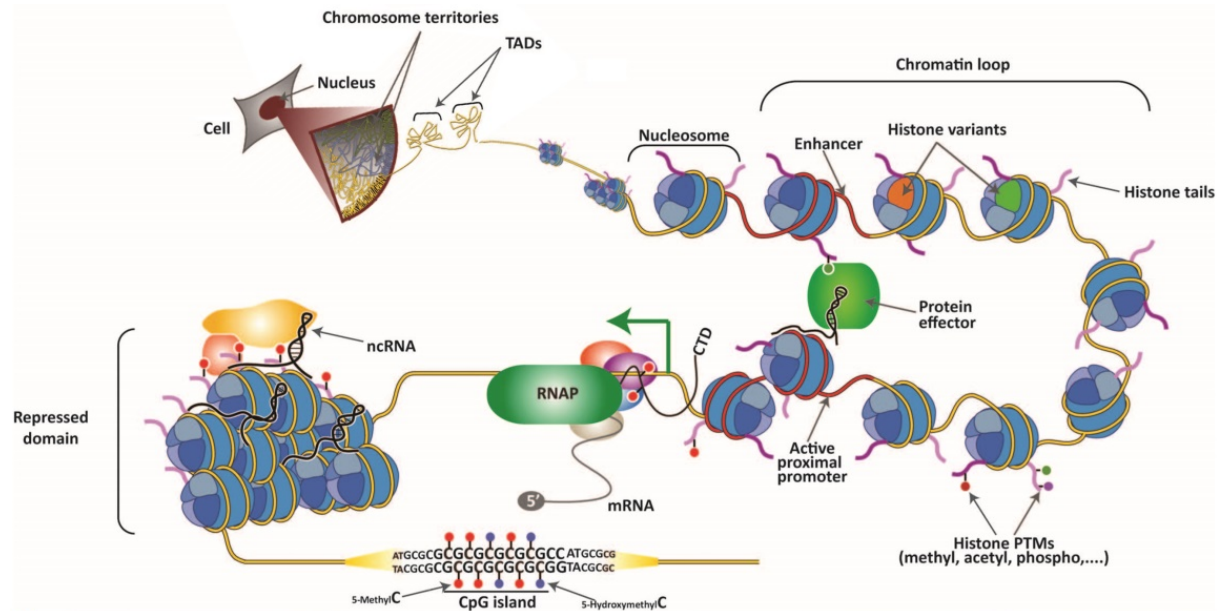


Figure 4: **Hierarchical chromatin organization of mammalian cells, Arana et. al 2015 [138].** DNA wrapped around histones with different modifications, leading to chromatin loops and TADs (TAD: Topologically associated domains, CTD: C-terminal domain, RNAP: RNA polymerase II).

Due to the rarity of recurring mutations and the deregulation of certain pathways, hepatoblastoma was examined for epigenetic alterations over the last decade. Recently, our group identified several tumor suppressor genes (TSG) to be epigenetically modified in hepatoblastoma. These TSGs included members of the three major derailed pathways in hepatoblastoma. As an inhibitor of the Wnt pathway, *SFRP1* was found to be highly repressed through DNA methylation and a high level of H3K9me2 [139]. This was also shown for *HHIP*, an inhibitor of the Hedgehog pathway [52] and *IGFBP3*, an inhibitor of the IGF2 signaling [122]. These TSGs are silenced in hepatoblastoma, thus allowing tumor progression [139].

## INTRODUCTION

### 1.2. BCL6 Corepressor Like 1

BCL6 Corepressor Like 1 (BCORL1) is a transcriptional corepressor [140] and its gene is located on the X chromosome. There are two transcript variants, which both consist of 12 exons, but the 1a transcript variant has an additional exon 9. Important features of the BCORL1 protein are the C-terminal binding protein (CtBP) binding-site in form of a PDXLS-motif [140], a nuclear localization signal, some nuclear receptor recruiting motifs and an ankyrin repeat (Figure 5).

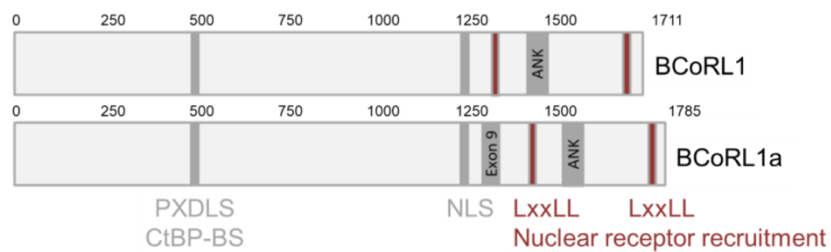


Figure 5: **The two transcript variants of BCORL1** (CtBP-BS: C-terminal Binding Protein-Binding Site, NLS: Nuclear Location Signal, ANK: Ankyrin repeat).

BCORL1 is closely related to the BCL6 Corepressor (BCOR), which potentiates BCL6 repression [141]. Moreover, BCORL1 is known to be part of the Polycomb repressive complex 1.1 (PRC1.1) also known as the BCORL1-complex [142-145]. PRC1.1 belongs to the group of non-canonical PRC1 (ncPRC1) complexes, all including a Ring Finger Protein 1 (RING1), one Polycomb Group Ring Finger (PCGF) protein, and RING1 And YY1 Binding Protein (RYPB), also called YY1 Associated Factor 2 (YAF2) as essentials [143, 146-148]. The PRC1.1 obtains its catalytic activity from the E3 ligase RING1B with H2Aub1 at lysine 119 as main substrate. PCGF1 enhances this RING1B function [144, 149, 150]. Moreover, PRC1.1 consists of Lysine Demethylase 2 (KDM2B), a histone demethylase with a CxxC domain for DNA binding and CGI targeting [142, 150, 151], the H2B-deubiquitinating Ubiquitin Specific Peptidase 7 (USP7)[138], and S-Phase Kinase Associated Protein 1 (SKP1)[143, 152]. Interaction of BCORL1 and the PRC1.1 is established through interaction of a RAWUL domain in PCGF1 and the PCGF Ub-like fold discriminator (PUFD) domain of BCORL1 [152].

## INTRODUCTION

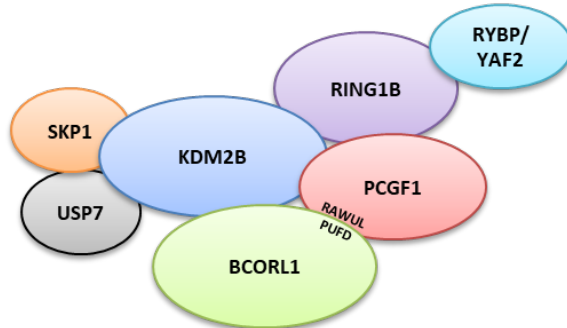


Figure 6: **Polycomb repressive complex 1.1/BCORL1 complex.** BCORL1 directly interacts with PCGF1 through interaction of PUFD and RAWUL motif.

BCORL1 was also reported to interact with class II histone deacetylases (HDAC) 4/5/7 [140] and perform gene repression by ubiquitination of histone 2A in cooperation with PCGF1 [153], which is also known to cooperate with RUNX1 to regulate self-renewal and differentiation of hematopoietic cells through downregulation of HOXA-cluster genes [153].

In 2007, Pagan *et al.*, exposed the interaction of BCORL1 and CtBP upon repression of target genes like *CDH1* [140]. CtBP has different functions in epithelial mesenchymal transition (EMT), apoptosis, cell proliferation, evasion of growth suppressors, and genome stability [154-160]. In mammals, there are two forms, CtBP1 and CtBP2, which are highly homologous and both involved in developmental processes [161, 162]. Furthermore, CtBP associates with the PRCs to mediate repression [163-166]. The effects of altered CtBP expression reach from embryonic lethality upon complete depletion [167] to development of cancer hallmarks, like evasion of cell death, EMT, increased proliferation, and loss in genome stability upon overexpression [154-160].

*BCORL1* was found to be mutated in different kinds of cancers. In breast cancer, mutations were found in exon 4, intron 5, and intron 13 but they have tolerable effects if even an effect at all. So *BCORL1* is most unlikely a high-risk predisposition gene in breast cancer, but eventually has middle to low penetrance [168]. In acute myeloid leukemia, *BCORL1* was reported to be mutated in 6 % of cases [145, 169]. Most mutations are frameshift, nonsense, splice-site, or missense mutations [169]. *BCORL1* was also found to be mutated in intracranial germ cell tumors. The six identified mutations were frameshift or missense mutations [170]. Other diseases like myelodysplastic syndrome or chronic myelomonocytic leukemia show lower mutation rates with 0.8 % and 1.9 %, whereas acute myeloid leukemia with myelodysplasia-related changes has a mutation rate of 9.1 % [145]. Another liver cancer, the hepatocellular carcinoma was reported to occur with a gene fusion of the *BCORL1* gene to the *ELF4* gene [145]. Due to the *BCORL1* gene position on the X-chromosome, *BCORL1* is affected by the X-inactivation especially in breast cancer [168].

### **1.3. Hepatocellular carcinoma**

---

Besides hepatoblastoma, the hepatocellular carcinoma (HCC) is the second most common pediatric liver tumor. It potentially affects children over 6 years (predominantly boys) [16]. Mostly, HCC develops *de novo*, but pre-existing conditions like metabolic diseases, cirrhosis, and hepatitis B virus (HBV) infection are at a high risk for HCC development [171-173]. Treatment faces difficulties through high chemotherapy resistance and advanced disease at time of diagnosis. Since only complete resection of the primary tumor is a cure, tumor resectability and mortality are directly correlated and thus, results in a survival rate of 25 % after 3 years [173].

### **1.4. Transitional liver cell tumor**

---

The third kind of pediatric liver tumors, which is neither hepatoblastoma nor HCC, is called TLCTs. These tumors differ from hepatoblastoma and HCC in clinical presentation, morphology, immunophenotype as well as reaction to treatment [174]. These aggressive hepatic tumors are bigger, show high AFP levels and high *CTNNB1* expression. Affected children are also older than hepatoblastoma patients. TLCTs are descendants of hepatoblastomas and stem from a neoplastic extension of oncogenic differentiation pathways between hepatoblastoma and HCC. Thus, they show clinical and histological features of both pediatric liver cancer types [174].

### **1.5. Aim**

---

The origin of hepatoblastoma is widely unknown, even though development and progression has been associated with mutations of *CTNNB1*, *NFE2L2* and *TERT*. Moreover, deregulation of signaling pathways like the IGF2, Wnt, and HH signaling pathway contribute to hepatoblastoma development and progression as well as some genetic syndromes. Thus, we attempted to investigate the genetic basis of hepatoblastoma.

Recent exome sequencing data generated by our lab revealed one *BCORL1* mutation aside from mutations that were already in focus of other research [52]. Hence, we focused on targeted Sanger sequencing for *BCORL1* mutations of additional hepatoblastoma cases, TLCTs, and cell lines. Moreover, we intended to perform functional analyses of *BCORL1* mutations, concerning the effects on tumor biology and gene regulation. This included the truncation of the *BCORL1* protein by CRISPR-Cas9, resembling the patient situation and analysis of morphology, proliferation, and clonogenicity. Due to the unavailability of a commercial antibody meeting our criteria to perform protein analysis, we wanted to establish a custom-made antibody. Considering *BCORL1* being a transcriptional corepressor, we also aimed to identify novel target genes of *BCORL1* and their functional involvement. Moreover, our studies intended to define clinical relevance of *BCORL1* mutations and restoration.

## 2. MATERIALS

---

### 2.1. Cell culture

---

#### 2.1.1. Cell lines

HepT1 <i>Homo sapiens</i> (human), liver, hepatoblastoma	Pietsch et al., 1996 [175]
Hep3B <i>Homo sapiens</i> (human), liver, pediatric HCC	ATCC, Manassas, USA
HepG2 <i>Homo sapiens</i> (human), liver, TLCT	ATCC, Manassas, USA
HUH6 <i>Homo sapiens</i> (human), liver, hepatoblastoma	JCRB, Osaka, Japan
HUH7 <i>Homo sapiens</i> (human), liver, adult HCC	JCRB, Osaka, Japan
HEK293T <i>Homo sapiens</i> (human), embryonic kidney	ATCC, Manassas, USA

#### 2.1.2. Cell Culture Reagents

---

Dimethyl Sulfoxide (DMSO), sterile	Merck, Darmstadt, Germany
Dulbecco's Modified Eagle Medium (DMEM)	Invitrogen, Karlsruhe, Germany
Dulbecco's Phosphate-Buffered Saline (DPBS)	Invitrogen, Karlsruhe, Germany
Fetal Calf Serum (FCS), sterile	Sigma-Aldrich, Taufkirchen, Germany
Penicillin-Streptomycin (10 x)	Invitrogen, Karlsruhe, Germany
Roswell Park Memorial Institute Medium (RPMI)	Invitrogen, Karlsruhe, Germany
Trypsin - EDTA 0.05 %	Invitrogen, Karlsruhe, Germany
G418	Millipore, Darmstadt, Germany
Puromycin	Sigma-Aldrich, Taufkirchen, Germany

#### 2.1.3. Cell Culture Material

---

Biosphere® Filtertips 1-10 µL, sterile	Sarstedt AG & Co., Nümbrecht, Germany
Biosphere® Filtertips 1-100 µL, sterile	Sarstedt AG & Co., Nümbrecht, Germany
Biosphere® Filtertips 100-1000 µL, sterile	Sarstedt AG & Co., Nümbrecht, Germany
Cell scraper	Sarstedt AG & Co., Nümbrecht, Germany
Costar® Stripette® Serologic Pipettes (5ml, 10 ml and 25 ml, sterile)	Corning GmbH, Wiesbaden, Germany
Cryotubes, Nalgene	Thermo Scientific, Wilmington, USA
EasyFlasks™, Cell culture flasks, 25 cm <sup>2</sup>	NUNC, Langenselbold, Germany

## MATERIALS

EasyFlasks™, Cell culture flasks, 75 cm <sup>2</sup>	NUNC, Langenselbold, Germany
Plastic tubes, 15 ml, sterile	greiner bio-one, Frickenhausen, Germany
Plastic tubes, 50 ml, sterile	greiner bio-one, Frickenhausen, Germany
Petri dishes 100 x 20 mm, non-pyrogenic, sterile	NUNC, Langenselbold, Germany
6-Well Plates, non-pyrogenic, sterile BD	NUNC, Langenselbold, Germany
12-Well Plates, non-pyrogenic, sterile BD	NUNC, Langenselbold, Germany
24-Well Plates, non-pyrogenic, sterile BD	NUNC, Langenselbold, Germany
96-Well Plates, non-pyrogenic, sterile BD	NUNC, Langenselbold, Germany

### **2.1.4. Cell Culture Transfection Reagents**

---

FuGene HD Transfection Reagent	Promega, Madison, USA
--------------------------------	-----------------------

## **2.2. Prokaryotic Cultures**

---

### **2.2.1. Bacteria**

---

*Escherichia coli* DH5α (Invitrogen, Karlsruhe, Germany)

Genotype: F<sup>-</sup>Φ80lacZΔM15 Δ(lacZYA-argF)U169 recA1 endA1 hsdR17(r<sub>K</sub><sup>-</sup>, m<sub>K</sub><sup>+</sup>) phoA supE44 λ<sup>-</sup> thi-1 gyrA96 relA1

### **2.2.2. Culture Media**

---

Lysogeny Broth (LB) Medium: pH: 7.0	Roth, Karlsruhe, Germany
-------------------------------------	--------------------------

- 10 g/L Tryptone
- 5 g/L Yeast extract
- 10 g/L NaCl

LB-Agar for plates: pH: 7.0	Roth, Karlsruhe, Germany
-----------------------------	--------------------------

- 10 g/L Tryptone
- 5 g/L Yeast extract
- 10 g/L NaCl
- 15 g Agar

Super Optimal Broth Medium with glucose (S.O.C)	Invitrogen, Karlsruhe, Germany
---	--------------------------------

## MATERIALS

### 2.3. Primers

Table 1: Genes and dedicated primer sequences.

Gene	Use	FWD: 5' → 3'	RV: 5' → 3'
<i>ACTB</i>	qRT-PCR	CCGAGGACTTGTATTGCACATT	AAGTGGGGTGGCTTTAGGAT
<i>ACTB</i>	qRT-PCR, ChIP	GCCAACGCCAAAACCTCTCC	CAGTGCAGCATTTTTACCCC
<i>BCORL1</i>	qRT-PCR	GGGCCAACGTGAACGTCA	CCCATAGGACAGCAGGAGCC
<i>BCORL1</i> (431-1360)	PCR, sequencing	AGTGCTACAGAAAAACTGGGC	TGTAGGGCTGGAGTAAAGATG
<i>BCORL1</i> (484-1628)	PCR, sequencing	GCCAAAATGGACTACGCTG	CGTAAGAGTGGAGGAAACCC
<i>BCORL1</i> (764-1699)	PCR, sequencing	CCCCTGGTTACCACTAACTCA	CACAGAAAATGCATACGGTAA
<i>BCORL1</i> (from 951)	sequencing	TAGCACCTGTCCCGGCTC	
<i>CDCP1</i>	qRT-PCR	AGTAGCAACCTCACCTGAC	GTGGTCTGTGCAGCTTATGG
<i>CDH1</i>	qRT-PCR	CGAGAGCTACACGTTACGG	TTGTCGACCGGTGCAATCT
<i>CDH1</i>	qRT-PCR, ChIP	CGAGAGCTACACGTTACGG	TTGTCGACCGGTGCAATCT
<i>CDH26</i>	qRT-PCR	ACCGAGGGAGTTAAGGATCT	GCTAAAGGGCTGCCATAA
<i>CDH3</i>	qRT-PCR	ATCATCCGACACCCATGTA	TCTCTCCCTCCCTCAATTA
<i>CDH4</i>	qRT-PCR	CCTGAACGCCATACATCA	TTGGGCATAGTCACCGTTCA
<i>CDKN2B</i>	qRT-PCR	AGCTGAGCCCAGGTCTCTAG	CACCGTTGGCGTAAACTAAC
<i>EHF</i>	qRT-PCR	ACCAAAAGCACAACCCGAG	ATCCTGGTTCTGTCTGGG
<i>EPCAM</i>	qRT-PCR	ATCGTCAATGCCAGTGTACTTCA	TGAGCCATTCACTGCCT
<i>ESRP1</i>	qRT-PCR	CGAAATGGTTATCCCCACC	GCTGGAAATGGCAGCTTCT
<i>GAPDH</i>	qRT-PCR	GGCACCGTCAAGGCTGAG	CCCACTTGATTTGGAGGGAT
<i>GAPDH</i>	qRT-PCR, ChIP	GAGAGAGCCGCTGGTGCAC	GAGGTTCTGCACGGAAGGTC
<i>HHIP</i>	qRT-PCR	CAGAACTGAAAATGTGAGCCA	ATCAAGAATACCTGCCCTGGTC
<i>HHIP</i>	qRT-PCR, ChIP	TTCCCACCTCCTACGGCC	TCCTCTCTCCCTCCCCGCTT
<i>IFGBP3</i>	qRT-PCR, ChIP	GCTCCCTGAGACCCAAATGTAA	GCTGGCATTCTGTGTAC
<i>JAG2</i>	qRT-PCR	TGCATCTGTGACAGTGGCTTA	TGCATGTGCCCTATTG
<i>Li3-1 (BCORL1)</i>	Sequencing		CCTGTTGCTCATTTGGGTGT
<i>Li3-2 (BCORL1)</i>	Sequencing		AACCTGGAATGCATCTGGAAC
<i>Li3-4 (BCORL1)</i>	Sequencing	TAGCACCTGTCCCGGCTC	
<i>Li3-5 (BCORL1)</i>	Sequencing		ACAGGGAGCGTAAGAGTGGAG
<i>Li3-6 (BCORL1)</i>	Sequencing		AGGTATCTGCCAAAGGCC
<i>Li3-7 (BCORL1)</i>	Sequencing	TTCCCTCACTCTTACGCTCC	
<i>Li3-8 (BCORL1)</i>	Sequencing	ATCTGTCCTCCAAGTCCAACC	
<i>Li3-10 (BCORL1)</i>	Sequencing	GAAACGATATACTCCAGCCCC	
<i>Li3-11 (BCORL1)</i>	Sequencing	GTGCCAAACCAAGGAACCTC	
<i>Li3-13 (BCORL1)</i>	Sequencing	GCAGGAGACACGAAGCCTAAG	
<i>KRT19</i>	qRT-PCR	GCCACTACTACACGACCATCCA	AGCCAGACGGCATGGTC
<i>MFAP4</i>	qRT-PCR	GGACTCATAGCATGGGGAA	CCAGGAGTGCAGTTCAAG
<i>NANOG</i>	qRT-PCR	AGAACTCTAACATCCTGAACCT	TCGGCCAGTTGTTCTGC
<i>NOXA</i>	qRT-PCR	CGCGCAAGAACGCTAAC	CCGGAAGTTCAGTTGCTCCA
<i>NR2E1</i>	qRT-PCR	ACTGGGTTCCCTTAGGCT	ATCTAAAATGCGGCCCTCTG
<i>OCT4</i>	qRT-PCR	CACTGCAGCAGATCAGCCA	GCTTGATCGCTGCCCTTC
<i>PCDH19</i>	qRT-PCR	GCCCATTAAATCAAGAGCAGC	TGTTCAGCACATCGTTGACA
<i>PCDHA1</i>	qRT-PCR	TCCAAGTCTAACACGTCAGAA	GGCTGTCGTGGATTACCAAG
<i>PCDHAC2</i>	qRT-PCR	CAGGAATCTCACAGGCCAAAG	GGCTGTCGTGGCTATT
<i>SFPR1</i>	qRT-PCR, ChIP	ACGCCGTGATCCATTCCC	CGGCTCAACACCCCTAAAAAA
<i>SFRP1</i>	qRT-PCR	CATGACGCCGCCAAT	GATGGCCTCAGATTCAACTCG
<i>TIMP2</i>	qRT-PCR	CTCATTGCAGGAAAGGCCG	CTCTTCTCTGGGTGGTGCT
<i>U6</i>	Sequencing	GAGGGCCTATTCCATGATTCC	

## MATERIALS

### 2.4. Antibiotics

---

Kanamycin (50 µg /ml)	Sigma, Steinheim, Germany
Ampicillin (100 µg /ml)	Sigma, Steinheim, Germany
Puromycin (10 mg/ml)	Sigma, Steinheim, Germany

### 2.5. Plasmids

---

pTER <sup>+</sup>	provided by Prof. Dr. Westermann
pEGFP-N1	Clontech, Mountain View, CA, USA
pEGFP-BCORL1	provided by Dr. Khanna
pEGFP-BCORL1 <sup>T6</sup>	provided by Dr. Beck
eSPCas9 (1.1)-2a-Puro	provided by Prof. Dr. Schnurr

### 2.6. Short-hairpin RNAs (shRNAs)

---

Self-designed Oligonucleotides	Eurofins, Ebersberg, Germany
	5'-GATCCCCGTGGCAGAGGCTGAGGGCTTCAAGAGAGGCCCTCAGCCTCTGCCACGTTTGGAAA-3'
	5'-AGCTTTCCAAAAACGTGGCAGAGGCTGAGGGCTCTTGAAGCCCTCAGCCTCTGCCACGGG-3'

### 2.7. Guide RNAs (gRNAs)

---

Self-designed Oligonucleotides	Eurofins, Ebersberg, Germany
Oligo 1:	5'-CACCGGAGGCAGGGATATATACCAAG-3' 5'-AAACCTGGTATATATCCGCCTCC-3'
Oligo 2:	5'-CACCGTCCAAAGCCTTACTCCGG-3' 5'-AAACCCGGAGTAAAGGCTTGGAC-3'

### 2.8. Antibodies

---

#### 2.8.1. Primary Antibodies

---

Anti-Histone H3 antibody (#2897200)	Millipore, Darmstadt, Germany
Anti-Histone H3K4me3 antibody (ab8580)	Abcam, Cambridge, UK
Anti-Histone H3K27me3 antibody (ab6002)	Abcam, Cambridge, UK
Anti-RNA polymerase II antibody (ab817)	Abcam, Cambridge, UK
Normal mouse IgG antibody (sc-2025)	Santa Cruz, Heidelberg, Germany
Rabbit anti-human β-actin (# 4970)	Cell signaling technology, Danvers, USA

## MATERIALS

Rabbit anti-BCORL1 (Ap50363PU-N)	Acris Antibodies, Herford, Germany
Rabbit anti-BCORL1 (PA5-24333)	Thermo Scientific, Wilmington, USA
Rat anti-BCORL1 (various supernatants)	Helmholtz center, Munich, Germany
Rabbit anti-CDH1 (#3195)	Cell signaling technology, Danvers, USA
Rabbit anti-GFP (NB600-308)	Novus, Wiesbaden, Germany
Rabbit anti-KRT19 (#HPA002465)	Sigma-Aldrich, Steinheim, Germany
Rabbit IgG, polyclonal - Isotype Control (ab37415)	Abcam, Cambridge, UK
Rat (IgG2a) anti-GFP 3H9	Helmholtz center, Munich, Germany

### 2.8.2. Secondary Antibodies

Horseradish peroxidase-conjugated goat anti-rabbit immunoglobulins (P0488)	DakoCytomation, Hamburg, Germany
Horseradish peroxidase-conjugated goat anti-mouse immunoglobulins (P0488)	DakoCytomation, Hamburg, Germany
Goat-Anti Rabbit (H+L) AlexaFluor 555	Thermo Scientific, Wilmington, USA
Goat-Anti Rat (H+L) AlexaFluor 555	Thermo Scientific, Wilmington, USA
Mouse-Anti Rat IgG2a/IgG2b/IgG2c/IgG1-HRP	Helmholtz center, Munich, Germany

### 2.9. Chemicals/Reagents

6x orange DNA Loading Dye	Thermo Scientific, Wilmington, USA
Acetic Acid	Carl Roth, Karlsruhe, Germany
Agarose	VWR, Munich, Germany
Albumin Fraction V (BSA)	Carl Roth, Karlsruhe, Germany
β-Mercaptoethanol	Sigma-Aldrich, Steinheim, Germany
Bio Rad Protein Assay	Bio-Rad, Munich, Germany
Boric acid	Carl Roth, Karlsruhe, Germany
Bromophenolblue	SERVA, Heidelberg, Germany
CaCl <sub>2</sub>	Calbiochem, San Diego, USA
Chloroform	Carl Roth, Karlsruhe, Germany

## MATERIALS

cOmplete Protease Inhibitor Cocktail Tablets (PI)	Roche, Mannheim, Germany
Crystal violet	Sigma-Aldrich, Steinheim, Germany
ddH <sub>2</sub> O	Invitrogen, Karlsruhe, Germany
dNTPs	Roche, Mannheim, Germany
Dimethyl sulfoxide (DMSO)	Merck, Darmstadt, Germany
Disodium hydrogen phosphate	Merck, Darmstadt, Germany
Dithiothreitol (DTT) (0.1 M)	Invitrogen, Karlsruhe, Germany
Ethylenediaminetetraacetic acid (EDTA)	Carl Roth, Karlsruhe, Germany
Ethanol, absolut	Merck, Darmstadt, Germany
Ethidium bromide (EtBr), 10 mg /ml	Sigma, Steinheim, Germany
Formaldehyde 37 %	Merck, Darmstadt, Germany
Glycerol	Applichem, Darmstadt, Germany
Glycine	Carl Roth, Karlsruhe, Germany
HCl	Carl Roth, Karlsruhe, Germany
HEPES	Applichem, Darmstadt, Germany
Isopropyl alcohol	Sigma-Aldrich, Steinheim, Germany
IGEPAL CA-630	Sigma-Aldrich, Steinheim, Germany
Potassium chloride	Carl Roth, Karlsruhe, Germany
Lithium chloride	Carl Roth, Karlsruhe, Germany
Magnesium chloride	Carl Roth, Karlsruhe, Germany
Methanol	Merck, Darmstadt, Germany
MG-132 proteasome inhibitor	Sigma-Aldrich, Steinheim, Germany
Nonidet P-40	Roche, Basel, Switzerland
Paraformaldehyde	Carl Roth, Karlsruhe, Germany
Phenol	Carl Roth, Karlsruhe, Germany
Phosphate buffered saline (PBS)	Invitrogen, Karlsruhe, Germany
PIPES	Sigma-Aldrich, Steinheim, Germany

## MATERIALS

Potassium chloride	Merck, Darmstadt, Germany
Potassium dihydrogen orthophosphate	Merck, Darmstadt, Germany
Powdered milk	Carl Roth, Karlsruhe, Germany
Propidium iodide	Sigma-Aldrich, Steinheim, Germany
Sodium acetate	Carl Roth, Karlsruhe, Germany
Sodium chloride	Carl Roth, Karlsruhe, Germany
Sodiumdeoxycholate	Carl Roth, Karlsruhe, Germany
Sodium dodecyl sulfate (SDS)	Biomedicals, Eschwege, Germany
Thiazolyl Blue tetrazolium (MTT1)	Sigma-Aldrich, Steinheim, Germany
TRI Reagent® RNA Isolation Reagent	Sigma-Aldrich, Steinheim, Germany
Tris (hydroxymethyl) aminomethane	Carl Roth, Karlsruhe, Germany
Triton X-100	Sigma-Aldrich, Steinheim, Germany
Tween 20	Sigma-Aldrich, Steinheim, Germany
Ultra Pure™ DNase/RNase-Free Distilled water	Invitrogen, Karlsruhe, Germany
Vectashield® Mounting Medium with DAPI	Vector Laboratories Inc., Burlingame, USA

### 2.10. Buffers and Solutions

Buffers and solutions were prepared in dH<sub>2</sub>O, autoclaved if needed and pH adjusted with NaOH or HCl.

#### 2.10.1. Cloning

Buffer R	Thermo Scientific, Wilmington, USA
5 x TBE Buffer, pH 8.0:	445 mM Tris
	445 mM Boric acid
	10 mM EDTA

#### 2.10.2. Proliferation assay

MTT1:	0.5 % Thiazolyl Blue tetrazolium in DPBS
MTT2 stock solution:	4.15 ml 37 % HCl 45.85 ml dH <sub>2</sub> O
MTT2 working solution:	500 µl Stock solution 49.5 ml 10 % SDS

## MATERIALS

### 2.10.3. Western Blot

---

5 x SDS Buffer:	312.5 mM Tris-HCl (pH 6.8) 50 % Glycerol 5 % SDS 5 % $\beta$ -Mercaptoethanol 0.05% Bromophenol blue
Cell Lysis Buffer:	50 mM Hepes 1 mM EDTA 0.7 % DOC 1 % NP40 0.5 M LiCl
PBS-T:	50 % PBS (2 x) 0.1 % Tween 20
Running Buffer:	10 % Novex™ Tris-Glycine SDS Running Buffer (10X), Thermo Scientific, Wilmington, USA
Transfer Buffer:	25 mM Tris 192 mM Glycine (pH 8.3) 20 % Methanol

### 2.10.4. Immunoprecipitation

---

Lysis Buffer/ Wash Buffer 1:	50 mM Tris-HCl (pH 7.5) 150 mM NaCl 1 % NP40 0.1 % SDS 0.5 % DOC 1 $\mu$ M MG-132 proteasome inhibitor
Wash Buffer 2:	50 mM Tris-HCl (pH 7.5) 500 mM NaCl 0.1 % NP40 0.1 % SDS 0.05 % DOC
Wash Buffer 3:	50 mM Tris-HCl (pH 7.5) 0.1 % NP40 0.05 % DOC

## MATERIALS

### 2.10.5. ChIP

---

Cell Lysis Buffer:	5 mM PIPES (pH 8.0) 85 mM KCl 0.5 % Nonidet P-40 (NP40)
Mnase Digestion Buffer (pH 8):	50 mM Tris-HCl 5 mM CaCl <sub>2</sub>
Nuclei Lysis Buffer:	1 % SDS 10 mM EDTA 50 mM Tris-HCl (pH 8.1)
ChIP Dilution Buffer:	0.01 % SDS 1 % Triton X-100 1.2 mM EDTA 16.7 mM Tris-HCl (pH 8.1) 167 mM NaCl
High Salt Wash Buffer:	0.1 % SDS 1 % Triton X-100 2 mM EDTA 20 mM Tris-HCl (pH 8.1) 500 mM NaCl
Low Salt Wash Buffer:	0.1 % SDS 1 % Triton X-100 2 mM EDTA 20 mM Tris-HCl (pH 8.1) 150 mM NaCl
LiCl Wash Buffer:	250 mM LiCl 1 % NP40 1 % Sodiumdeoxycholate (DOC) 1 mM EDTA 10 mM Tris-HCl (pH 8.1)
TE Buffer:	10 mM Tris-HCl (pH 7.8) 1 mM EDTA

## MATERIALS

### 2.10.6. Immunocytochemistry

---

IF-Buffer: 3 % BSA

10 % FCS

DPBS

### 2.11. Molecular Size Markers

---

Gene Ruler™ 100 bp DNA Ladder	Thermo Scientific, Wilmington, USA
Gene Ruler™ 1 kb DNA Ladder	Thermo Scientific, Wilmington, USA
Page Ruler™ Prestained Protein Ladder	Thermo Scientific, Wilmington, USA
Spectra™ Multicolor Broad Range Protein Ladder	Thermo Scientific, Wilmington, USA

### 2.12. Enzymes

---

Bgl II	Fermentas GmbH, St. Leon-Rot, Germany
Fast Digest <i>Bbs</i> I	New England Biolabs, Ipswich, USA
Hind III	Fermentas GmbH, St. Leon-Rot, Germany
iTaq SYBR Green Supermix with ROX	Bio-Rad, Munich, Germany
Maxima Hot Start Taq DNA – Polymerase	Fermentas, St. Leon-Rot, Germany
Micrococcal Nuclease	Thermo Scientific, Wilmington, USA
Proteinase K, 10 mg/ml	Sigma-Aldrich, Steinheim, Germany
Plasmid Safe buffer	New England Biolabs, Ipswich, USA
Plasmid Safe Endonuclease	New England Biolabs, Ipswich, USA
Q5 Hot Start High-Fidelity DNA - Polymerase	New England BioLabs, Ipswich, USA
RNase A	QIAGEN GmbH, Hilden, Germany
Super Script™ II Reverse Transcriptase	Invitrogen, Karlsruhe, Germany
T4 DNA Ligase	Fermentas, St. Leon-Rot, Germany
T4 polynucleotide kinase (PNK)	New England Biolabs, Ipswich, USA

### 2.13. Kits

---

QIAquick PCR Purification Kit	QIAGEN GmbH, Hilden, Germany
QIAquick Gel Extraction Kit	QIAGEN GmbH, Hilden, Germany
QIAprep Spin Miniprep Kit	QIAGEN GmbH, Hilden, Germany

## MATERIALS

### 2.14. Consumables

---

BD Falcon™ Round-Bottom Tubes	BD, Heidelberg, Germany
Biosphere® Filtertips	Sarstedt AG & Co., Nümbrecht, Germany
Pipette tips (10 µl, 100 µl, 1000 µl)	Sarstedt, Nümbrecht, Germany
8-Well PCR stripes	Eppendorf, Hamburg, Germany
PCR 96 Well Plates	PeQLab, Erlangen, Germany
Novex™Wedge Well™ 4 - 12 % Tris-Glycine Gel	Invitrogen, Karlsruhe, Germany
Safe-lock Eppendorf tube (1.5 ml, 2 ml)	Eppendorf, Hamburg, Germany
Trans-Blot®Turbo™ Mini PVDF Transfer Packs	Biorad, Munich, Germany
ibiTreat µ-Plate 96 Well Black	ibidi, Munich, Germany

### 2.15. Equipment

---

XCell SureLock™ Mini-Cell	Invitrogen, Karlsruhe, Germany
Biofuge fresco, Heraeus	Kendro, Langenselbold, Germany
Biofuge pico, Heraeus	Kendro, Langenselbold, Germany
Camera AxioCam MRM	Zeiss, Jena, Germany
Camera Power Shot G6	Canon, Krefeld, Germany
Cell screen Olympus IX50	Innovatis, Bielefeld, Germany
Centrifuge 5702	Eppendorf, Hamburg, Germany
Centrifuge J2-21	Beckman Coulter, Krefeld, Germany
Centrifuge LMC-3000	G. Kisker, Steinfurt, Germany
ChemiDoc XRS+	Biorad, Munich, Germany
CO <sub>2</sub> -Incubator MCO-20AIC	Sanyo, Tokio, Japan
Excella E24 Incubator Shaker Series	New Brunswick Scientific, Enfield, USA
Heat block MR 3001	Heidolph, Kehlheim, Germany
Heatblock „Thermomixer comfort“	Eppendorf, Hamburg, Germany
Homogenizer Micra	ART, Mühlheim, Germany
GelJet Imager Version 2004	Intas, Göttigen, Germany

## MATERIALS

GENios Microplate reader	Tecan, Crailsheim, Germany
Mastercycler RealPlex2	Eppendorf, Hamburg, Germany
Mastercycler personal	Eppendorf, Hamburg, Germany
Microlitercentrifuge MZ014	G. Kisker, Steinfurt, Germany
Microscope Axiovert 40 CFL	Zeiss, Jena, Germany
Microscope Axiovert 135	Zeiss, Jena, Germany
Microtom Leica SM 2000R	Leica, Solms, Germany
Micro scales Te1245	Sartorius, Göttingen, Germany
Microwave	Panasonic, Hamburg, Germany
Minilys	bertin TECHNOLOGIES, France
Mini®-Sub Cell GT	Biorad, Munich, Germany
NanoDrop 1000 instrument	Thermo Scientific, Wilmington, USA
Incubator	Memmert, Schwabach, Germany
pH-Meter inoLab pH720	WTW, Weilheim, Germany
Pipette Accu-Jet	Brand, Wertheim, Germany
PowerPac Basic™	Bio-Rad, Munich, Germany
PyroMark Q24 system	QIAGEN GmbH, Hilden, Germany
PyroMark Q24 Vacuum Workstation	QIAGEN GmbH, Hilden, Germany
Scales Vic-5101	Acculab, Edgewood, USA
Shaker, Rock-N-Roller	G. Kisker, Steinfurt, Germany
Shaker, Unimax 1010	Heidolph, Schwabach, Germany
Suctionsystem „EcoVac“	Schütt, Labortechnik, Göttingen, Germany
Thermal Printer DPU-414	Seiko Instruments, Neu-Isenburg, Germany
Thermomixer Compact	Eppendorf, Hamburg, Germany
Vortexer „Genie2“	Scientific Industries, NY, USA
Water bath GFL 1083	GFL, Wien, Austria
Work flow, Hera Safe	Kendro, Hanau, Germany

## MATERIALS

XCell II™ Blot Module	Invitrogen, Karlsruhe, Germany
XCell SureLockTM Electrophoresis Cell	Invitrogen, Karlsruhe, Germany
Brandon Digital Sonifier® W450	Emerson, St. Louis, USA

## **2.16. Software**

---

CHROMAS v1.45 software	Griffith University, Queensland, Australia
SeqMan NGen, Arraystar, GenVision Pro	DNAstar, Madison, USA
GraphPad Prism 5.0	GraphPad Software, La Jolla, USA
Methyl Primer Express® Software v1.0	Applied Biosystems, Darmstadt, Germany
PyroMark Q24 Advanced Software	QIAGEN GmbH, Hilden, Germany
Realplex	Eppendorf, Hamburg, Germany
AxioVision Release 4.8.2	Zeiss, Oberkochen, Germany

### **3. METHODS**

---

#### **3.1. Patient samples**

---

In order to obtain tumor samples from hepatoblastoma cases, patients undergoing surgery in the department of pediatric surgery of the Dr. von Hauner Children's Hospital in Munich were asked for their consent in participation of the study protocol (Munich, Germany; no. 431-11), approved by the Ludwig-Maximilians-University Ethics Committee. Therefore, written consent was obtained from each patient before taking hepatoblastoma tumor samples along with corresponding liver tissue.

#### **3.2. Polymerase chain reaction (PCR)**

---

For amplification of candidate exons, 50 ng DNA, 2 µl hot start buffer, 500 nM forward and reverse primer, 0.4 µl 10 mM dNTPs, 13.2 µl ddH<sub>2</sub>O, and 1 U Taq-polymerase were mixed and incubated with the following protocol in the Mastercycler personal.

Hot start:	4 min at 94 °C
Denaturation:	40 sec 94 °C
Annealing:	40 sec 59 °C
Extension:	1 min 72 °C
Final extension:	10 min 72 °C
Hold:	4 °C

#### **3.3. RNA extraction**

---

For the extraction of RNA, patient samples as well as different cell lines were used. To extract RNA from cells, the culture medium was exchanged for PBS to wash the cells. Then, cells have been mixed with 1 ml TRI Reagent and transferred to Eppendorf tubes. Tissue samples needed to be cut up first. Then tumor and the corresponding normal liver tissue samples were homogenized with the homogenizer Micra with 1 ml TRI Reagent. Cells and tissue samples were incubated for 5 min at RT. In the next step, 200 µl chloroform have been added to each sample and, after vortexing for 15 s. For phase separation, the samples were then centrifuged for 15 min at 12,000 rpm (4 °C). After transfer of the aqueous phase to a new tube, 1 volume of isopropanol was added and incubated for 1 min at RT. Afterwards, the samples were centrifuged for 15 min at 12,000 rpm (4 °C). To wash the pellet, 1.5 ml of 70 % cooled ethanol were used, followed by centrifugation at 7,500 rpm (4 °C). After air drying of the pellet at RT for 10-15 min, the pellet was dissolved in 20-50 µl DNase/RNase-free water at 55 °C for at least 15 min. The concentration of RNA was quantified using the NanoDrop 1000.

## METHODS

### **3.4. Reverse Transcription**

---

To synthesize cDNA of the extracted RNA, 2 µg RNA were used. Samples were diluted with RNase/DNase-free water to a volume of 7 µl and incubated for 10 min at 70 °C with 5 µl random hexamers (20 ng/µl). Afterwards 4 µl 5x 1<sup>st</sup> strand buffer, 1 µl 10 mM dNTPs, and 2 µl 0.1 M DTT have been added and the mixture was incubated at 25 °C for 10 min. After incubation at 42 °C for 2 min, 1 µl SuperScriptII was added by gently pipetting up and down and incubated at 42 °C for 1 h. To stop the reaction, the mixture was heated for 10 min to 70 °C. Samples were filled up with ddH<sub>2</sub>O to 100 µl.

### **3.5. Quantitative real-time PCR (qRT-PCR)**

---

For qRT-PCR the Master cycler RealPlex2 in combination with the Software Realplex were used for detecting mRNA abundance. The protocol for qRT-PCT was SYBR green based. For one reaction, cDNA corresponding to 40 µg RNA of sample, 10 µl iTaq-SYBR Green-Supermix, 6 µl DNase/RNase-free water (ddH<sub>2</sub>O), 500 nM forward primer, and 500 nM reverse primer were used with the following protocol. The primers, which were used, are listed in Table 1 (p. 22).

SYBR green protocol:	Initial denaturation:	2 min at 95 °C	
	Denaturation:	15 sec at 95 °C	
	Annealing:	15 sec at 58 °C	40-45 cycles
	Extension:	20 sec at 68 °C	

After analyzing the melting curve, relative expression was calculated and normalized to TATA-Box binding Protein (TBP) expression according to the  $\Delta\Delta Ct$  method [176].

### **3.6. Knockdown/knockout of BCORL1**

---

#### **3.6.1. Generation of a short-hairpin RNA vector**

---

To anneal the oligonucleotides, 5 µl annealing buffer, 1 µl oligo sense (100 pmol/µl), 1 µl oligo antisense (100 pmol/µl), and 43 µl ddH<sub>2</sub>O were mixed, boiled at 95 °C for 5 min and slowly cooled down to RT.

1 µg of the pTER<sup>+</sup> plasmid was digested by using the restriction enzymes BamHI and BgIII as indicated by the manufacturer's manual.

For ligation, 1 µl annealed oligos, 50-100 ng digested vector, 2 µl T4 ligase buffer and 1 µl T4 ligase were mixed on ice and filled up to 20 µl with ddH<sub>2</sub>O. After overnight incubation at 16 °C, ligase inactivation was accomplished by 10 min at 65 °C.

## METHODS

### 3.6.2. Generation of a CRISPR-Cas9 vector

Oligonucleotides (Table 2), which recognize the target sequence (Exon 4 of *BCORL1*) and use the Protospacer Adjacent Motif (PAM) of the CRISPR-associated endonuclease 9 (Cas9) are shown in Figure 7 and were designed using the CRISPR design tool [177].

Table 2: Oligonucleotides as guideRNAs (gRNA) to recognize Exon 4 of *BCORL1*, provided by the company Eurofins.

gRNA	Sense	Antisense
1	5'-CACCGGAGGCAGGATATACCAAG-3'	5'-AAACCTGGTATATATCCCGCTCC-3'
2	5'-CACCGTCAAAGCCTTACTCCGG-3'	5'-AAACCCGGAGTAAAGGTTGGAC-3'

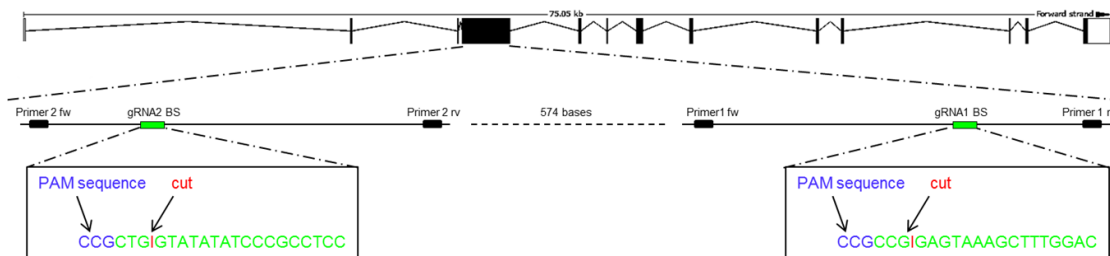


Figure 7: Location of designed gRNAs in the *BCORL1* gene (gRNA BS: guideRNA binding site, PAM: Protospacer Adjacent Motif).

For phosphorylation and annealing of the oligonucleotides, 10  $\mu$ M oligo sense, 10  $\mu$ M oligo antisense, 1  $\mu$ l T4 PNK and 1  $\mu$ l T4 ligase buffer were mixed with 6  $\mu$ l ddH<sub>2</sub>O incubated in the Master cycler personal for 30 min at 37 °C, for 5 min 95 °C, then ramping down at 5 °C per min to 25 °C. To clone the annealed gRNAs into the eSPCas9 (1.1)-2a-Puro plasmid, the gRNAs were diluted 1:200. 2  $\mu$ l of this dilution, 100 ng plasmid, 2  $\mu$ l 10x Tango buffer, 0.5 mM ATP, 0.5 mM DTT, 0.5  $\mu$ l T4 ligase and 1  $\mu$ l FastDigest *Bbs*I were added up with ddH<sub>2</sub>O to 20  $\mu$ l. For ligation, this mixture was incubated for 5 min at 37 °C and for 5 min at 21 °C in 1-6 cycles. Afterwards, 11  $\mu$ l of ligation reaction were digested with 1 mM ATP, 1.5  $\mu$ l 10x PlasmidSafe buffer, and 1  $\mu$ l PlasmidSafe exonuclease for 30 min at 37 °C, followed by 30 min at 70 °C, to get rid of any residual linearized DNA.

For plasmid propagation DH5 $\alpha$  were used as described below. For sequence validation, the plasmid had been Sanger sequenced by using a forward primer for the U6 promoter. For functional validation, different liver tumor cell lines were transfected with the plasmid and put under puromycin selection (100  $\mu$ g/ml) for 3 days. To establish single clones, one cell per well was seeded out in a 96-well plate and grown until DNA extraction was possible. DNA was extracted using phenol-chloroform-extraction and thus, used to perform a PCR of exon 4 of the *BCORL1* gene (primers *BCORL1* (484-1628), table 1). The PCR product had been extracted using the Qiagen Gel extraction kit and Sanger sequenced for mutation analysis by using the primers for *BCORL1* (764-1699) (see Table 1).

### **3.7. Plasmid propagation**

---

#### **3.7.1. Transformation of DH5 $\alpha$**

One aliquot of 50  $\mu$ l DH5 $\alpha$  was thawed on ice for each ligation or plasmid. After adding either 2-20  $\mu$ l of ligation or 5 ng of plasmid, the DH5 $\alpha$  were cooled on ice for 30 min. After a 40 s heat shock at 42 °C, the mixture was incubated two more min on ice. Then 250  $\mu$ l of S.O.C. medium had been added to the DH5 $\alpha$  and incubated at 37 °C for a minimum of 1 h with shaking at 350 rpm. When grown enough, 50 to 100  $\mu$ l of bacteria have been plated on an agar dish.

#### **3.7.2. Colony picking and MiniPrep**

---

One colony per sample was picked from the agar dish and incubated shaking at 37 °C overnight with 10 ml LB medium. The plasmid preparation was done according to the Qiagen MiniPrep manual.

### **3.8. Cell culture**

---

#### **3.8.1. Thawing of cells**

To thaw cells, an aliquot was taken from liquid nitrogen and thawed fast in a water bath (37 °C). Then cells were transferred to falcons with pre-warmed medium. After centrifugation for 5 min at 1,200 rpm, the cell pellet was resuspended in 5 ml medium, transferred to T25 cell culture flasks and incubated at 37 °C.

#### **3.8.2. Passaging of cells**

---

After three days, medium was discarded and cells were washed with PBS. To detach the cells, an incubation with 1 ml Trypsin/EDTA for 1 min at 37 °C followed. The reaction was stopped by adding 3-4 ml medium (10 % FCS and 1 % P/S in RPMI 1640). After gently mixing the cell suspension to detach them from each other, part of the suspension was diluted and transferred to a new flask. The cell suspension was then incubated until further use at 37 °C.

#### **3.8.3. Freezing of cells**

---

The remaining cell suspension from passaging was transferred to a falcon and centrifuged by 1,200 rpm. After resuspending the cell pellet in 0.5 ml DMEM, 5 to 10 ml ice cold freezing medium (12.5 % DMSO and 50 % FCS in DMEM) were added dropwise and the suspension was transferred to cryotubes. These were incubated for 1 to 3 days at -80 °C before moving them to the liquid nitrogen tank.

#### **3.8.4. Transient/stable transfection of cells**

---

Based on the FuGene manufacturer's manual, cells were transfected with the pEGFP-N1 vector as a positive control and with a pEGFP-BCORL1 construct. To obtain stably transfected cells, a pool of transfected cells was propagated under G418 selection and selected by fluorescence-activated cell

## METHODS

sorting (FACS) for high expression of EGFP. This process has been done twice to exclude remaining non-transfected cells.

### **3.9. Phenol-Chloroform extraction of DNA**

---

After passaging, the remaining cell suspension was used for DNA extraction. Thus, the suspension was centrifuged for 5 min at 2,000 rpm, then the pellet was washed with PBS. After resuspending the pellet in 500  $\mu$ l STE buffer, incubation with 30  $\mu$ l proteinase K (10 mg/ml) shaking overnight at 55 °C followed.

The next day, 1 volume phenol was added, after mixing, the emulsion was centrifuged at 3,000 rpm for 10 min. The upper phase was moved to a new Eppendorf tube with 1 volume chloroform, mixed and centrifuged again. Again, the upper phase was transferred to another tube and mixed with 2.5 volumes 100 % ethanol. This was followed by an incubation for 10 min at -20 °C for DNA precipitation. After centrifuging the mixture at 12,000 rpm for 10 min, the supernatant was discarded, the pellet was washed with 70 % ethanol and air dried. Finally, the DNA pellet was dissolved for 15 min in 30  $\mu$ l ddH<sub>2</sub>O at 50 °C and quantified with the Nanodrop1000.

### **3.10. Proliferation assay**

---

Depending on the cell line, between 2,000 and 5,000 cells per well were seeded a 96-well plate and incubated with 10  $\mu$ l MTT1 per well at different time points (0 h, 48 h, 96 h, 144 h, 192 h, 240 h). After 4 hours, 100  $\mu$ l MTT2 was added to each well to lyse cells. The next morning, absorbance was measured with the GENios Microplate reader at 592 nm.

### **3.11. Clonogenicity assay**

---

To assess the clonogenicity of the different cell types, between 1,000 and 5,000 cells were seeded per 6-well. After 8 to 10 days, the cells were washed with cold PBS and fixed with methanol for 5 min. Staining was done by a 15 min incubation with a 0.5 % crystal violet solution. Afterwards, the number of colonies was counted and the percentage of colony forming units was calculated by dividing the counted cell number by the seeded cell number.

### **3.12. Immunocytochemistry**

---

For fluorescent labeling of different protein, 10,000 cells per well were seeded in an ibiTreat  $\mu$ -Plate (96 wells). After adhesion of cells to the surface, cells were washed two times with DPBS and then fixed for 20 min at RT with 100  $\mu$ l of 3.7 % formaldehyde in DPBS. To stop this process, the formaldehyde solution was exchanged with 100  $\mu$ l of 0.1 M glycine in DPBS and incubated at RT for 10 min. After this step, the fixed cells could remain in DBPS in the dark at 4 °C until further use.

For fluorescent labeling, the next step was permeabilization, which was done by adding 100  $\mu$ l 0.5 % triton X-100 in DPBS for 10 min at RT. In the next step, the cells were washed twice with DPBS and

## METHODS

subsequently blocked with IF-buffer at RT for 30 min. After washing twice with DPBS, 60 µl of the primary antibody solution was added (1:150-1:200 for established antibodies, 1:2 for test serums) for overnight incubation at 4 °C in the dark.

To remove non-bound first antibody, two washes with DPBS followed. Then 60 µl of secondary antibody were added for 45 min at RT. Following this, the cells were again washed with DPBS and incubated with a few drops of Vectashield Mounting Medium, containing DAPI overnight at RT in the dark.

Storage of fluorescent-labeled cells continued at 4 °C in the dark until further use. For imaging and analysis of the fluorescent-labeled cells, the microscope Zeiss Axiovert 200M and the AxioVision software was used.

### **3.13. Immunodetection of proteins/Western Blot**

---

#### **3.13.1. Protein extraction**

---

Tissue samples were sliced into small pieces with a clean razor blade and supplemented with 500 µl lysis buffer supplemented with protease inhibitors. This mixture was homogenized using the Minilys homogenizer for 5 x 30 s with breaks on ice in between. After lysis for 20 min on ice and vortexing multiple times, the mixture was centrifuged for 30 min at 13,000 x g and 4° C. Presenting the whole cell lysate, the supernatant was then transferred to a new tube.

For cell line samples, cells were washed with and scraped into 1 ml PBS. This suspension was transferred to an Eppendorf tube on ice and centrifuged for 5 min at 2,000 rpm and 4 °C. The cell pellet was subsequently resuspended in 400 µl lysis buffer and incubated for 25 min on ice. Before centrifuging for 1 min at 13,000 rpm, 25 µl of 10 % IGEPAL were added and vortexed. The supernatant presents the whole cell lysate, the pellet can be used to generate nuclear extracts.

For nuclear extracts, 75 µl nuclear extraction buffer were used to resuspend the pellet, followed by an 1 h incubation on ice with vortexing every few minutes. Afterwards, the suspension was centrifuged for 10 min at 13,000 rpm and 4° C, leaving the supernatant as the nuclear extract.

Bradford analysis was used to determine protein concentrations of lysates and nuclear extracts. Thus, lysates and extracts were diluted 1:10 in a 96-well plate and incubated with 1:5 diluted Bradford reagent for 15 min at RT. The adsorption was measured with the GENios Microplate reader at 595 nm. To calculate the protein content, a dilution curve with BSA was used.

## METHODS

### **3.13.2. SDS-PAGE and Western blot**

---

25 µg of protein extract were diluted to 20 µl and mixed with 5 x SDS loading buffer. After denaturation at 99 °C for 10 min, the samples were loaded onto a 4-20 % Tris-Glycine SDS gel, which was run with 225 V for 30 min. Subsequently, the gel was blotted onto a PVDF membrane using the Trans-Blot Turbo Transfer System for 10 min at 25 V. The membrane was washed with PBS-T three times for 5 min and then blocked with 5 % milk in PBS-T at room temperature for one hour. Afterwards, the membrane was washed for 15 min with refreshing of the PBS-T and incubated at 4 °C shaking with the primary antibody overnight. The next day, the membrane was washed three times for 15 min and followed by a one-hour incubation with secondary antibody. After washing for 15 min three times, the immunostained proteins were detected by using the ChemiDoc XRS+ system.

### **3.13.3. Antibody establishment**

---

For the BCORL1 protein, new antibodies were generated against different epitopes of the protein and produced in rats by the monoclonal antibody core facility in the Helmholtz center in Munich. The sera of these rats were tested by Western Blot as primary antibody with a 1:10 dilution. The specific secondary antibody was diluted 1:1,000.

### **3.14. Immunoprecipitation (IP)**

---

HEK293 cells have been transiently transfected with pEGFP-BCORL1<sup>WT</sup> or pEGFP-BCORL1<sup>T6</sup> and cultivated for 48 h. Following this, the cells were washed two times with DPBS, scraped of the culture plates with lysis buffer ( $10^6$ - $10^7$  cells/ml) and homogenized five times for 30 s with the Minilys system. In between, the tubes were incubated on ice. The cell suspension was centrifuged at 12,000 x g and 4 °C for 10 min. After transferring the supernatant to a new tube, it was blocked with 50 µl Protein G Agarose at 4 °C on a rotator for 1 h. The blocking agent was removed by centrifugation and transfer of the supernatant to a new tube. The precleared protein lysate was incubated with 10 µl Rat (IgG2a) anti-GFP 3H9 for 4-5 h and then 50 µl Protein G Agarose were added rotating overnight, both at 4 °C. The next day, the coupled protein-antibody-beads mixture was washed by centrifuging and incubation on a rotator in new wash buffer for 20 min. After two washes with the first two wash buffers, followed by a wash with wash buffer 3, 40 µl of SDS-loading dye were added. The suspension was directly denatured by 3 min incubation at 99 °C and centrifuged again for elution. The supernatant was directly used for immunodetection of proteins with the BCORL1 antibody supernatants.

### **3.15. Chromatin Immunoprecipitation (ChIP)**

---

#### **3.15.1. Chromatin preparation**

To perform ChIP with cell lines, around  $20 \times 10^6$  cells were seeded one day prior. For tissue-ChIP, 100-400 µg liver or tumor tissue was cut into tiny pieces on dry ice. Cells, as well as the tissue pieces, were incubated with a RPMI solution, containing 10 % FCS, 1 % P/S, and 1 % formaldehyde at RT for 15 min while shaking. In order to quench the crosslinking, glycine was added to a final concentration of 125 mM and incubated for 5 min at RT. Cells and tissue pieces were washed twice with pre-chilled PBS and put on ice. The cells were scraped off and collected in 1 ml cell lysis buffer in Eppendorf tubes on ice. The tissue pieces were incubated with 1 ml cell lysis buffer per sample in tubes for the Minilys homogenizer. The samples were homogenized 4 times for 30 s at maximum speed with breaks on ice. After an incubation for 10 min, all the samples were centrifuged at  $0.3 \times g$  and 4 °C for 10 min. The residual supernatant was discarded.

#### **3.15.2. Chromatin shearing**

500 µl Mnase reaction buffer were used to resuspend the chromatin pellet. To shear the chromatin, an incubation at RT with 100 U Mnase followed for 5-15 minutes depending on the cell line. Then EGTA was added to a final concentration of 20 mM and by putting the sample on ice to stop this reaction. After centrifuging at  $0.3 \times g$  (4 °C) for 10 min, the pellet was resuspended in nuclei lysis buffer supplemented with protease inhibitor. Nuclei lysis was accomplished by a 10 min incubation on ice. Afterwards, samples were sonified 3-5 times for 30 s (pulse on 0.8 s, pause 0.2 s) on ice. Subsequently, the sonified samples were centrifuged for 10 min at  $17.0 \times g$  (4 °C). The sheared chromatin in the supernatant was then transferred into a new tube and stored at -20 °C until further use.

#### **3.15.3. Chromatin quality check**

To check the chromatin length, 5 µl chromatin were used to prepare an input control. 200 µl elution buffer, 4 µl 0.5M EDTA, 8 µl 1M Tris-HCl (pH 8), and 1 µl RNase A (10 µg/µl) were incubated with the input control at 37 °C for 15-30 min shaking (650 rpm). To reverse crosslinks, 1 µl proteinase K (10 mg/ml) and 8 µl 5 M NaCl were added overnight at 65 °C shaking (650 rpm). The next day, 500 µl ice-cold 100 % ethanol, 20 µl 3 M NaAc and 1 µl glycogen were supplemented for DNA precipitation for at least 10 min at -20 °C. Afterwards, the input samples were centrifuged for 15 min at 13,300 rpm (4 °C). 70 % ethanol was used to wash the pellet, which was then air-dried. 5 µl DNase/RNase-free water had been used to solve the pellet at 50 °C. To quantify the DNA, the Nanodrop1000 was used. To check the chromatin length, 500 µg DNA were resolved using a 1 % agarose gel containing EtBr at 120 V. When the DNA length was between 600 Mb and 1 kb, the chromatin was blocked with 100 µl Protein G Agarose in dilution buffer containing protease inhibitor to final volume of 2 ml for 1 h shaking

## METHODS

at 4 °C. 100 µg chromatin per antibody were filled up to 1 ml with dilution buffer and incubated with a ChIP-grade antibody overnight at 4 °C shaking.

### 3.15.4. Immunoprecipitation

---

The next day, 60 µl Protein G Agarose were added to each sample for a 4-5 h incubation at 4 °C while shaking. Subsequently, the samples were washed once with low and high salt buffer, once with LiCl buffer and two times with TE buffer at 4 °C for 5 min shaking with centrifugation steps of 1 min at 4.0 x g (4 °C) to pellet the Protein G Agarose. The beads were eluted using a 15 min incubation at 30 °C shaking (1,250 rpm) with 100 µl elution buffer and the antibody-coated Protein G Agarose twice with subsequent centrifugation at 4.0 x g (4 °C) for 1 min and transferring the supernatant to a new tube. The eluted chromatin was digested afterwards with 1 µl RNase A (10 µg/µl), 8 µl 1 M Tris-HCl, and 4 µl 0.5 M EDTA for 30 min at 37 °C. 1 µl proteinase K (10 mg/ml) and 8 µl 5 M NaCl were used to reverse crosslinks overnight at 65 °C shaking (650 rpm). On the following day, the DNA was purified by using the Qiagen PCR purification kit.

### 3.15.5. Evaluation of ChIP

---

To test the ChIP efficiency, a small amount of DNA was used to do a qRT-PCR with a SYBR green based protocol with primers for known active and inactive loci. Samples were sent to the Helmholtz center for library prep and ChIP-sequencing.

## 3.16. Sequencing

---

### 3.16.1. Sanger sequencing

---

Different *BCORL1* exons were amplified by PCR (primers for *BCORL1*, see table 1) and evaluated on a 1 % agarose gel by gel electrophoresis. Using the Qiagen Gel extraction kit, the desired band was extracted and used for sequencing. Sequencing was done with the primers (Li3-1 to Li3-13, see Table 1) in the LMU Sequencing Facility using the ABI BigDye Terminator kit on an ABI 3730 capillary sequencer. The CHROMAS v1.45 software was used to perform the sequence analysis.

### 3.16.2. RNA sequencing

---

3,000 ng of RNA were used to prepare a library with subsequent NGS sequencing by Illumina, performed in the institute of Human Genetics in the Helmholtz center.

### 3.16.3. ChIP sequencing

---

The ChIP DNA was checked for quality and quantity by nanodrop, gel electrophoresis, and bioanalyzer before performing a library preparation with subsequent NGS sequencing by Illumina in the Helmholtz center.

## 4. RESULTS

### 4.1. Genetic investigation

For a better understanding of childhood liver cancers, our lab performed an initial genome wide exome sequencing of 15 hepatoblastoma patient samples, 3 transitional liver cell tumor samples as well as the corresponding normal tissue samples [52]. Besides the most common recurrent mutation in *CTNNB1*, a frameshift mutation in the *BCORL1* gene was identified in case T528. Hence, our lab Sanger sequenced 79 additional HB samples and 5 cell lines for *BCORL1* mutations and found 3 further mutations (Table 3), which sums up to a 5 % mutation rate (performed by Dr. Alexander Beck and Sebastian Sigl).

Table 3: ***BCORL1* mutations in hepatoblastoma samples.**

Case	Mutation	Protein
T6	c.3001_3001delC	p. Q1001Rfs*49
T4	c.3607G>A	p. G1203S
HepT1	c.3765_3767delAGA	p. E1257del
T528	c.4262_4262delA	p. K1421Sfs*29

Two mutations were frameshift mutations. Three of the mutations were located in front of the nuclear location signal (Figure 8).

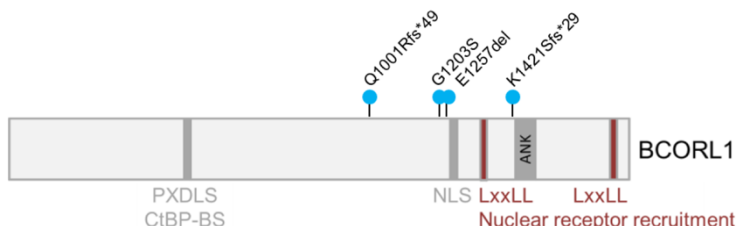


Figure 8: **Mutations in the BCORL1 protein** (CtBP-BS: C-terminal Binding Protein-Binding Site, NLS: Nuclear Location Signal, ANK: Ankyrin repeat, frameshift (fs)).

All these mutations were introduced into the pEGFP-BCORL1 vector by site-directed mutagenesis and expressed in HEK293 cells (performed by Dr. Alexander Beck). Interestingly, only the Q1001Rfs\*49 mutation of case T6 resulted in a loss of function (LOF) mutation that led to BCORL1 exclusion from the nucleus (Figure 9).

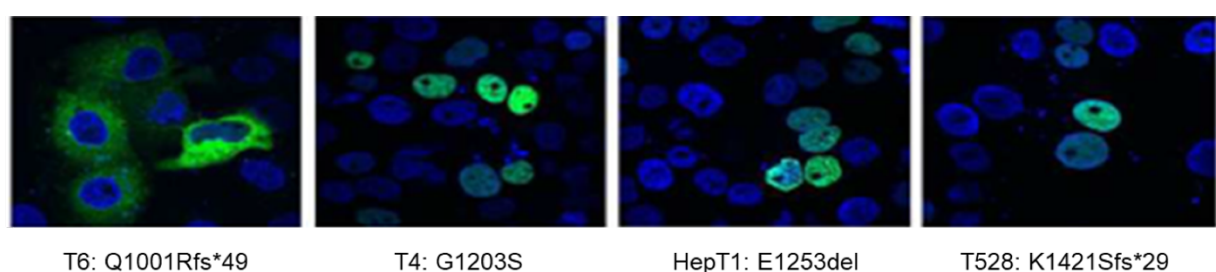


Figure 9: **BCORL1 mutant EGFP-tagged plasmids expressed in HEK293 cells.**

#### 4.2. Protein level

Due to the obvious LOF effect in case T6, we aimed to further investigate this on the protein level. Hence, we examined our hepatoblastoma, TLCT, and HCC cell lines for their *BCORL1* expression by qRT-PCR to identify a high expressing cell line for immunodetection. Expression levels of *BCORL1* vary strongly between the cell lines. The HepT1 cell line, which has a *BCORL1* mutation, exhibited the highest *BCORL1* expression. The second highest expression showed the HUH7 cell line, followed by the normal liver tissue, which we have chosen for comparison. HUH6 and Hep3B cells showed rather low *BCORL1* expression and HepG2 cells exhibited the lowest *BCORL1* expression (Figure 10).

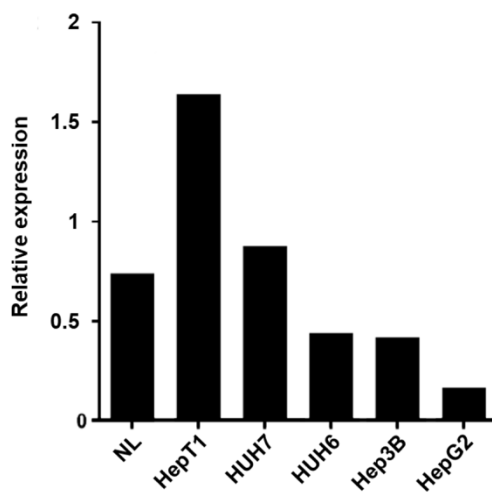


Figure 10: ***BCORL1* expression** relative to *TBP* in normal liver tissue (NL) and the different hepatoblastoma (HepT1 and HUH6), TLCT (HepG2) and HCC (HUH7 and Hep3B) cell lines.

To detect the *BCORL1* protein by immunoblotting, we selected the HUH7 cell line due to the high *BCORL1* expression and their expression of the wildtype *BCORL1* protein. Thus, we probed whole cell lysates with two commercially available antibodies, one from Thermo Scientific and the other from Acris Antibodies. These antibodies revealed multiple bands with molecular weights varying from 15 kDa to 170 kDa. The molecular weight of wildtype *BCORL1* is 189 kDa, but no band of this weight could be detected (Figure 11).

## RESULTS

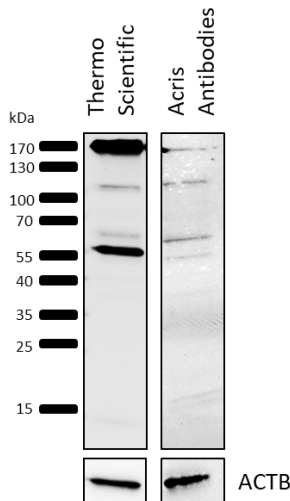


Figure 11: **BCORL1 protein detection.** Whole cell lysates of HUH7 wildtype cells were used for detection of BCORL1 with antibodies from Thermo Scientific (left) and Acris Antibodies (right). As loading control, ACTB was used.

Unfortunately, the commercially available antibodies from Thermo Scientific and Acris Antibodies could not be used for further investigation of the mutated BCORL1 protein due to their inability to detect the wildtype BCORL1. Moreover, both antibodies were not specific enough for further experiments. Thus, our lab decided to order a custom-made antibody for BCORL1 detection that would detect the wildtype version of the protein, as well as the truncated version. Therefore, different antibody epitopes were manufactured for different domains of the BCORL1 protein near the N-terminus in order to detect the wildtype and the truncated BCORL1 protein. The manufacturing was done by the Monoclonal Antibody Core Facility at the Helmholtz Center.

### 4.2.1. Improvement of protein extraction

Prior to testing the supernatants for BCORL1 detection, different lysis buffers were tested to enhance BCORL1 levels in the lysate. This was accomplished by detecting an EGFP-tagged wildtype BCORL1 (estimated size: 216 kDa) with a GFP antibody. Hence, HepG2 O1.1 cells were used to overexpress the EGFP-tagged wildtype BCORL1, because these cells contain no wildtype BCORL1 and are easily transfectable. Thus, unspecific binding of the GFP antibody with the wildtype BCORL1 protein could be ruled out. After visual proof of the overexpression (GFP positivity) by fluorescent microscopy, the cells were incubated with 1  $\mu$ M MG-132 proteasome inhibitor before cell lysis and different lysis buffer compositions were tested. These lysates were used for SDS-PAGE and subsequent immunoblotting. Detection was performed using a GFP antibody (Figure 12). Buffer 1 and 5 exhibited the most intense GFP signal, but in direct comparison, buffer 1 has the more intense GFP to ACTB ratio. Thus, buffer 1 was used for further experiments.

## RESULTS

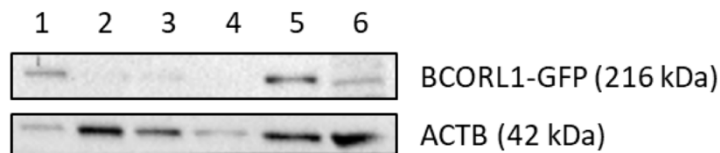
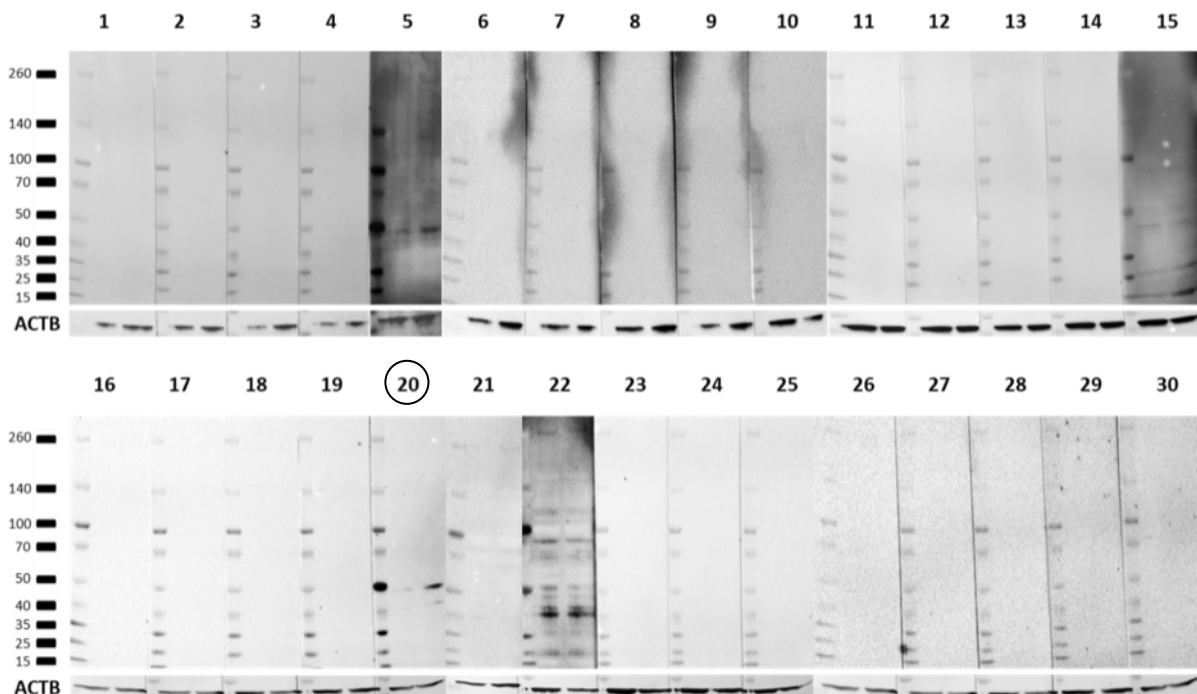


**Figure 12: Testing of different protein extraction methods.** One exemplary immunoblot out of five, showing the detection of protein lysates of HepG2 O1.1 cells transfected with pEGFP-BCORL1<sup>WT</sup> with anti-GFP antibody. Protein lysates were obtained by using different lysis buffers containing a proteinase inhibitor cocktail and 1  $\mu$ M MG-132 (1: 25 mM Tris, 150 mM NaCl, 1 % Triton-X 100, 1 % DOC, 0.1 % SDS; 2: 50 mM Hepes, 1 mM EDTA, 0.7 % DOC, 1 % NP40, 0.5 M LiCl; 3: 10 mM Hepes, 2.5 mM KCl, 0.5 mM MgCl<sub>2</sub>, 1 mM DTT, 0.1 mM EDTA; 4: 20 mM Hepes, 0.42 M NaCl, 1.5 mM MgCl<sub>2</sub>, 1 mM DTT, 0.2 mM EDTA, 25 % Glycerol; 5: 5 mM PIPES, 85 mM KCl, 0.5 % NP40; 6: 1 % SDS, 10 mM EDTA, 50 mM Tris). As loading control, ACTB is shown.

### 4.2.2. BCORL1 antibody screening

For the antibody screening, the cellular supernatants were tested with immunoblotting and immunocytochemistry. For immunoblotting, whole cell lysates of HepG2 (Figure 13) or HUH7 (Figure 14) wildtype, knockout and rescue cells were produced and used for SDS-PAGE with subsequent immunoblotting. These cells contain different versions of the BCORL1 protein. Wildtype cells should show a band with a molecular weight around 189 kDa, whereas the knockout versions both carry a truncated version of approximately 47 kDa. The rescue cells contain the 47 kDa version and additionally the EGFP-tagged BCORL1 of 216 kDa. Seventeen supernatants exhibited a difference in the detection between wildtype and knockout cells. Moreover, these blots did not show bands over the whole blot, so the supernatants were more specific than the rest, which either did not reveal any bands or the blot exhibited bands of all weights, like blot #22 and #68 (Figure 13).



## RESULTS

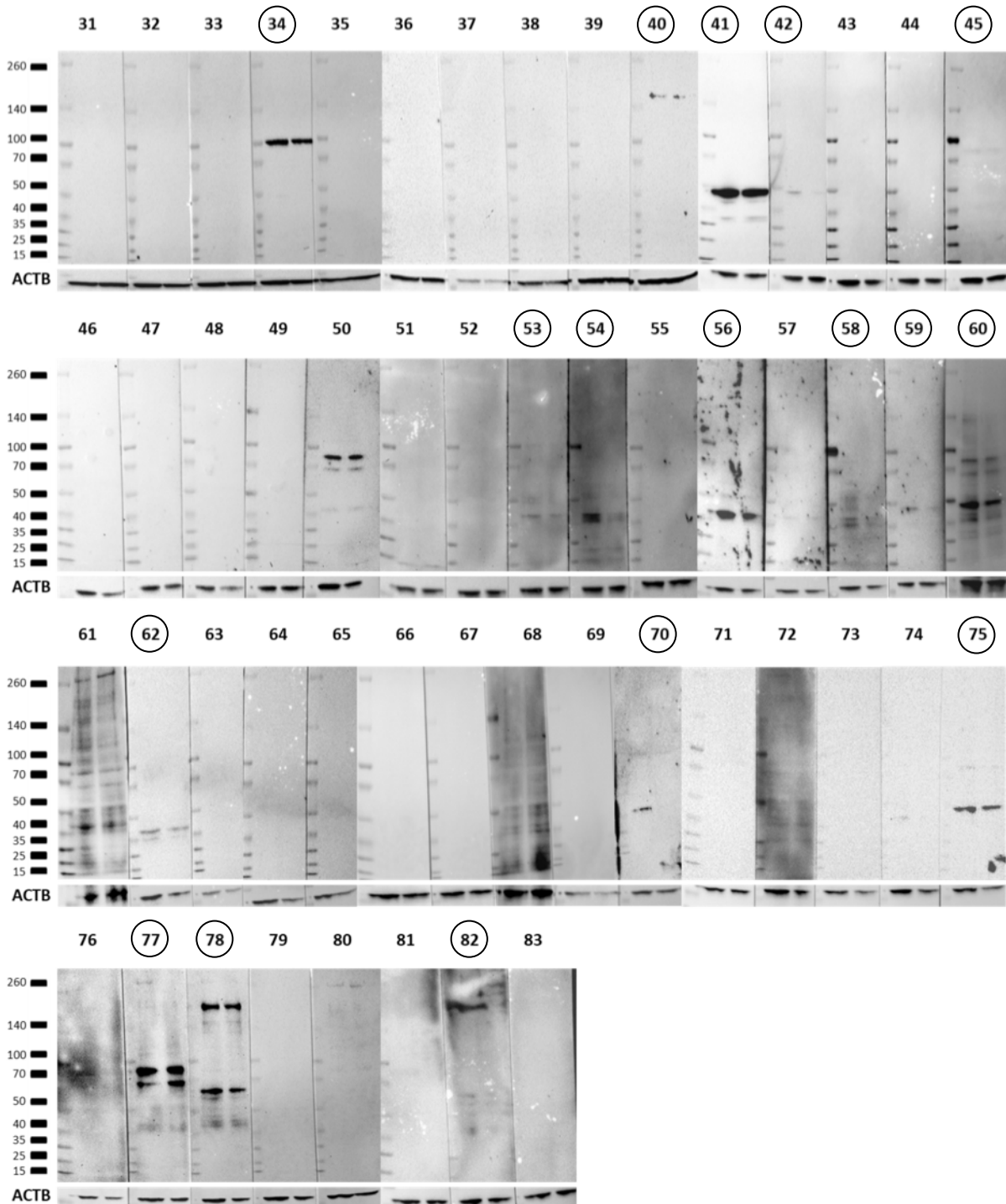


**Figure 13: BCORL1 detection by using supernatants of clone 1-83.** For detection of BCORL1, immunoblotting of whole cell lysates of HepG2 wildtype (left lane) versus HepG2 O1.1 knockout cells (right lane) was performed against supernatants of clone 1-83. ACTB, which has a molecular weight of 42 kDa, was used as loading control. Circled numbers were used for further experiments.

The second batch of supernatants (84-105) was tested on nuclear extracts of HUH7 cells due to their high *BCORL1* expression (Figure 10). From the second batch, only #86 and #103 were chosen for further testing. #86 exhibited a clear difference in bands around the wildtype BCORL1 and showed a faint band in the knockout cells, which had approximately the calculated size of the truncated BCORL1.

## RESULTS

#103 showed a slight difference between the different samples and was therefore further investigated as well (Figure 14).

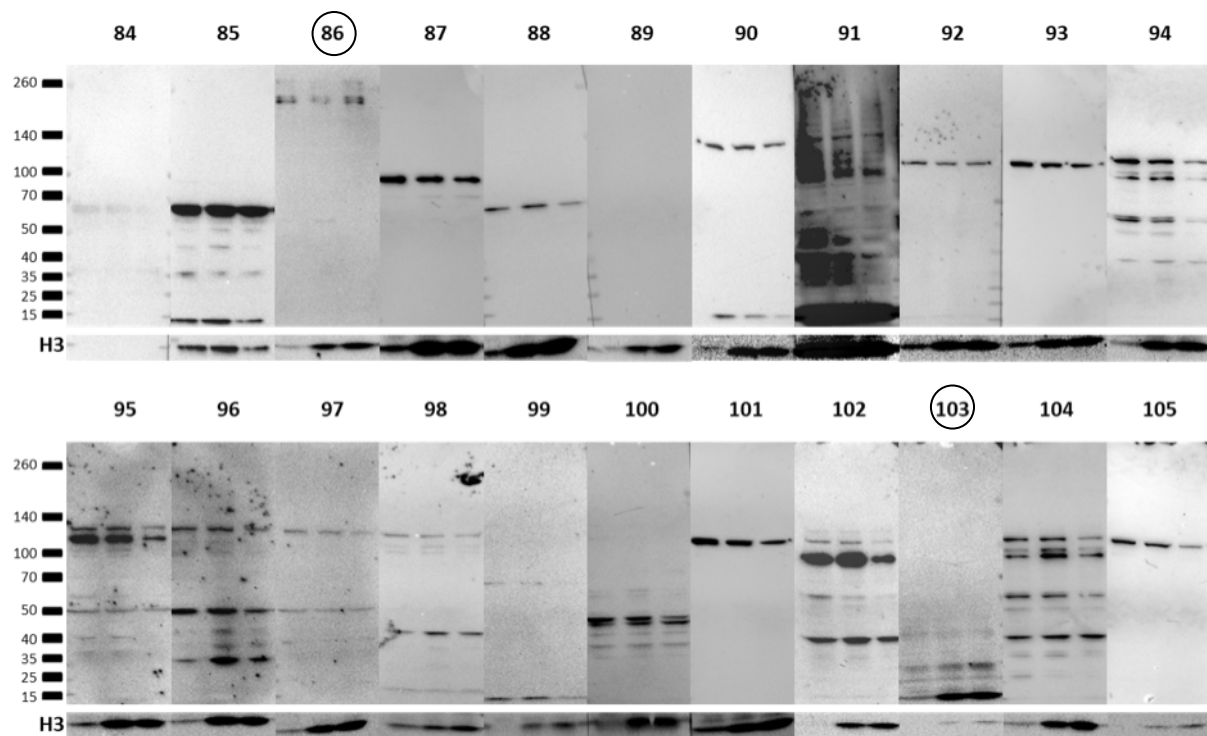


**Figure 14: BCORL1 detection by using supernatants of clone 83-105.** Immunoblotting of whole cell lysates of HUH7 wildtype (left lane), HUH7 O1.1 (middle lane) and HUH7 O1.1 knockout, stably transfected with pEGFP-BCORL1<sup>WT</sup> plasmid against supernatants of clone 83-105. Histone 3, which has a molecular weight of 17 kDa, was used as loading control. Circled numbers were used for further experiments.

Collectively, we identified twenty supernatants as possible candidates to detect BCORL1 protein. In a next step, we examined the ability of the candidate supernatants to detect the truncated BCORL1 by immunofluorescence. We hypothesized that BCORL1 should not be able to translocate to the nucleus due to the missing NLS in BCORL1 knockout cells. As an internal control, HepG2 O1.1 knockout cells were transiently transfected with pEGFP-BCORL1<sup>WT</sup> plasmid and used for immunofluorescent labeling of BCORL1 with the candidate supernatants. For comparison, two commercially available antibodies (Acris Antibodies and Thermo Scientific) were also tested (Figure 15).

As anticipated, pEGFP-BCORL1<sup>WT</sup> transfected cells showed localization of the exogenous EGFP-tagged wildtype BCORL1 protein in the nucleus depicted in green, which was also detected by all candidate supernatants depicted in red (Figure 15). However, non-transfected HepG2 O1.1 cells that showed no green signal and should only show endogenous truncated BCORL1 protein predominantly outside the nucleus was only amenable for eight candidate supernatants as marked in Figure 15.

## RESULTS

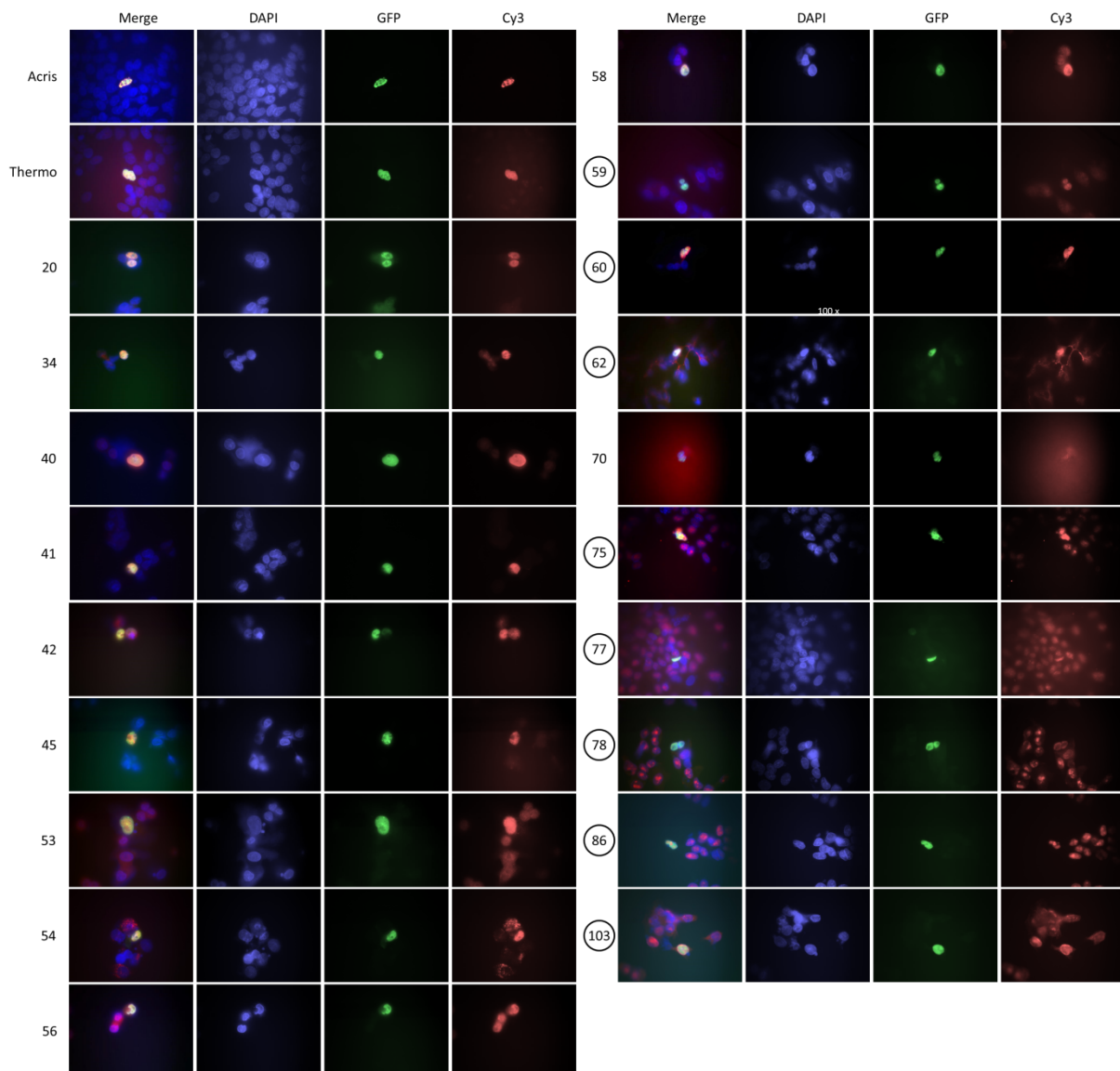


**Figure 15: Fluorescent labeling of HepG2 O1.1 transiently transfected with pEGFP-BCORL1<sup>WT</sup> to detect BCORL1 with candidate supernatants.** DAPI (blue) staining marks nuclei, GFP fluorescence (green) detects cells transfected with pEGFP-BCORL1<sup>WT</sup>. Cy3 (red) shows the BCORL1 labeled by commercially available antibodies from Acris Antibodies and Thermo Scientific or the candidate supernatants. Circled supernatants detected plasmatic truncated BCORL1.

In order to validate detection in a cell line known to express high levels of endogenous BCORL1, HEK293 cells were transfected with pEGFP-BCORL1<sup>WT</sup> or mutant pEGFP-BCORL1<sup>T6</sup>. Figure 16 shows the fluorescent labeling with three antibodies, which marked the BCORL1<sup>WT</sup> predominantly in the nucleus, whereas the truncated version was found in the cytoplasm.

## RESULTS

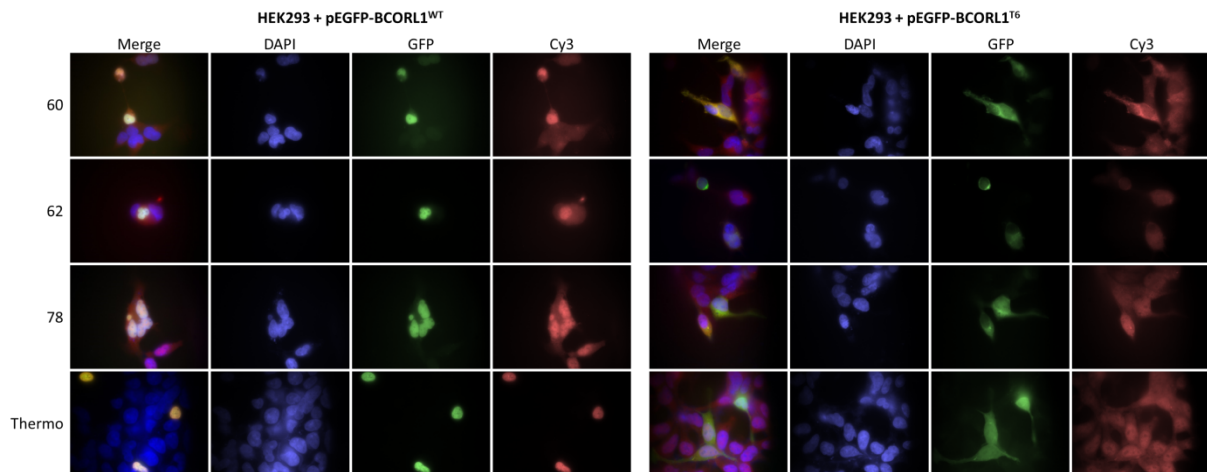


**Figure 16: Fluorescent labeling of HEK293 cells transiently transfected with pEGFP-BCORL1<sup>WT</sup> (left) or pEGFP-BCORL1<sup>T6</sup> (right).** DAPI (blue) staining marks nuclei and the GFP fluorescence detects the transfected cells (green). Cy3 (red) shows BCORL1 labeled by the candidate supernatant or Thermo Scientific antibody.

Since all three supernatants exhibited positive colocalization of the wildtype and truncated EGFP-tagged BCORL1, the following step was to see their performance in an immunoblotting setup with transfected HEK293 cell. Hence, HEK293 cells were transfected with pEGFP-BCORL1<sup>WT</sup> or pEGFP-BCORL1<sup>T6</sup> and were used for preparation of whole cell lysates. These lysates were then used to perform an immunoprecipitation to exclude any unspecific binding of the supernatants to other proteins. The precipitated lysate was then used for SDS-PAGE with subsequent immunoblotting with candidate supernatants. Due to the insufficiency of supernatant #60 and #62 in detection of EGFP-tagged BCORL1, they were removed from the candidate list, which left #78 as the best candidate for production of a BCORL1 antibody (Figure 17).

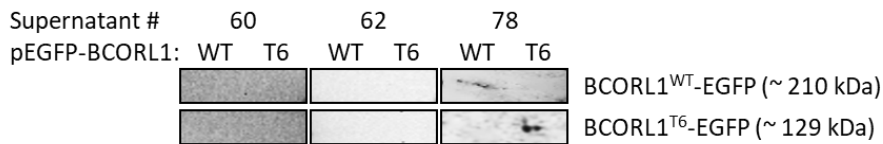


**Figure 17: Immunoblot of immunoprecipitated BCORL1-EGFP from transiently with pEGFP-BCORL1<sup>WT</sup> (left lane) or pEGFP-BCORL1<sup>T6</sup> (right lane) transfected HEK293 cells.** Detection with supernatant #60 (left), #62 (middle) and #78 (left) as primary antibodies.

The use of supernatant #78 not only confirmed that the BCORL1 protein of case T6 is indeed truncated (Figure 17), but also clearly demonstrated that the truncated BCORL1<sup>T6</sup> was not translocated to the nucleus (Figure 16) as predicted due to the loss of the nuclear location signal.

### 4.3. Creation of BCORL1 knockout cells

To further investigate the consequences of *BCORL1* LOF mutation, different approaches of *BCORL1* knockout were evaluated. Due to the fact that the LOF mutation still produces a truncated version of *BCORL1*, siRNA and shRNA based knockdown or knockout would not be able to reflect the patient situation. The existence of the truncated *BCORL1* might have unknown effects. Thus, a CRISPR-Cas9 mediated knockout of *BCORL1* was performed. Therefore, two different guideRNAs (gRNA), targeting the middle and the end of the *BCORL1* gene, were designed (Table 2, Figure 7). We used two different loci to exclude target dependent effects. Both gRNAs were designed to guide Cas9 to the designated loci for introducing a double strand break, leading to frameshift mutations and thus, truncated versions of *BCORL1* (performed by Sebastian Sigl).

#### 4.3.1. CRISPR efficiency

To evaluate the efficiency of the two gRNAs in the performed CRISPR-Cas9 mediated knockouts, multiple single clones of the HepG2 cell line were cultivated until DNA could be extracted and used for proofing the mutagenesis. Figure 18 displays the ratio of frameshift and in-frame mutations. Furthermore, it depicts remaining wildtype clones and clones where sequencing did not work or a double sequence indicated that the colony was not grown from a single clone. The use of gRNA1 led to frameshift mutations in 33 % of clones and gRNA2 resulted in frameshift mutations in 53 % of clones.

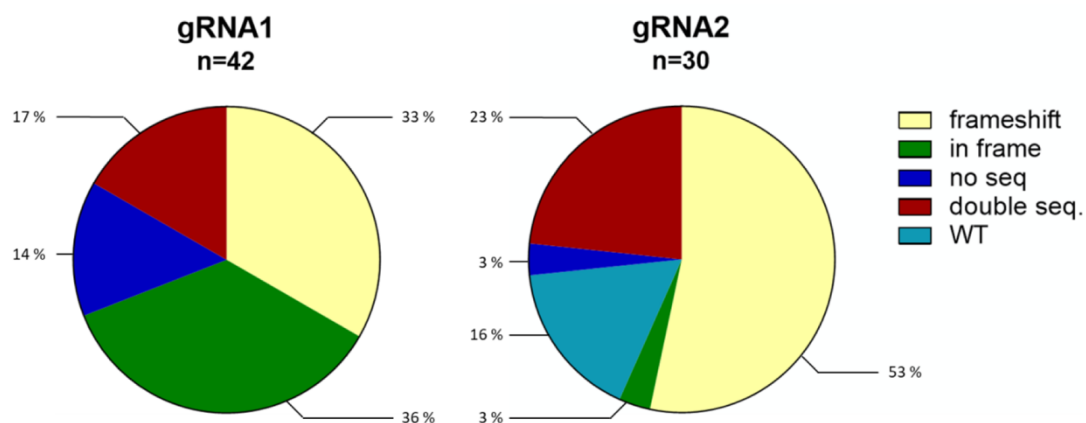


Figure 18: **CRISPR clones of HepG2 obtained using gRNA1 or gRNA2** (no seq: no sequencing possible, double seq: no single clone, WT: wildtype).

In the exemplary HepG2 cell line, both gRNAs induced frameshift mutations in at least one third of cells undergoing CRISPR-Cas9 editing. Thus, both gRNAs could be used to generate CRISPR-Cas9 mediated knockout clones from other cell lines.

## RESULTS

### 4.3.2. Mutation analysis of knockout clones

For further experiments, two clones of each cell line were picked. Mutation analysis was done by forward Sanger sequencing of genomic DNA (gDNA) and verified by reverse Sanger sequencing (Figure 19). In Hep3B clone O1.1, HepG2 clone O1.1, and HUH6 clone O2.2 CRISPR-editing resulted in large insertions at the CRISPR locus. Both HUH7 clones obtained single deletions. For HUH6, two clones from gRNA2 were selected due to lethality of the CRISPR clones. HUH6 clone O2.1 showed a small deletion. Hep3B clone O2.5 and HepG2 clone B2.24 both presented with the same insertion of a single cytosine. All mutations caused frameshifts leading to a stopcodon shortly after and thus, loss of CtBP-binding site, nuclear location signal, and PUFD domain.

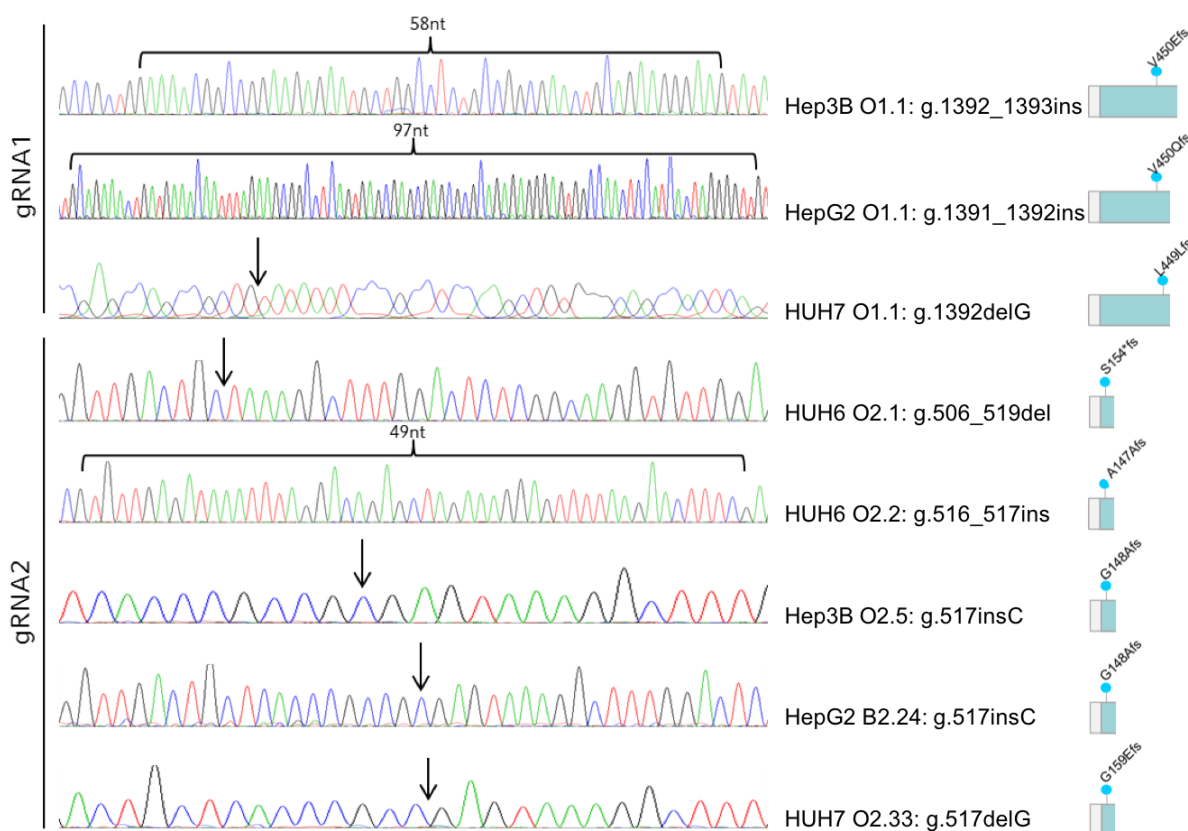


Figure 19: **Sequencing of the BCORL1 gene mutations in different knockout clones.** The knockout was mediated by CRISPR-Cas9 system using gRNA1 or gRNA2 for different loci in exon 4 of BCORL1. Arrows point at the location of insertion or deletion, brackets mark longer insertions. On the right side the corresponding protein changes of each mutation in BCORL1 are shown.

To see if genome editing of BCORL1 is also reflected on the transcriptional level, RNA was extracted, reverse transcribed into cDNA and sequenced. Sanger sequencing of the cDNA verified all mutations found on the DNA level (not shown).

## RESULTS

### 4.3.3. Effects of genome editing on protein level

To investigate the effect of the CRISPR-Cas9 mediated mutagenesis on the BCORL1 protein, whole cell lysates of HepG2 knockout clone O1.1 and wildtype HepG2 cells were produced and used for SDS-PAGE with subsequent immunoblotting with the above selected BCORL1 antibody (#78). In case of the wildtype, the detection of the immunoblot showed a band of 189 kDa, whereas the knockout exhibited a band of approximately 47 kDa (Figure 20A) as predicted [178]. This clearly confirmed that the CRISPR-Cas9 induced mutation is also translated into a truncated BCORL1 protein. As the truncated BCORL1 lacks the nuclear localization signal, it should not be translocated to the nucleus. To verify this theory, wildtype HepG2 cells and HepG2 knockout clone O1.1 cells were analyzed for the localization of BCORL1 by immunofluorescent staining. The immunostaining clearly showed that the wildtype BCORL1 protein is exclusively located in the nucleus, whereas the truncated BCORL1 is located in the cytoplasm (Figure 20B).

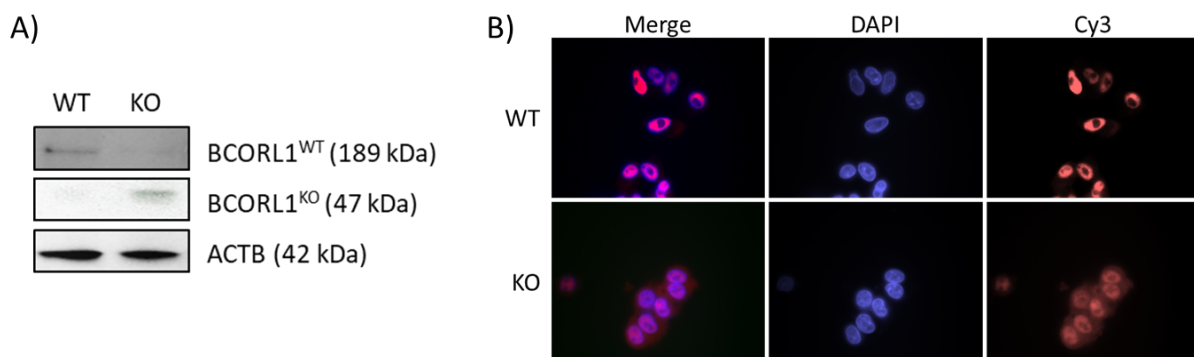


Figure 20: **BCORL1 levels in HepG2 cells.** A) Immunoblot with whole cell lysates of wildtype HepG2 (WT) and HepG2 clone O1.1 (KO) against BCORL1 (supernatant #78). The upper line shows the WT version of BCORL1, the second line shows the truncated BCORL1 version. B) Immunofluorescent staining of BCORL1 (#78) of HepG2 WT and HepG2 KO cells. DAPI (blue) marks the nuclei, Cy3 (red) marks BCORL1 detection.

### 4.4. Effect of BCORL1 knockout on tumor biology

The creation of CRISPR-Cas9 mediated BCORL1 knockout cell lines was the first step of investigating BCORL1. After ensuring that the wildtype version of the protein is actually lost, the knockout cell lines could be examined for changes in tumor biology. Hence, morphology of the knockout cell lines was compared to the wildtype cell line morphology.

#### 4.4.1. Morphology

Cell morphology and growth are indicators for aggressiveness of a tumor and can have different causes [14-17]. Hence, our lab examined wildtype cells and two knockout clones of each cell line for their growth patterns using microscopy. The wildtype cell lines of the hepatoblastoma cell line HUH6, as well as the pediatric HCC cell line Hep3B, the TLCT cell line HepG2 and the adult HCC cell line HUH7 exhibited a flat growth pattern. The colonies expanded in one layer until the cell patches closed the

## RESULTS

gaps in between, so there was no more space. Neither the two knockout clones from the HUH6 cell line, nor the two clones from the Hep3B cell line changed their growth pattern upon knockout of BCORL1. However, the two knockout clones of the HepG2 and HUH7 cell line revealed a completely different growth pattern. All four knockout clone colonies started to expand horizontally and vertically. This growth pattern was continued after passaging the knockout clone lines. When grown until confluence, the vertical expansion of cells was even visible without a microscope. Thus, the knockout clones from the HepG2 and HUH7 cell line changed their growth pattern from flat to a three-dimensional crowded or stem cell-like phenotype (Figure 21).

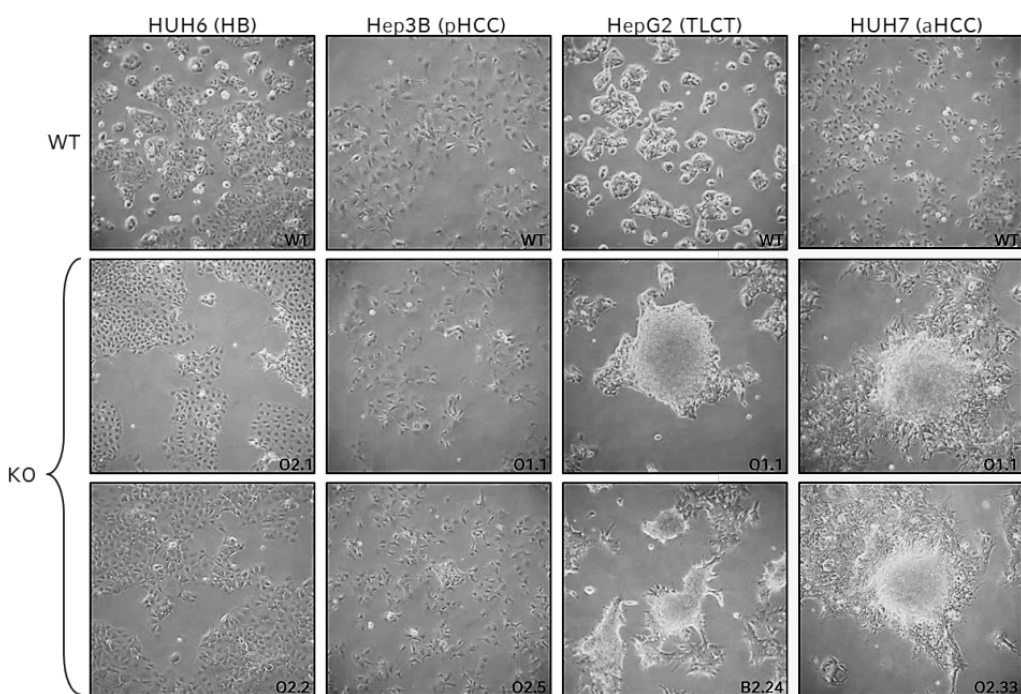


Figure 21: **Morphology of wildtype (WT) and knockout (KO) cell lines.** From each cell line, one exemplary picture of the wildtype cell line (upper line) as well as two knockout clones is shown. In the right corner, the number of the clone is indicated (HB: Hepatoblastoma, pHCC: Pediatric HCC, TLCT: Transitional liver cell tumor, aHCC: adult HCC).

Next, we examined more CRISPR-Cas9 treated HepG2 cells for their morphological changes. Of the 42 single clones generated using gRNA1, about 40 % showed stem-cell like morphology. The use of gRNA2 led to 30 clones, of which 50 % exhibited stem-cell like morphology (Figure 22).

Subsequently, the clones with stem-cell like morphology were sequenced for correlation of the morphological change and the knockout. The use of gRNA2 demonstrated a higher amount of frameshift mutations than gRNA1. Moreover, less gRNA2 clones revealed in-frame mutations, could not be sequenced, or revealed double sequences, indicating that this sample contained more than one clone. Unfortunately, the use of gRNA2 resulted in a small amount of wildtype clones, whereas gRNA1 did not (Figure 22).

## RESULTS

Collectively, these data demonstrate that most clones with stem-cell like morphology also carried truncating frameshift mutations in the *BCORL1* gene (taking the clones out of the equation, which could not be sequenced or showed double sequences). This clearly corroborates the connection of *BCORL1* and the observed morphological changes.

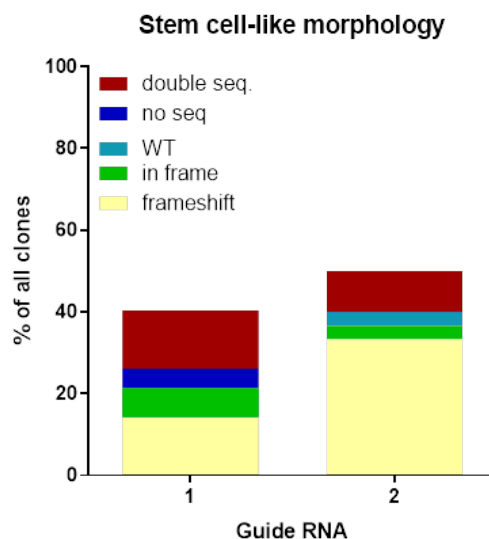


Figure 22: **CRISPR-Cas9 mediated knockout clones of HepG2 with stem-cell like morphology**, grouped by the used gRNA (no seq: no sequencing possible, double seq: no single clone, WT: Wildtype, n=72).

### 4.4.2. Cell proliferation

Besides morphological changes, an important aspect of tumor behavior is cell proliferation. Hence, our lab performed cell viability assays of all four cell lines and the associated two *BCORL1* knockout clones of every cell line to measure proliferation. This was done by seeding cells in equivalent amounts of wildtype and knockout cells and performing a MTT assay at indicated time points (Figure 23).

In the HUH6 cell line, the wildtype cells showed the lowest increase in proliferation. Both knockout clones exhibit considerable higher proliferation rates. This situation is reversed in *BCORL1* knockout clones from the cell lines Hep3B, HepG2, and HUH7. In all three cell lines, the wildtype has the highest proliferation rate. In Hep3B and HepG2 cells, the decrease in knockout clones from gRNA2 was more prominent than gRNA1 clones. The HUH7 cell line and the two HUH7 knockout clones showed the same proliferation pattern. Both knockout clones showed a similar cell viability curve, which was dramatically lower than the wildtype.

The knockout of *BCORL1* led to decreased proliferation levels in most cell lines. The biggest difference was observed in HepG2 B2.24 cells, which reached growth saturation at day 6 with 3-fold the starting cell number. HepG2 wildtype cells almost doubled in comparison to B2.24 (Figure 23).

## RESULTS

Interestingly, the clones with stem cell-like morphology also demonstrated the most prominent decreases of proliferation rates.

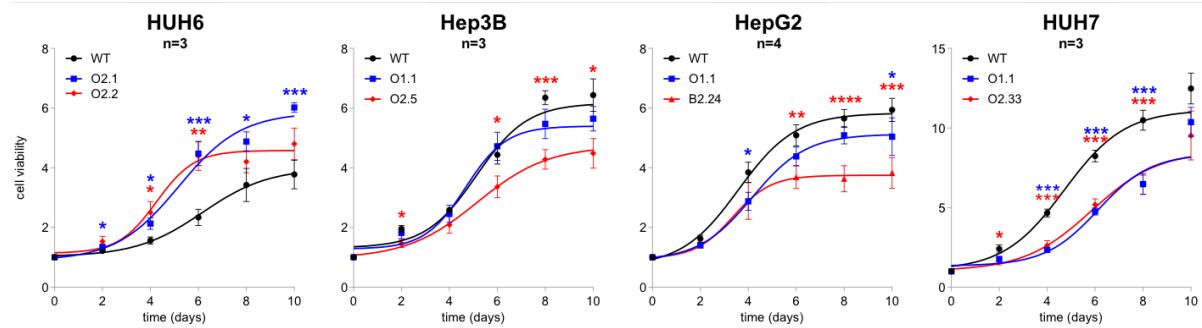


Figure 23: **Proliferation rate** of all liver tumor cell lines over 10 days. Wildtype cell lines are depicted in black and two knockout clones in blue and red (\* p < 0.05, \*\* p < 0.01, \*\*\* p < 0.005, \*\*\*\* p < 0.001).

### 4.4.3. Clonogenicity

For further investigation of changes in tumor biology, we subsequently examined the four cell lines and the two BCORL1 knockout clones of each cell line for changes in clonogenicity. Increased clonogenicity is a feature of stemness, meaning the stem cell characteristics of a certain cell. Therefore, wildtype and knockout cells were seeded in an equally low number and grown to observe how many colonies would grow from the seeded cells.

The percentage of colony forming units increased significantly in all cell lines upon BCORL1 knockout with the highest increase in HepG2 clone B2.24 (Figure 24).

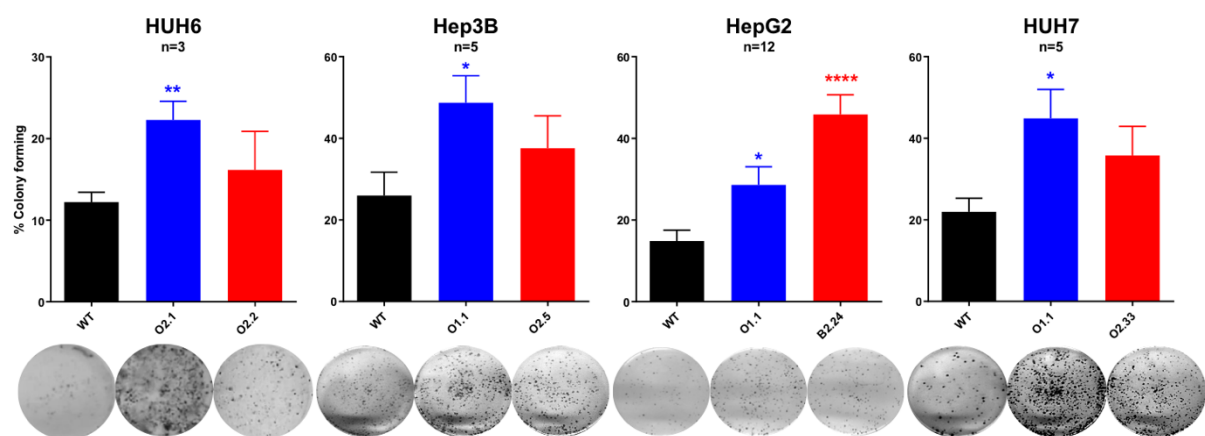


Figure 24: **Colony formation assay** of wildtype liver tumor cell lines (black) versus knockout (blue and red) clones of each cell line 10 days after seeding (\* p < 0.05, \*\* p < 0.01, \*\*\* p < 0.005, \*\*\*\* p < 0.001). Underneath are representative photographs of the culture plates.

Taken together with the observed decreased proliferation rates of most knockout clones, these results indicate that the observed morphological changes are indeed connected to a stem cell characteristic growth.

## RESULTS

### 4.5. Effect of BCORL1 knockout on gene regulation

Since we observed definite effects on tumor biology upon BCORL1 knockout, we started to examine the knockout cells for effects on the molecular level. BCORL1 works as a transcriptional corepressor [179] and is part of the PRC1.1 [138], which regulates histone marks like the ubiquitination of H2A and thus, affects transcription [136]. Hence, we established the ChIP method in our lab to examine the effects of BCORL1 on the distribution of the transcriptionally activating histone mark H3K4me3 and the silencing histone mark H3K27me3.

#### 4.5.1. Establishment of ChIP

To establish ChIP, positive and negative controls needed to be found for enrichments of H3K4me3 and H3K27me3. Thus, different genes were tested for their expression in normal liver tissue and all wildtype cell lines (Figure 25). The housekeeping genes Actin Beta (*ACTB*) and Glyceraldehyde-3-Phosphate Dehydrogenase (*GAPDH*) are normally highly expressed in tissues and cells. Therefore, they should show enrichments of H3K4me3. The normal liver tissue and all cell lines showed high *ACTB* expression. *GAPDH* exhibited lower expression than *ACTB* in all samples. As a negative control for expression and thus H3K4me3 enrichment, we selected the tumor suppressor gene Secreted Frizzled Related Protein 1 (*SFRP1*), which demonstrated a low expression ( $=0.511$ ) in normal liver tissue and was silenced in the hepatoblastoma cell line HUH6 ( $=0.0002$ ), the TLCT cell line HepG2 ( $<0.0001$ ) and the HCC cell lines Hep3B ( $=0.007$ ) and HUH7 ( $=0.0001$ ).

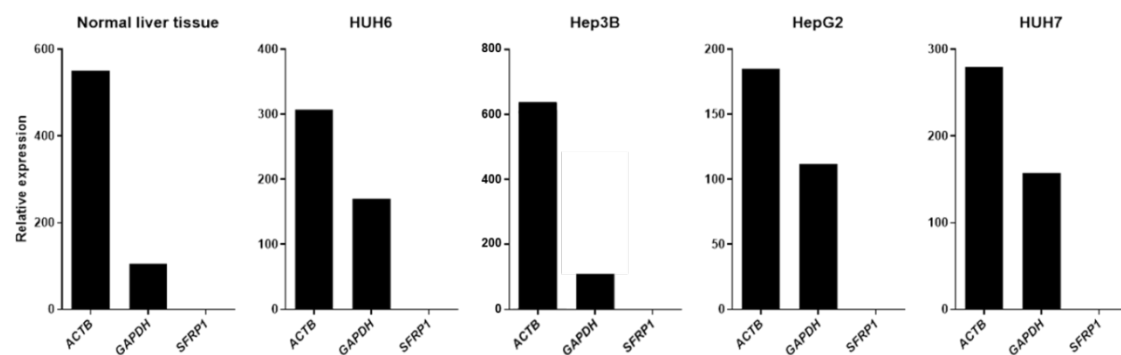


Figure 25: **Relative mRNA expression of control genes.** Expression of Actin Beta (*ACTB*), Glyceraldehyde-3-Phosphate Dehydrogenase (*GAPDH*) and Secreted Frizzled Related Protein 1 (*SFRP1*) normalized to TATA-binding Protein (*TBP*).

According to the expression analysis, the housekeeping genes *ACTB* and *GAPDH* were chosen as positive control and *SFRP1* was selected as negative control for H3K4me3 enrichment. Thus, the parameters for ChIP establishment were defined and ChIP could be performed on normal liver tissue as well as the wildtype cell lines. In every case, there was a clear H3K4me3 enrichment at the housekeeping gene loci as predicted by the expression analysis. The tumor suppressor gene locus

## RESULTS

*SFRP1* showed small enrichment in normal liver tissue confirming the low expression observed above and no or very low enrichment in the cell lines (Figure 26).

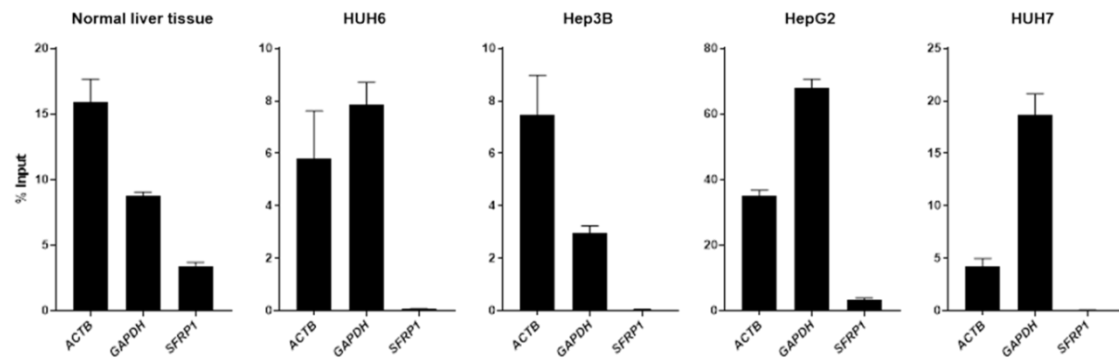


Figure 26: **H3K4me3 enrichments at control loci.** Enrichments in normal liver tissue and the cell lines HUH6, Hep3B, HepG2 and HUH7 at *ACTB*, *GAPDH* and *SFRP1* loci, evaluated from qRT-PCR with ChIP-DNA as template in % of input.

For the silencing mark H3K27me3, the housekeeping gene loci served as negative control and *SFRP1* has been used as positive control for enrichment. Enrichment analysis by qRT-PCR confirmed low enrichments for the housekeeping gene loci in normal liver tissue and all of the four cell lines. The normal tissue, as well as the cell lines, presented by far the largest enrichment at the *SFRP1* locus. The absolute quantity of ChIP-DNA enrichment pointed to HepG2 as the best proof for enrichment at *SFRP1*. However, the ratios between positive and negative loci emphasized that HUH7 and Hep3B cells showed the highest enrichment over negative loci (Figure 27).

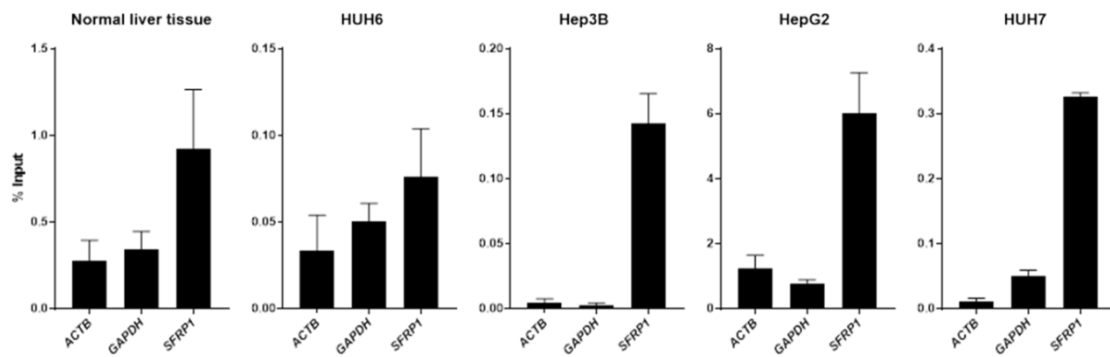


Figure 27: **H3K27me3 enrichments at control loci.** Enrichments of normal liver tissue and the cell lines HUH6, Hep3B, HepG2 and HUH7 at *ACTB*, *GAPDH* and *SFRP1* loci, evaluated from qRT-PCR with ChIP-DNA as template in % of input.

In summary, the enrichments of H3K4me3 at the housekeeping gene loci proofed the high expression of these genes. Thus, *ACTB* and *GAPDH* work as positive controls for H3K4me3 ChIP. Moreover, the observed H3K27me3 enrichments of the cell lines at the *SFRP1* locus corroborated the silencing of *SFRP1*. In normal liver tissue, the basal expression of *SFRP1* could be linked to a low H3K4me3 enrichment, but also H3K27me3 enrichment. However, *SFRP1* can be used as positive control for H3K27me3 enrichment.

## RESULTS

### 4.5.2. Establishment of ChIP-seq

The verification of H3K4me3 and H3K27me3 target loci allowed us to upscale the ChIP approach from single genes to the whole genome by subsequent sequencing of the enriched ChIP-DNA. Out of the global data we first examined the housekeeping genes *ACTB* and *GAPDH*, as well as the tumor suppressor gene *SFRP1*, in order to confirm the enrichments of H3K4me3 and H3K27me3 observed by qRT-PCR. The sequencing results of the ChIP-DNA were also compared to expression, derived from RNA sequencing results. The housekeeping genes showed high expression in the hepatoblastoma cell line HUH6, the TLCT cell line HepG2, and the HCC cell line HUH7. This coincides with a high level of H3K4me3, but almost no H3K27me3. The tumor suppressor gene *SFRP1* exhibited a marginal expression in HUH6, but no expression in HepG2 and HUH7 cells. This was corroborated by very low H3K4me3 and high H3K27me3 levels (Figure 28).

These results clearly presented similar patterns of the small scale qRT-PCR approach and the large-scale global approach. Both corroborated the link of high expression with the enrichment of H3K4me3 and marginal expression with enrichment of H3K27me3.

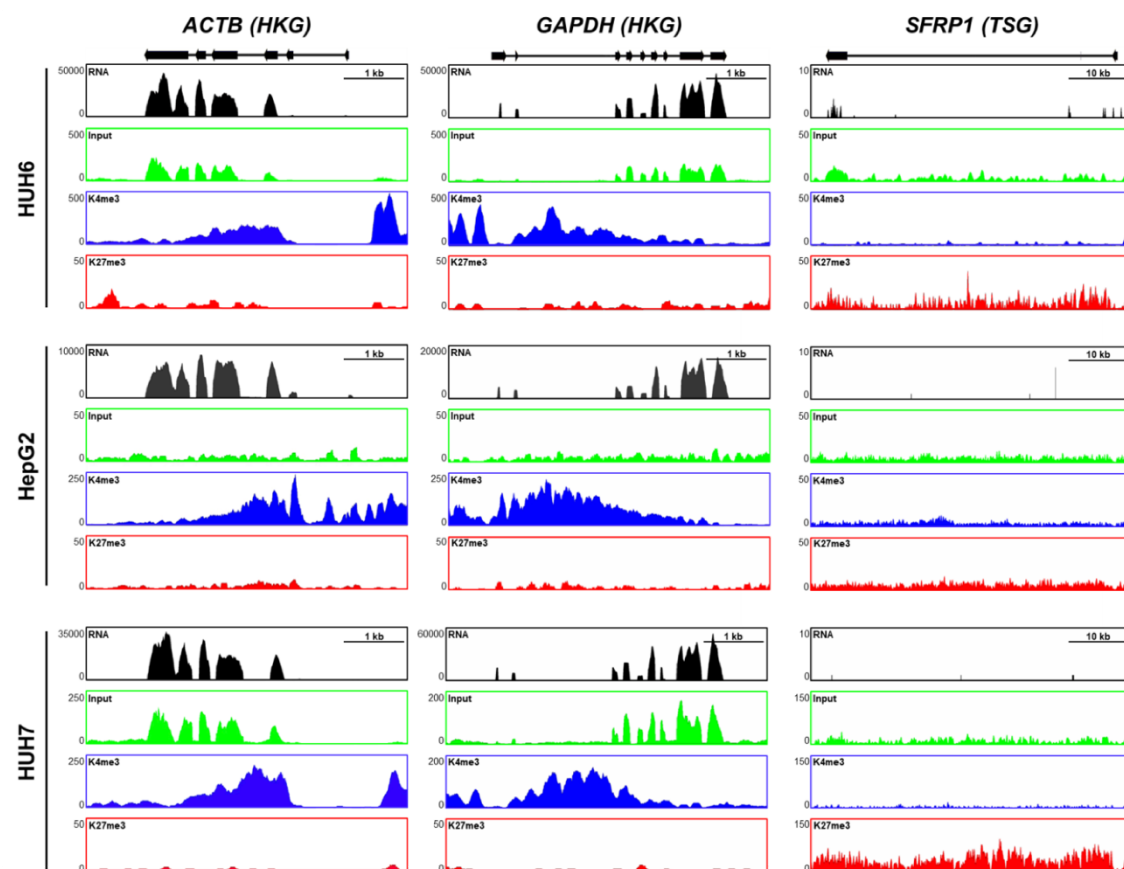


Figure 28: RNA and ChIP-seq of the control genes *ACTB*, *GAPDH*, and *SFRP1* in HUH6, HepG2 and HUH7 cells. Expression (black), trimethylation of H3K4 (blue) and H3K27 (red) was measured in reads per kilobase per million.

## RESULTS

### 4.5.3. Target genes of BCORL1 regulation

In regard to the above observed effects of BCORL1 LOF on tumor biology, the next step was to identify novel target genes of BCORL1, responsible for these changes. Thus, after confirming the successful establishment of the ChIP-seq, global data was generated for one CRISPR-Cas9 mediated knockout clone of the hepatoblastoma cell line HUH6, the TLCT cell line HepG2, and the HCC cell line HUH7. The global RNA-seq and ChIP-seq (H3K4me3 and H3K27me3) data of wildtype cells and knockout cells were then used for identification of new target genes of BCORL1 regulation.

#### 4.5.3.1. CDH1 – the known target gene

As the *CDH1* gene has been described as a gene regulated by BCORL1 [140], we first looked at this locus to see if this is also true for liver cancer cell lines. In HepG2 cells, knockout clone O1.1 exhibited a drastic increase of *CDH1* expression and H3K4me3 levels, but no changes of H3K27me3 levels were observed. The observation of HUH7 cells exhibited an increase of *CDH1* expression upon knockout of BCORL1. H3K4me3 and H3K27me3 levels slightly decreased. HUH6 cells showed no increase in *CDH1* expression after knockout. H3K4me3 levels, as well as H3K27me3 levels, showed no changes upon BCORL1 knockout in the HUH6 clone O2.2 (Figure 29). Collectively, these expression and H3K4me3 enrichment data demonstrated the reactivation of *CDH1* upon BCORL1 knockout only in the HepG2 cell line as Pagan [179] presented. This might also be the case for the HUH7 cell line, but not the HUH6 cell line.

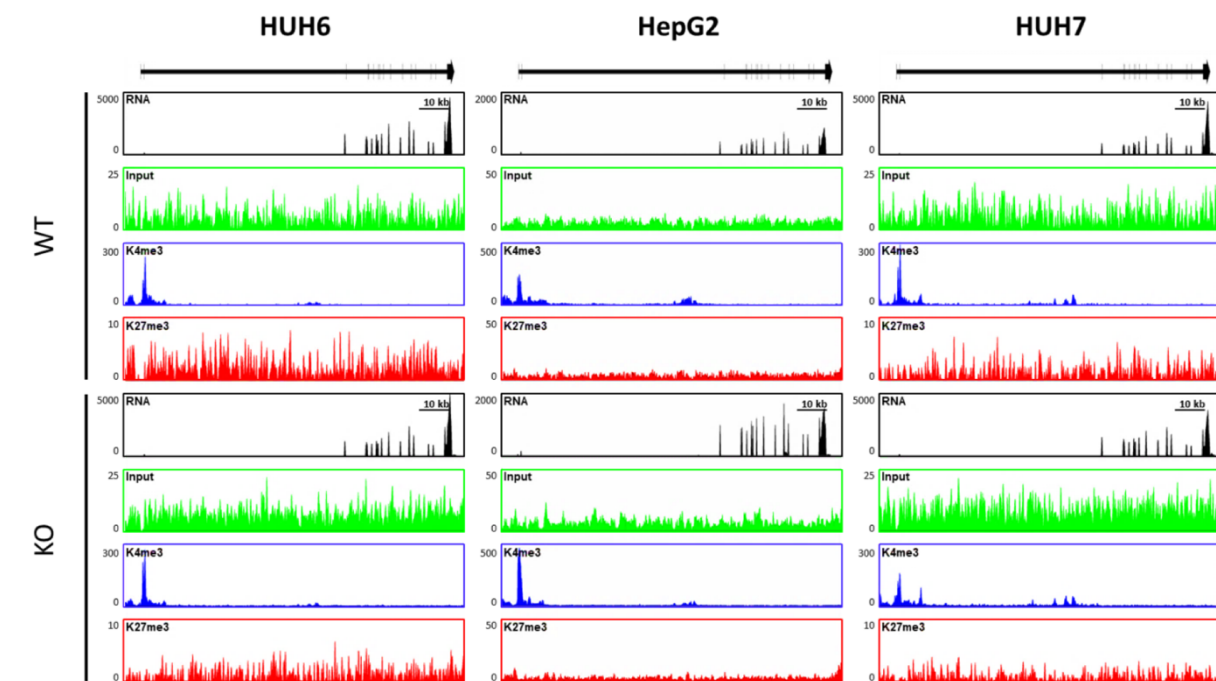


Figure 29: **Reactivation of *CDH1* upon BCORL1 knockout in HepG2 and HUH7.** Expression (black) and levels of H3K4me3 (blue) and H3K27me3 (red), measured in reads per kilobase per million.

## RESULTS

To see if these findings actually affect the *CDH1* protein level, immunoblotting for *CDH1* was performed with the three wildtype cell lines and two knockout clones of each cell line. The HepG2 and HUH7 knockout cells exhibited increased in *CDH1* levels, which were more prominent in HUH7 knockout clones. HUH6 knockout cells exhibited no changes (Figure 30). This data verified the effect on *CDH1* protein levels in HepG2 and HUH7 cells and thus, the regulation of *CDH1* transcription through BCORL1 in HepG2 and HUH7 cells.

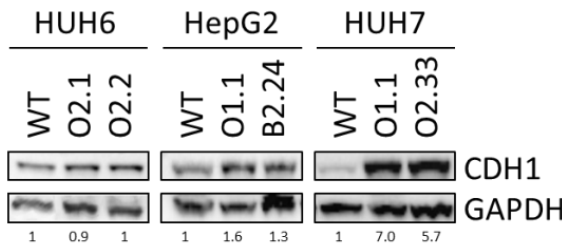


Figure 30: **CDH1 protein levels of wildtype cells and BCORL1 knockout clones.** For immunoblotting, whole cell lysates of wildtype HUH6, HepG2 and HUH7 cell lines and two BCORL1 knockout clones of each cell line were used to detect *CDH1* levels with GAPDH as control. Quantification was calculated relative to GAPDH and expressed in fold change to wildtype.

### 4.5.3.2. Candidate target genes of BCORL1 regulation

After conformation of the known target gene *CDH1*, we aimed to identify new target genes of BCORL1 regulation. As the HUH6 cell line revealed completely different features upon BCORL1 knockout compared to the other cell lines in terms of its inability to change morphology and to reactivate *CDH1* expression, we compared the expression data of HUH6 wildtype cells with HepG2 and HUH7 wildtype cells and a normal liver tissue sample (N528) for genes, which are differentially expressed. Hierarchical clustering showed a close relationship between the HepG2 and HUH7 cell lines. Both cell lines also cluster close to the normal liver sample. The HUH6 cell line reveals a completely different pattern (Figure 31).

Next, we used a 2.3-fold increase or decrease to filter out genes which are highly differentially expressed between HUH6 and the other samples (HepG2, HUH7 and N528) and found this to be the case for 8,437 genes. These genes were cross-examined for a relationship to BCORL1 and/or *CDH1*. Interestingly, *CtBP2* as well as *RING1B* revealed to be one of these genes (Figure 31). *CtBP* acts as a transcriptional repressor on certain target loci like *CDH1*. This repression is partially mediated by BCORL1 [179]. The expression of *CtBP2* in wildtype HUH6 cells at least 3.2-fold higher than normal liver tissue, wildtype HUH7, and HepG2 cells. *RING1B* is a component of the many PRC complexes [138]. BCORL1 is known to associate with PRC1.1 [142-145] through interaction with PCGF1 [152]. The expression of *RING1B* in wildtype HUH6 cells is at least 2.3-fold higher than the other samples. In wildtype HUH7 cells the expression of *RING1B* is highly suppressed (Figure 31).

## RESULTS

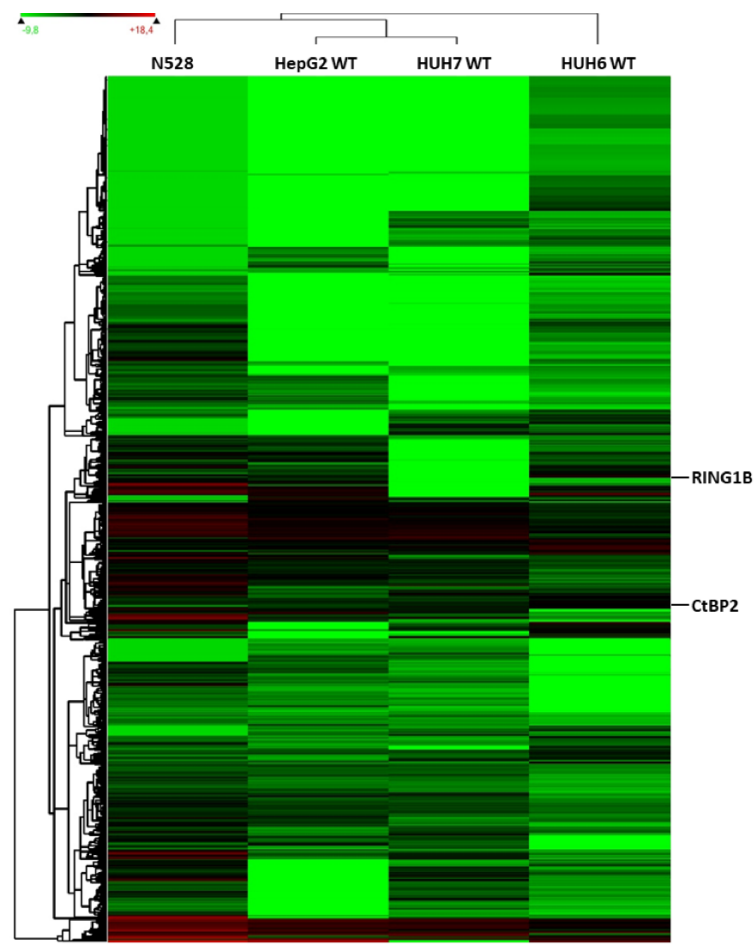


Figure 31: **Hierarchical clustering of differentially expressed genes between the normal liver sample 528 and the cell lines HepG2, HUH7, and HUH6.** These genes were filtered by 3-fold change between HUH6 and the other samples and shown as a heat map with suppressed genes marked green and highly expressed genes marked red (N528: normal liver tissue of patient 528, WT: wildtype, CtBP2: C-terminal binding protein 2).

Considering the differential clustering and the morphological differences upon knockout of BCORL1, we decided to examine the expression data exclusively for 2-fold increased expression in HepG2 and HUH7 knockout clones. The two data sets were overlapped using a Venn diagram as shown in Figure 32.

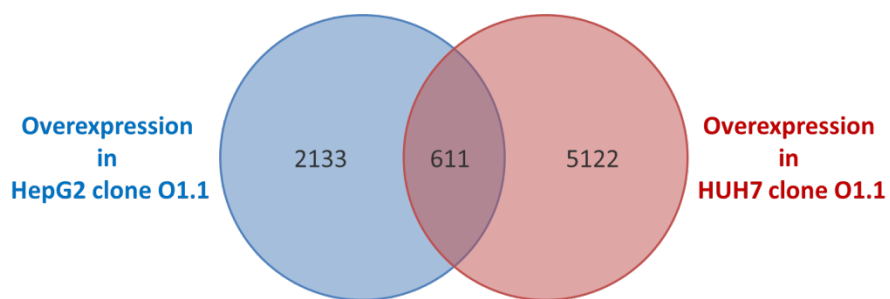


Figure 32: **Venn diagram showing genes with 2-fold overexpression in HepG2 clone O1.1 compared to wildtype HepG2 cells (left) and in HUH7 clone O1.1 compared to wildtype HUH7 cells (right).** The overlap exhibits the amount of genes, which showed a 2-fold increase of expression in both knockout clones.

## RESULTS

Furthermore, we examined the ChIP-seq data of HepG2 clone O1.1 and HUH7 clone O1.1 to confirm if these 7,866 genes also show changes of H3K4me3 levels compared to the according wildtype. Hence, the both clones were cross-examined unaltered or increased H3K4me3 levels. Due to the low H3K27me levels in general, these were not used for filtering. The 2,547 genes, which are overexpressed and show unaltered or increased H3K4me3 levels in one cell line were used for functional annotation with the DAVID database. Figure 33 shows the functional annotation with Gene ontology (GO) terms related to biological processes or cellular compartments, selected for significant p-value and a false discovery rate less than 5 %.

The analysis of GO terms revealed terms related to plasma membrane with the highest enrichment scores and gene counts. Other terms like cell adhesion, cell proliferation and cell division also showed high enrichment scores. Considering the observed effects of BCORL1 knockout on morphology, we examined genes belonging to the GO term plasma membrane, which are also associated with adhesion more closely (Figure 33).

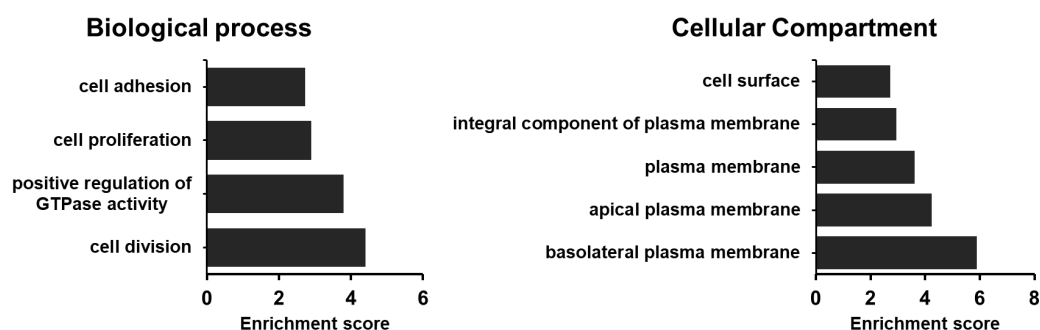


Figure 33: DAVID analysis of genes with increased expression and H3K4me3 levels upon knockout in HepG2 and HUH7. The enrichment score is calculated from  $-\log_{10}(p\text{-value})$ . All samples have a false discovery rate <5 % and  $p < 0.05$ .

For further evaluation, five genes with the highest increases of expression and H3K4me3 levels in HepG2 clone O1.1 and HUH7 clone O1.1 were chosen. These genes were Cadherin 24 (*CDH24*), Endothelial Cell Adhesion Molecule (*ESAM*), Epithelial Cell Adhesion Molecule (*EPCAM*), Teratocarcinoma-Derived Growth Factor 1 (*TDGF1*), and Keratin 19 (*KRT19*).

*CDH24* belongs to the group of cadherins and is also linked to adhesion, but the GO term single organismal cell-cell adhesion. The combination of RNA-seq and ChIP-seq data revealed an increase of expression in HepG2 clone O1.1 and increased H3K4me3 levels in HUH7 clone O1.1. No changes of expression in HUH7 clone O1.1, H3K4me3 levels in HepG2 and H3K27me3 in both clones were observed (Figure 34). Even though expression was increased in HepG2 upon BCORL1 knockout, this pattern could not confirm *CDH24* as target gene of BCORL1, due to the missing increase of H3K4me3 levels.

## RESULTS

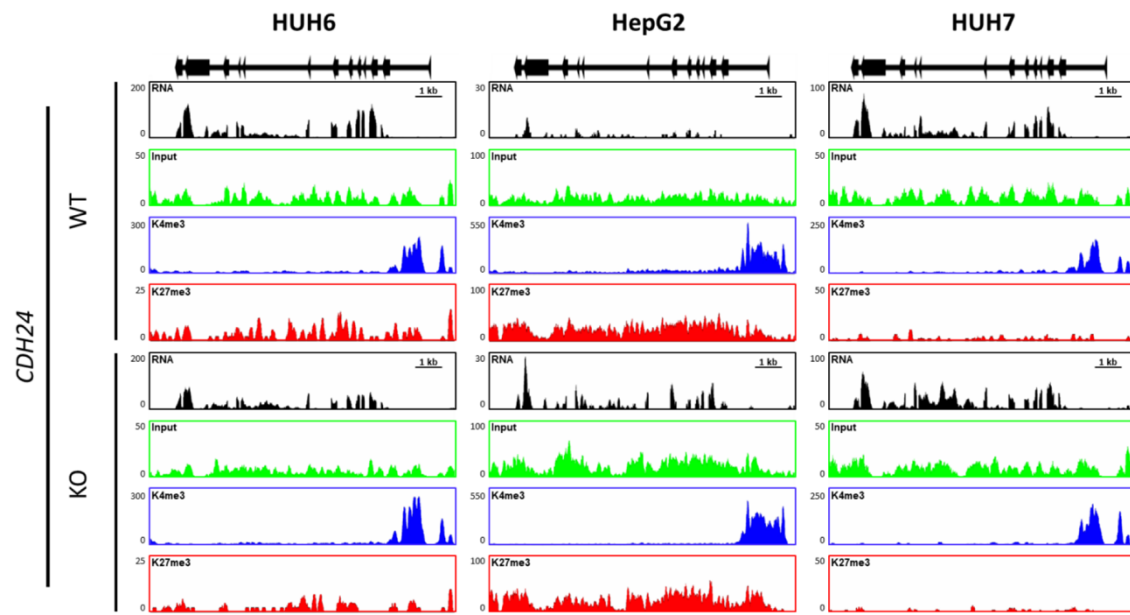


Figure 34: **RNA (black) and ChIP-seq results at the *CDH24* locus** in wildtype (WT) and knockout HUH6, HepG2 and HUH7 cells (KO) in reads per kilobase per million. The input control is depicted in green, H3K4me3 and H3K27me3 in blue and red.

Furthermore, we checked the gene *ESAM* for changes upon BCORL1 knockout in the cell lines HepG2 and HUH7. As an immunoglobulin-like transmembrane protein [180], *ESAM* also belongs to the GO terms related to single organismal cell-cell adhesion and plasma membrane. All three knockout clones exhibited increased expression as well as increased H3K4me3 levels, when compared to the wildtype cell lines. H3K27me3 levels stayed unchanged. While the expression pattern of *ESAM* (Figure 35) differed from *CDH1* (Figure 29), we observed similar changes of H3K4me3 levels as *CDH1*.

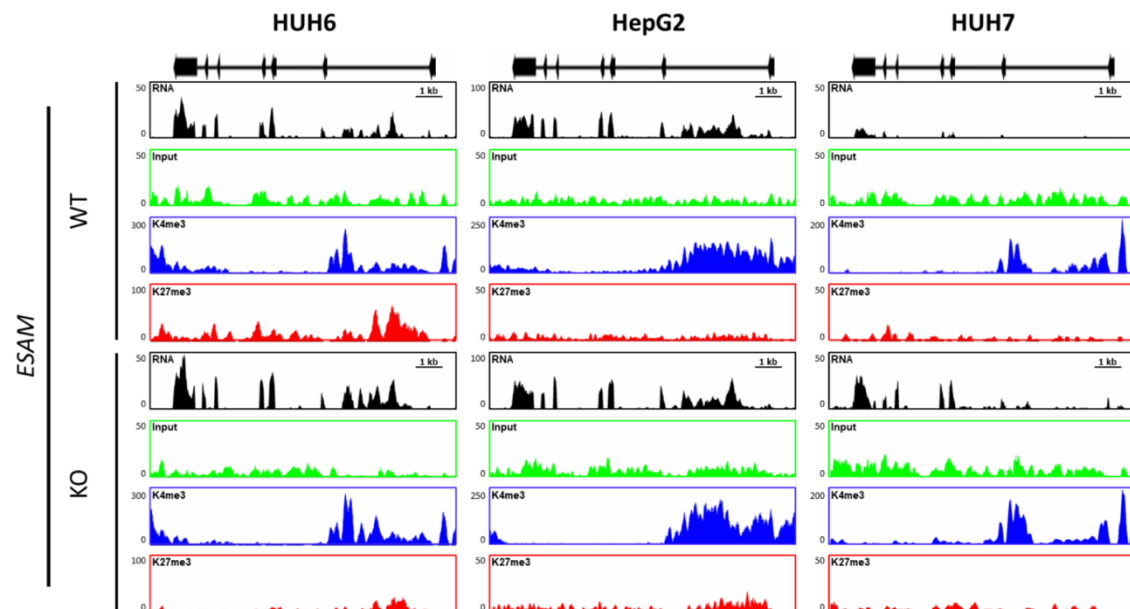


Figure 35: **RNA-seq (black) and ChIP-seq results at the *ESAM* locus** in wildtype (WT) and knockout (KO) HUH6, HepG2 and HUH7 cells. Input control is shown in green, H3K4me3 and H3K27me3 levels in blue and red. All data is depicted in reads per kilobase per million.

## RESULTS

The third plasma membrane-related gene, is *EPCAM*, a transmembrane glycoprotein, which mediates cell-cell adhesion in an  $\text{Ca}^{2+}$ -independent manner [181]. Observations of the sequencing data at the *EPCAM* locus exhibited huge expression increases in HepG2 and HUH7 knockout clones and increased H3K4me3 levels in HepG2 clone O1.1, but no changes in H3K27me3 levels (Figure 36). This expression and enrichment pattern resembles the one of *CDH1* (Figure 29) and thus, suggests *EPCAM* as a target gene of BCORL1.

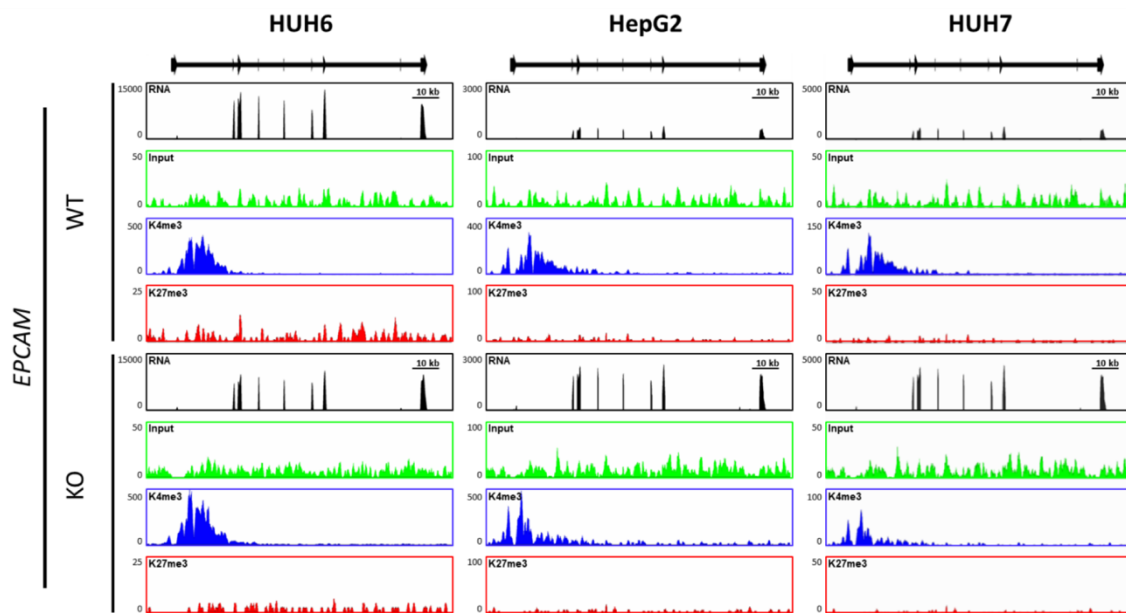


Figure 36: **RNA-seq (black) and ChIP-seq results at *EPCAM* locus in wildtype (WT) and knockout (KO) HUH6, HepG2 and HUH7 cells.** Input control is shown in green, H3K4me3 levels in blue and H3K27me3 levels in red. All data is depicted in reads per kilobase per million.

The fourth gene related to the GO term plasma membrane, is *TDGF1*. Expression analysis of *TDGF1* revealed a high increase in HepG2 clone O1.1. H3K4me3 levels decreased in HepG2 clone O1.1, while HUH7 clone O1.1 exhibited a high increase in H3K4me3 levels. H3K27me levels did not show any alterations (Figure 37).

After closer examination, the expression and enrichment pattern of *TDGF1* did not meet the dictated criteria and thus, is no target gene of BCORL1.

## RESULTS

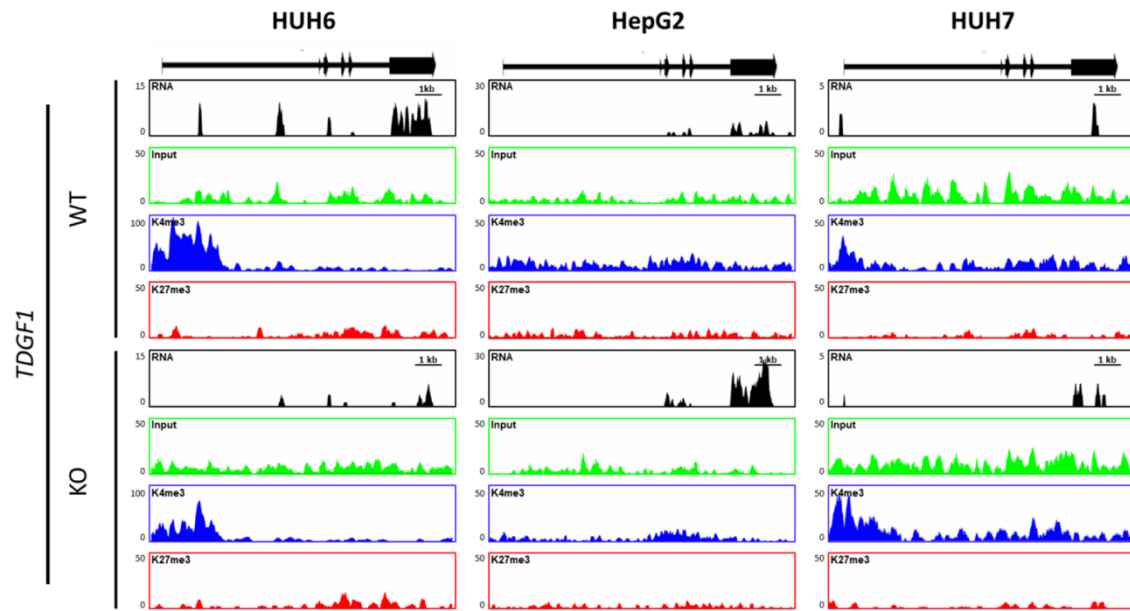


Figure 37: **RNA-seq and ChIP-seq results at *TDGF1* locus in wildtype (WT) and knockout (KO) HUH6, HepG2 and HUH7.** RNA levels are shown in black, input control in green, H3K4me3 levels in blue and H3K27me3 levels in red. All data is depicted in reads per kilobase per million.

Finally, we sought out effects on expression of *KRT19* upon knockout of BCORL1. As part of the Keratin family, *KRT19* is also associated with the GO term plasma membrane. Moreover, it was also associated with cell proliferation in breast cancer [182]. We observed increased expression in HepG2 and HUH7 knockout clones, as well as increased H3K4me3 levels in HepG2 clone O1.1. Moreover, H3K27me3 levels were strongly decreased in HUH7 clone O1.1 (Figure 38) in contrast to the other observed loci.

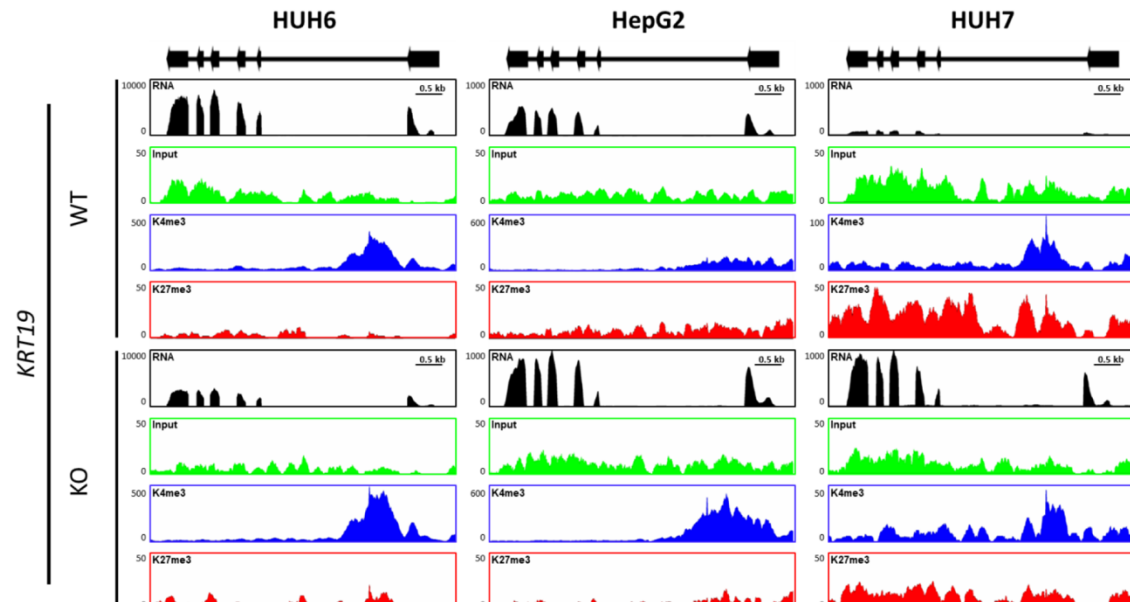


Figure 38: **RNA-seq (black) and ChIP-seq results at *KRT19* locus in HUH6, HepG2 and HUH7 wildtype (WT) and knockout (KO) cells.** The input control is shown in green, H3K4me3 levels in blue and H3K27me3 levels in red. All data is depicted in reads per kilobase per million.

## RESULTS

*KRT19* met the three criteria for being a target gene of BCORL1. The expression pattern, as well as the enrichment pattern for both histone methylations demonstrated that *KRT19* is regulated through BCORL1 in HepG2 and HUH7.

When looking into *ESAM*, *EPCAM*, and *KRT19*, one common term attracted our attention. All three genes are also connected to stemness [180, 183, 184]. This knowledge, combined with the stem cell-like morphology, the decreased proliferation and the increased clonogenicity suggests BCORL1 as regulator of *KRT19* expression and thus, stemness in HepG2 and HUH7 cells. In addition to the observed changes on RNA and chromatin level, we investigated the *KRT19* protein level upon BCORL1 knockout by immunoblotting.

Both HepG2 and HUH7 clones revealed increased *KRT19* protein levels. The HUH7 clone O1.1 showed the highest increase in *KRT19* protein level, which was followed by the HUH7 clone O2.33 (Figure 39). These results perfectly resemble the expression data observed (Figure 38) above and thus, confirm *KRT19* as a valid target gene of BCORL1.

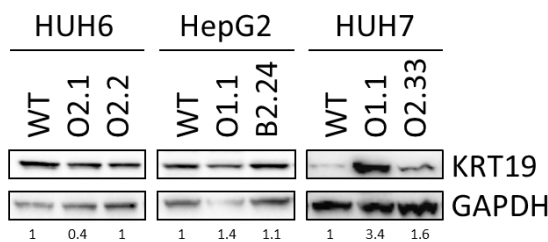


Figure 39: **KRT19 levels in wildtype (WT) cell lines and BCORL1 knockout clones.** For immunoblotting, whole cell lysates of HUH6, HepG2 and HUH7 cells were used. As the GAPDH loading control indicates, the HUH7 blot is the same as Figure 30.

## RESULTS

### 4.6. BCORL1 rescue

For the validation of the functional consequences of a BCORL1 LOF, rescue experiments were performed by transfecting EGFP-tagged BCORL1 wildtype into the knockout clones. Protein levels of BCORL1 were examined by immunoblotting using the BCORL1 antibody #78, as identified in 4.2.2. The two immunoblots clearly detected the EGFP-tagged BCORL1<sup>WT</sup> (216 kDa) and demonstrated the low endogenous BCORL1 levels (189 kDa). Moreover, both knockout cells revealed the loss of wildtype BCORL1 (Figure 40A). We also used immunoblotting to show again the inefficiency of the commercial BCORL1 antibody from Thermo Scientific to detect BCORL1 in liver cancer cell lines. Figure 40B clearly depicted the detection of some protein, but not BCORL1, and thus, corroborated the need for the custom-made antibody #78.

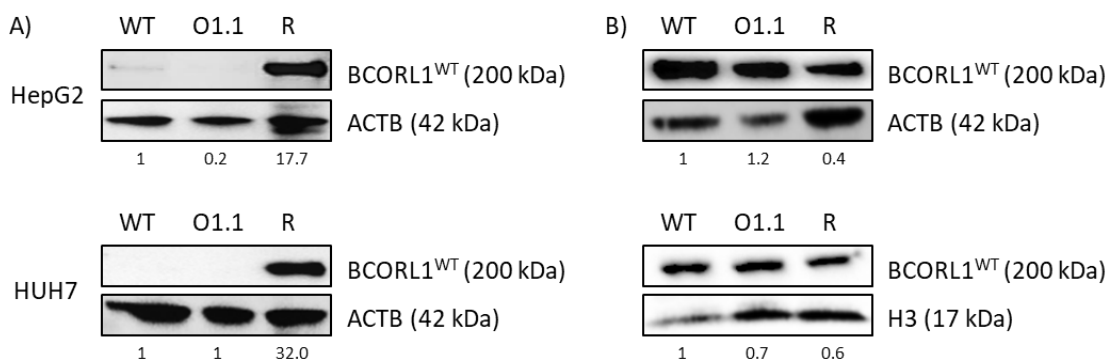


Figure 40: **BCORL1 protein levels of wildtype (WT) HepG2 and HUH7 cells, knockout clones O1.1 of both cell lines, and the respective rescue cells (R)**, which were generated by transfection with pEGFP-BCORL1<sup>WT</sup>. A) Immunoblotting was performed using the antibody #78 and ACTB as control. B) Detection using the commercially available antibody from Thermo Scientific on whole cell lysates (upper blot) and ACTB as control and nuclear extracts with H3 as loading control (bottom blot).

#### 4.6.1. Effect of BCORL1 rescue on morphology

The observed changes in morphology and *KRT19* expression observed upon knockout of BCORL1 indicated a connection with a more stem cell-like behavior of these cells.

Hence, we examined the BCORL1 rescue for effects on tumor biology after verification of the BCORL1 rescue on protein level. Cell morphology, as well as proliferation and clonogenicity, were examined. HepG2 and HUH7 knockout clones were transfected with a control plasmid (pEGFP-N1) or the EGFP-tagged BCORL1<sup>WT</sup> to examine the effects of BCORL1 restoration in the knockout clones. All clones exhibited a high expression of the according plasmids. Soon after fluorescent activated cell sorting, both HepG2 and HUH7 knockout clones showed the expected stem cell-like morphology. However, the four rescued clones exhibited a totally normal one-layered horizontal growth pattern. Even after extended culture periods, the rescue clones did not regain the stem cell-like morphology (Figure 41). Collectively, these results demonstrated the reversibility of the phenotypic alterations upon BCORL1 knockout.

## RESULTS

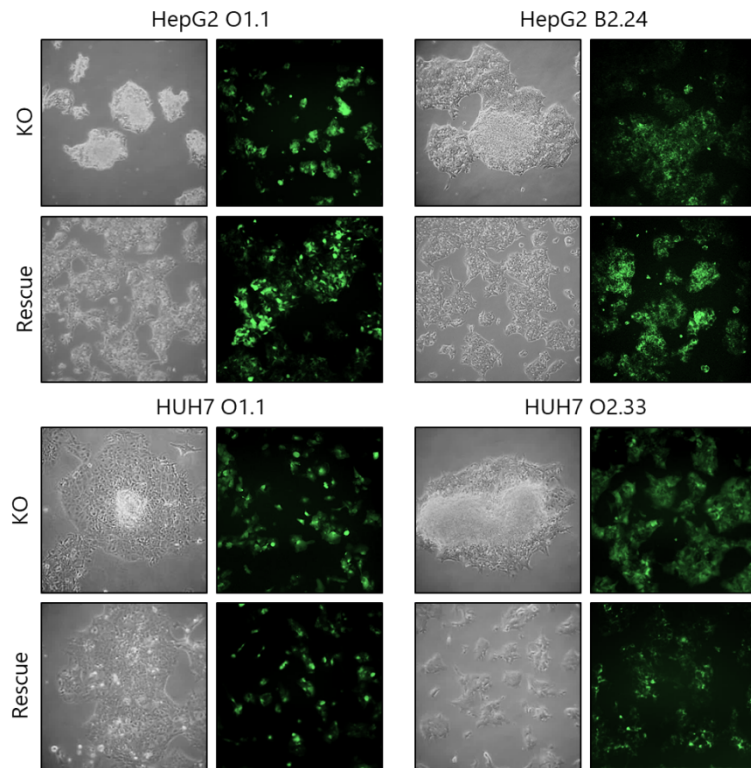


Figure 41: **HepG2 and HUH7 knockout clones and rescue clones.** All knockout clones were stably transfected with either pEGFP-N1 (KO) as a control or pEGFP-BCORL1<sup>WT</sup> (Rescue). Growth pattern were analyzed by conventional microscopy (grey), the FACS efficiency and fluorescence intensity was analyzed by fluorescent microscopy (green cells).

### 4.6.2. Effect of BCORL1 rescue on proliferation

The successful rescue of the normal cell morphology by restoring BCORL1<sup>WT</sup> expression indicated that restoration of BCORL1 could also reverse the other effects of BCORL1 loss. Thus, proliferation was investigated as the next aspect of tumor biology, which can also be regulated by *KRT19* expression [182].

Upon knockout of BCORL1, we observed significant decreases in proliferation rates of HepG2 as well as HUH7 clones (Figure 23). The proliferation rate of all knockout clones from HepG2 and HUH7 increased upon restoring BCORL1<sup>WT</sup> expression. The rescue of HepG2 clone B2.24 demonstrated a highly significant increase of proliferation until day 4, when it was matched by HepG2 clone B2.24 (Figure 42). Together, these results showed the reversibility of the effect of BCORL1 knockout on proliferation.

## RESULTS

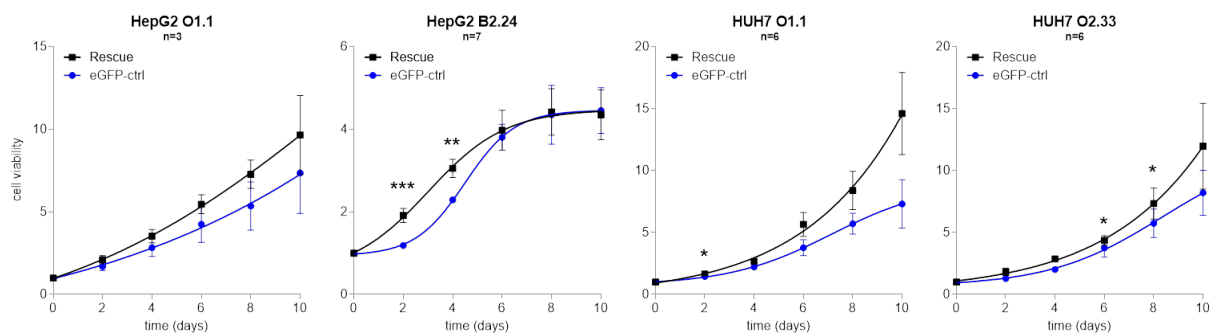


**Figure 42: Proliferation rate of knockout versus rescue.** HepG2 and HUH7 knockout clones were stably transfected with pEGFP-N1 as control (blue) and the rescue (black) of these clones by transfection with pEGFP-BCORL1<sup>WT</sup> (\* p < 0.05, \*\* p < 0.01, \*\*\* p < 0.005).

### 4.6.3. Effect of BCORL1 rescue on clonogenicity

The effects of BCORL1 knockout on morphology, as well as proliferation, proved to be reversible upon restoration of BCORL1<sup>WT</sup> expression. A third aspect of tumor biology is clonogenicity, which was highly affected by the loss of BCORL1. Increased clonogenicity is a trait of stemness and might also be regulated by deregulation of the stemness associated gene *KRT19*.

Upon knockout of BCORL1, all cell lines showed a high increase in colony formation (Figure 24). This situation was reversed by restoring the BCORL1<sup>WT</sup> expression. Upon rescue of BCORL1, all clones revealed significant decreases in colony formation (Figure 43). This is also clearly visible when looking at the culture plates underneath, which exhibit a high colony number in case of the rescue on the left and a low colony number for the knockout clone on the right. These results clearly demonstrate the inhibitory effect of BCORL1 restoration on clonogenicity and confirm that the effects of BCORL1 loss are reversible.

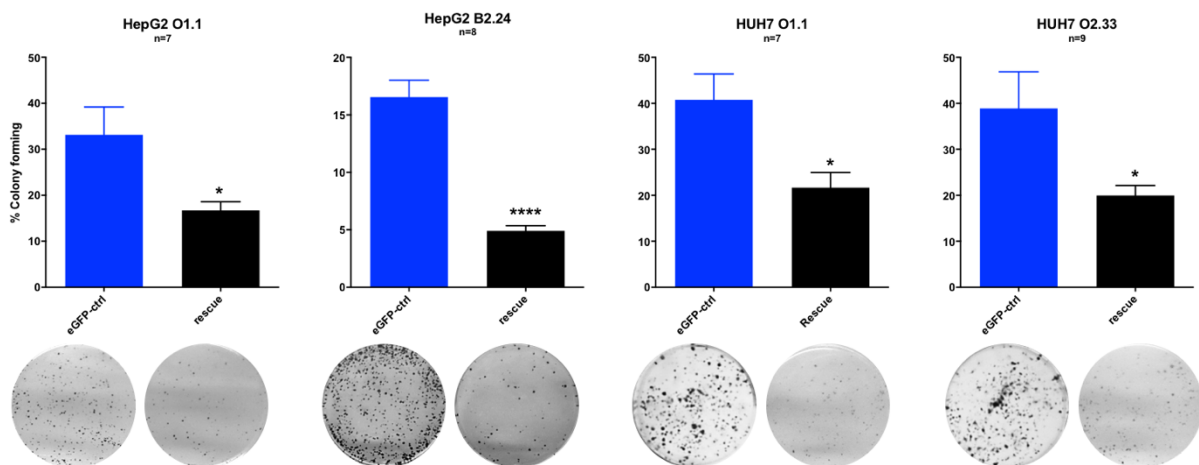


**Figure 43: Colony formation assay of knockout versus rescue.** Knockout clones (blue) were transfected with pEGFP-N1 as control versus rescue (black) of each knockout clone transfected with pEGFP-BCORL1<sup>WT</sup> 10 days after seeding. Underneath are representative photographs of the culture plates (\* p < 0.05, \*\*\*\* p < 0.0001).

## RESULTS

Summing up, the investigation of tumor biology pointed out the effects of BCORL1<sup>WT</sup> loss. All these effects were demonstrated to be reversible by restoration of BCORL1<sup>WT</sup> expression. This concerned the induction of the stem cell-like morphology, as well as changes in proliferation and clonogenicity.

### 4.6.4. Effect of BCORL1 rescue on gene regulation

Considering the effects of BCORL1 knockout on gene regulation, we intended to see if these are also reversible upon reintroduction of the wildtype BCORL1. Thus, RNA of rescue HepG2 clone O1.1 and rescue HUH7 clone O1.1 was sequenced and used for expression analysis.

For selection of candidate target genes of BCORL1 regulation, the expression data of HepG2 and HUH7 cells was filtered for genes, which are reactivated upon BCORL1 knockout and exhibit decreased expression upon restoration of BCORL1<sup>WT</sup> expression. The cross-examination of these potential target genes pointed out 195 genes, which occurred in both groups (Figure 44). These 195 genes were subsequently used for DAVID analysis.



Figure 44: Genes with 1.4-fold increased expression in knockout HepG2 (left) and HUH7 (right) clone O1.1 compared to the respective rescue and wildtype cells.

Functional annotation revealed different GO terms with a highly significant p-value, an enrichment score  $>1$  and FDR  $<1\%$  (Figure 45). The most striking GO term is plasma membrane, due to its identification in the DAVID analysis above (Figure 33).

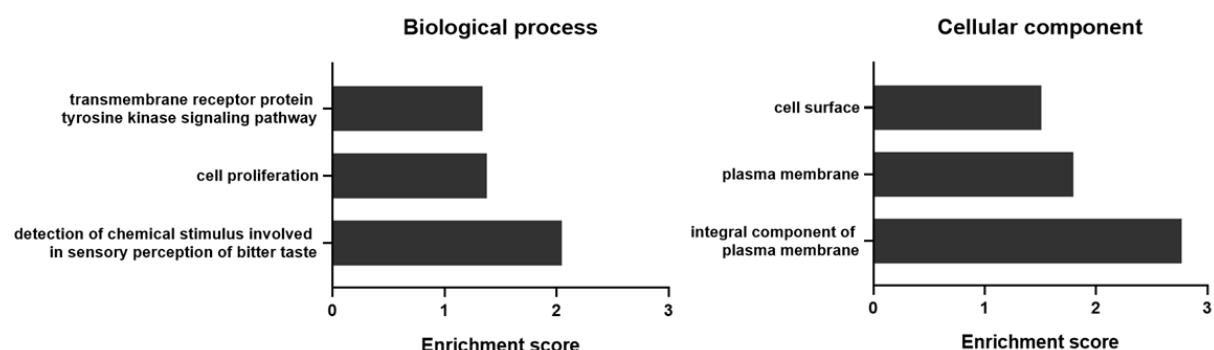
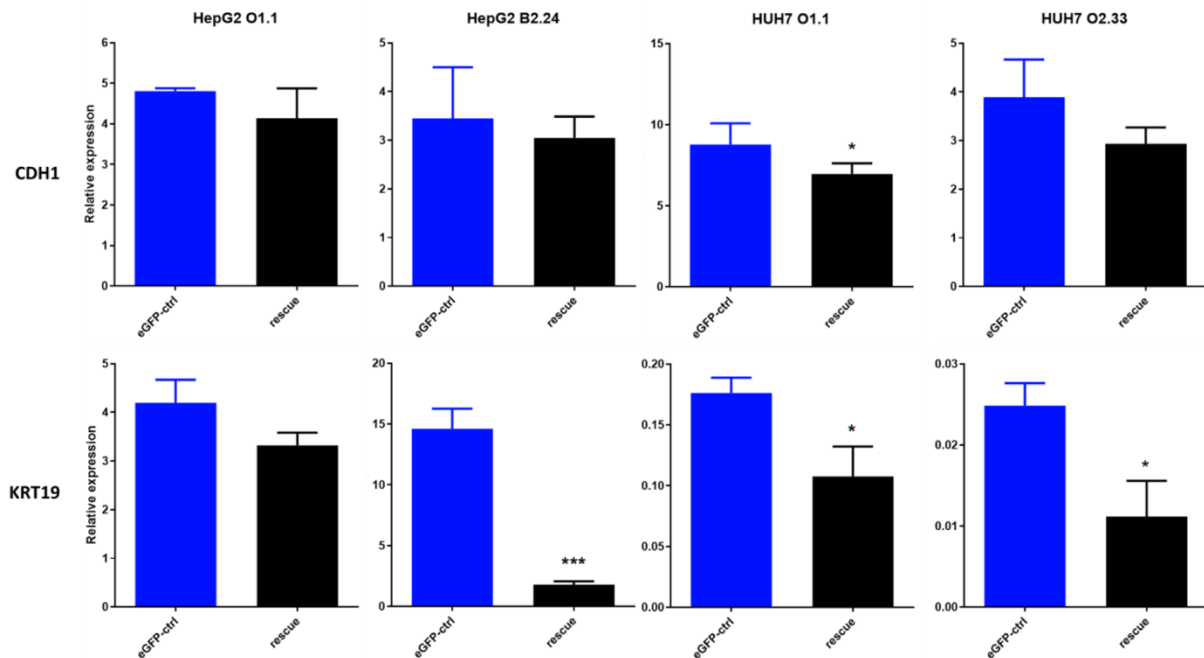


Figure 45: DAVID analysis of genes with increased expression in knockout clone O1.1 of HepG2 and HUH7 in comparison to wildtype and rescue cells.

Out of the group plasma membrane, we examined *KRT19* and the known target gene *CDH1*. Therefore, qRT-PCR was performed for the HepG2 and HUH7 clones and the respective BCORL1 rescue

## RESULTS

cells. Both HepG2 and HUH7 clones showed decreased *CDH1* expression upon restoration of BCORL1 expression. The expression of *CDH1* in HUH7 clone O1.1 was significantly decreased. Moreover, the restoration resulted in decreased *KRT19* expression in all rescue clones. Most clones demonstrated significantly decreased *KRT19* expression (Figure 46).



**Figure 46: Relative expression of candidate genes in knockout and rescue HepG2 and HUH7 clones** measured with qRT-PCR and normalized to *TBP*. The EGFP-control (ctrl) cells were stably transfected with pEGFP-N1, rescue cell lines with pEGFP-BCORL1<sup>WT</sup> (\* p < 0.05, \*\* p < 0.01, \*\*\* p < 0.005, \*\*\*\* p < 0.001).

In summary, the expression data verified the sequencing data and demonstrated the reverse effect of BCORL1 rescue on expression of *CDH1* and *KRT19* in HepG2 and HUH7 cells. Considering the reversible changes in morphology, proliferation, and clonogenicity, these results corroborated the regulation of stemness through BCORL1 via *KRT19* expression.

In regards of the above measured expression decrease of *CDH1* and *KRT19* expression, we also looked for changes on protein level in the knockout and rescue cell lines of HepG2 and HUH7. The immunoblotting demonstrated increased *CDH1* and *KRT19* protein levels in all knockout clones, which decreased upon restoration of the BCORL1<sup>WT</sup> expression. The increases in protein levels were higher in HUH7 clones, but the rescue proved higher efficiency in reversing the effects of BCORL1 knockout in HepG2 clone rescue (Figure 47).

## RESULTS

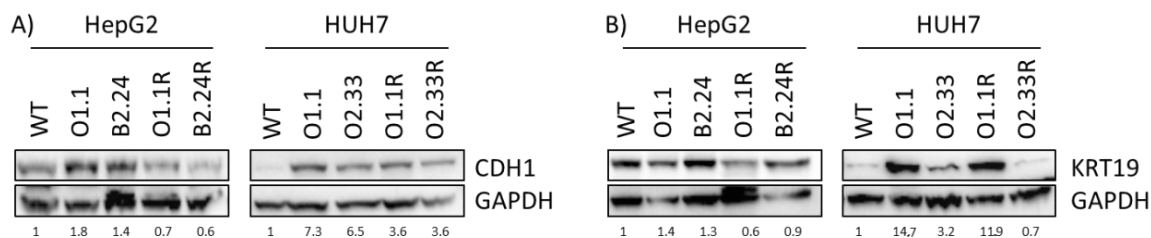


Figure 47: **Protein levels of A) CDH1 and B) KRT19 in wildtype (WT), knockout and rescue (R) HepG2 and HUH7 cells.** All samples were quantified for bands relative to the GAPDH loading control and expressed in fold wildtype (WT). As the GAPDH loading control indicates, the HepG2 blot A) is the same as Figure 30 and the KRT19 blots (B) are the same as Figure 39.

In summary, the restoration of BCORL1<sup>WT</sup> expression showed that the effects of BCORL1 knockout on tumor biology, as well as gene regulation, are reversible. Rescue of BCORL1 in knockout clones by transfection with an EGFP-tagged BCORL1<sup>WT</sup> reversed the stem cell-like morphology of HepG2 and HUH7 knockout cells and increased proliferation. Furthermore, clonogenicity decreased. The known target gene *CDH1*, which was reactivated by knockout of BCORL1, demonstrated decreased expression after restoration of BCORL1<sup>WT</sup> expression. This was also the case for the newly identified target gene *KRT19*. The inverse effects of rescue and knockout corroborated the role of BCORL1 as a regulator of stemness through KRT19.

## 5. DISCUSSION

---

Even though hepatoblastoma is the most common childhood liver cancer, it is still poorly understood. The prominent theory of tumorigenesis is based on differentiation errors of immature hepatocyte precursors. Deregulated pathways like the WNT-, IGF2- and hedgehog signaling pathway, genetic syndromes, and/or mutations can contribute to development and progression of hepatoblastoma. Due to a very low mutation rate, the only recurrent mutations identified so far, are in *CTNNB1*, *NFE2L2* and *TERT* genes.

In this study, we identified *BCORL1* mutations in 5 % of hepatoblastoma cases and uncovered the role of *BCORL1* in gene regulation and the resulting tumor biology. Our correlative data suggests *KRT19* as a target gene of *BCORL1*, through which *BCORL1* regulates stemness. Moreover, we demonstrated the reversibility of *BCORL1* LOF mutation effects and thus, revealed the clinical relevance of *BCORL1* mutations.

### 5.1. Mutations

---

With a mutation rate of 5 %, *BCORL1* is number four of the most common mutated genes in hepatoblastoma. The four identified *BCORL1* mutations are at different loci and result in different protein changes. The T4 and HepT1 mutation cause only an amino acid change and deletion without potential to cause damage to any known functional unit according to PROVEAN [185]. The T6 and T528 mutation are both truncating frameshift mutations (Figure 8). Interestingly, both patients have been tested positive for the aggressive C2 subtype of the 16-gene signature, including strong overexpression of *KRT19*. The immature C2 pattern indicates a hepatic stem-cell like phenotype of these tumor cells [33]. The patients also suffered from metastases, thus were marked high-risk hepatoblastoma by SIOPEL [26, 30] and received chemotherapy.

The T6 mutation is located between CtBP-binding site and the nuclear location signal (Figure 8). The CtBP-binding site is not affected, but the nuclear location signal, LxxLL motifs, ankyrin repeats, and PUFD domain get lost [140, 152]. The loss of the nuclear location signal denies *BCORL1* the access to the nucleus and causes *BCORL1* to accumulate outside the nucleus as shown in Figure 9. The *BCORL1* mutation in patient T528 only causes the loss of the PUFD domain [152] and one LxxLL motif, which normally facilitates the nuclear receptor recruitment [140, 186]. Loss of the LxxLL motif was shown to disturb IRF-1 dependent growth inhibitory activity in colon carcinoma and non-small cell lung carcinoma cell lines [187] and could also have an impact on growth of these tumors.

Due to the loss of the PUFD domain in both cases, *BCORL1* is also not able to bind PCGF1 anymore and thus cannot associate with Pcg proteins to form PRC1.1 [138]. PCGF1 was previously reported to be required for ESC differentiation [188]. With the immature C2 pattern, the T6 and T528 tumor cells are suspected to have the hepatic stem-cell like phenotype [33]. Thus, the inability to bind PCGF1 and

## DISCUSSION

thereby PRC1.1, due to the truncating mutations, could be the reason for the global deregulation, resulting in an immature pattern.

For further investigation of the role of BCORL1 in hepatoblastoma, it was crucial to have a model system for BCORL1 loss. Accordingly, we constructed cell lines with a truncated version of BCORL1, mediated by CRISPR-Cas9. This truncated BCORL1 missed the PUFD domain, the nuclear location signal, as well as the CtBP-binding site. These knockout cells clearly demonstrated that the loss of BCORL1 had dramatic effects. One of these effects is the complete morphological rearrangement, as suggested by the induction of a stem cell-like morphology in HepG2 and HUH7 cells (Figure 21). Depletion of PCGF1 alone is not able to cause any morphological changes [189], but depletion of CtBP can cause EMT deficiencies [154, 158]. The observed phenotypic changes are not the result of just one missing protein-protein interaction, but are probably caused by the inability of recruiting PRC1.1 and/or CtBP and thus, global rearrangements.

Moreover, we observed decreased proliferation in HepG2 and HUH7 cells (Figure 23), coinciding with findings of decreased proliferation in case of *CtBP* depletion in fibroblasts [154, 190]. Contrary to these effects, the depletion of *PCGF1* alone does not affect cell viability [189]. One of the potential target genes of BCORL1 that we identified is *KRT19*. Coincidentally, a recent study showed that *KRT19* expression inversely regulates proliferation in breast cancer cells. Moreover, Ju *et al.*, demonstrated that *KRT19* silencing abolished colony formation [182]. The induction of a stem cell-like phenotype and the decreased proliferation upon BCORL1 LOF are accompanied by an increased clonogenicity in HepG2 and HUH7 cells (Figure 24). These stem cell characteristics could indicate that the knockout cells behave like embryonal/hepatic stem or progenitor cells. *PCGF1*, as well as *CtBP2* were previously shown to be a crucial part of ESC differentiation [188, 191, 192]. The observed effects towards stem cell behavior indicate that this common role of *PCGF1* and *CtBP2* might be due to the combined regulation. Due to the truncating mutations, BCORL1 is not able to associate with the PRC1.1 and/or CtBP, leading to reactivation of target genes like *KRT19*, which then suppress proliferation and increase colony formation.

However, none of these proteins directly regulates any of the observed effects on tumor biology but both are part of a PRC1.1. Hence, potential target genes of BCORL1 needed to be identified and examined for the ability to induce such effects. Furthermore, we addressed functional relevance by restoration of BCORL1<sup>WT</sup> expression and were able to reverse all the observed effects on tumor biology as well as gene regulation. Since our findings demonstrated that BCORL1 loss led to stem cell characteristics, we assume that tumor cells harboring BCORL1 mutations might also show higher resistance to chemotherapeutical treatment like other cancer stem cells [193]. Unfortunately, the

## DISCUSSION

resistance provided by cancer stem cells makes using a higher dosage of chemotherapy pointless, but increases the therapeutic burden and thus, increases the occurrence of side and long-term effects.

However, the findings within this study suggest future treatment options for hepatoblastoma cases with BCORL1 mutations by restoring the normal BCORL1 function. We demonstrated the possible reversion of the stem cell-like behavior of these tumor cells. Using this approach in a clinical setting could dramatically ease the burden of chemotherapeutical treatment.

### **5.2. Target genes of BCORL1**

---

The previously identified target gene *CDH1* [140] is known to play major roles in cell adhesion upon interacting with  $\beta$ -catenin [194]. *CDH1* expression is regulated by BCORL1, CtBP and PCGF1 [140, 195, 196]. These proteins might act together in repressing *CDH1* in form of the PRC1.1, but were also shown to have an individual effect on *CDH1* (Figure 29) [140, 195, 196]. Interestingly, we found in our functional annotation analysis other adhesion-related genes belonging to the functional group “plasma membrane”, such as *CDH24*, *ESAM*, *EPCAM*, *TDGF1* and *KRT19*, which were highly enriched in the group of differentially expressed genes between knockout and wildtype cells (Figure 33). *CDH24* belongs to the group of cadherins [197], but is mostly uncharacterized [197]. Even though, *CDH24* was previously associated with gastric and colorectal cancers [198], our results could not definitely confirm *CDH24* as a target gene of BCORL1, because it did not meet all the criteria, meaning clearly increased expression and H3K4me3 levels and/or decreased K27me3 levels in the HepG2 and HUH7 knockout clones. Moreover, there are no previous reports of *CDH24*, being involved in any of the observed effects on tumor biology.

Upregulation of the immunoglobulin-like transmembrane protein *ESAM* [180] was reported to be relevant in metastatic lung tumors. Cangara *et al.*, connected the expression of *ESAM* to metastatic adenocarcinoma of the lung and the induction of migration, but did not report any effects on proliferation [199]. Moreover, high *ESAM* expression was associated with a subset of human leukemias [200] and increased expression was found in tumor vessels of head and neck squamous cell carcinoma and colorectal carcinoma [201]. Contrary to these reports, in case of the BCORL1 knockout, no induction of migration was observed, but reduced proliferation. These tumors differ strongly from the hepatoblastoma. Hence, we presume that the increased *ESAM* expression is not responsible for the decreased proliferation of the BCORL1 knockout cells. *EPCAM* mediates  $\text{Ca}^{2+}$ -independent adhesion [181] and is known to promote an aggressive tumor phenotype in HCC [183, 202]. Moreover, *EPCAM* was associated with promotion of proliferation [33, 203, 204], contrary to our results. Parallel to the decrease of proliferation, we detected an increase in *EPCAM* expression upon BCORL1 knockout (Figure 23) and therefore proliferation might be regulated via other target genes or a byproduct of the induction of the stem cell-like features observed (Figure 21, Figure 24). *ESAM* and *EPCAM* are not

## DISCUSSION

exclusively associated with the functional group plasma membrane, but also with stemness [183, 200]. Thus, the increased expression of *ESAM* as a result of BCORL1 knockout could induce increased clonogenicity (Figure 24) as it was shown for hematopoietic stem cells [200]. More convincingly is the relationship of *EPCAM* and stemness. Munz *et al.*, demonstrated a clear effect on colony formation upon *EPCAM* knockdown [203]. Moreover, multiple studies describe a relationship between *EPCAM* and cancer stem cells [183, 184, 204-206]. Hence, *EPCAM* might be involved in the development of stem cell-like features upon BCORL1 knockout.

Further investigation of plasma membrane-related genes exposed differential expression of *TDGF1* and *KRT19*, which are also related to stemness [205, 207]. The membrane bound *TDGF1* [208] plays a role in normal stem cells as well as cancer stem cell populations contributing to early cancer progression [209, 210]. Moreover, *TDGF1* expression is associated with poor prognosis and known to promote tumor resistance in HCC [211, 212]. Karkampouna *et al.*, demonstrated the induction of a more aggressive phenotype with stem cell characteristics upon overexpression of *TDGF1* in HepG2 cells [211]. Unfortunately, *TDGF1* did not meet all the criteria for being a valid target gene, even though we observed similar induction of stem cell characteristics, as mentioned before.

Finally, *KRT19* demonstrated to be a valid target gene of BCORL1. The expression pattern as well as the enrichment pattern of H3K4me3 and H3K27me3 changed as expected upon BCORL1 knockout. Coinciding with our findings, increased expression of *KRT19* expression was previously associated with hepatobiliary cancers [183, 213] and a hepatic stem cell-like phenotype [33]. *KRT19* revealed increased expression upon BCORL1 knockout as well as the other candidate genes, but also decreased expression upon restoration of BCORL1<sup>WT</sup> expression (Figure 46, Figure 47). Previously, *KRT19* was reported to suppress proliferation and enhance colony formation in breast cancer [182]. These findings corroborate the theory that reactivated *KRT19* expression due to BCORL1 loss is responsible for the observed effects on tumor biology. In line with other stem cell markers, *KRT19* is highly expressed in hepatic progenitor cells and liver cancer stem cells [202, 214]. Hence, increased expression of *KRT19* could induce stem cell or progenitor cell characteristics upon knockout of BCORL1.

Interestingly, the hepatoblastoma cell line HUH6 did not show any changes in morphology (Figure 21) or *CDH1* reactivation (Figure 29) upon BCORL1 knockout. The analysis of differentially expressed genes pointed out that the HUH6 cell line showed completely different expression patterns than all the other cell lines or even the normal liver tissue sample (Figure 31). Two genes connected to *CDH1* expression showed highly increased expression in HUH6 cells, compared to the normal liver tissue sample, HepG2 and HUH7 cells. These genes were *CtBP2* and *RING1B* (Figure 31). CtBP is known to partially mediate *CDH1* repression in a BCORL1-dependent manner [140], but most literature does not distinguish between CtBP1 and CtBP2 due to their closely related functions [162]. Recently, some

## DISCUSSION

research groups have started to distinguish between their individual functions [192, 195, 215]. Thus, it might be possible that *CDH1* repression is partially mediated by CtBP2 without BCORL1 [140]. More interesting is the differential expression of *RING1B*. BCORL1 is known to associate with the PRC1.1 [142-145] and RING1B as component of the PRC1.1 complex, which negatively regulates other stemness related genes like *NANOG* in embryonal carcinoma cells and mouse ESC [216, 217]. We also found increased *NANOG* expression (data not shown) upon BCORL1 knockout. Hence, upregulation of this stemness-related gene upon BCORL1 knockout corroborates the theory that BCORL1 together with PRC1.1 regulates the expression of *KRT19* and eventually also *ESAM*, *EPCAM*, and *TDGF1* in hepatoblastoma cells. RING1B is not exclusively associated with PRC1.1, but is also part of other PRC1 complexes [138]. One of these complexes is PRC1.2, which is defined by association with PCGF2. PCGF2 was recently shown to compensate loss of PCGF1 due to its enzymatical engagement of the same target sites in the absence of the other [189]. Moreover, PCGF2 target annotation revealed terms such as epithelial cell differentiation and embryonic pattern specification in HEK293 [143], which include the indirect target *CDH1*. *CDH1* expression is regulated through repression of the *CDH1*-repressors ZEB1/2 [218]. Hence, the highly increased expression of *RING1B* and the missing reactivation of *CDH1* and stemness-related target genes in HUH6 cell line (Figure 31) suggest that RING1B in fact represses these genes in association with PRC1.2. The above explained connections are depicted in Figure 48.

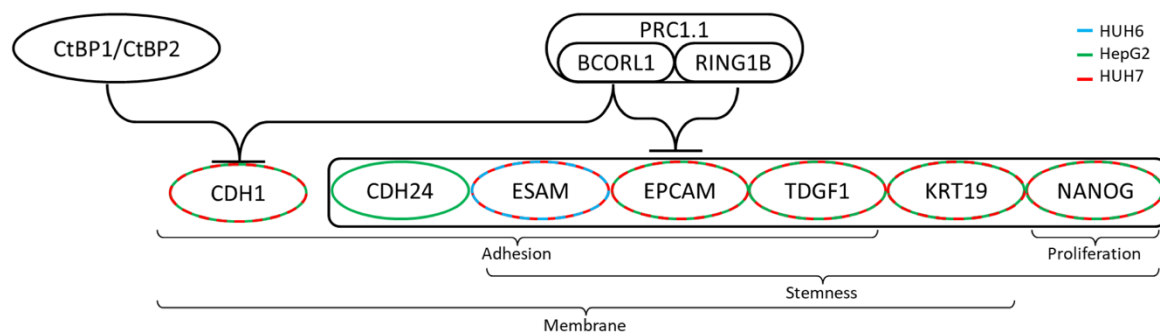


Figure 48: Hypothetical relational network of BCORL1.

### 5.3. Perspectives and future plans

Within this study, a novel antibody for BCORL1 was established. This antibody should be used for conformation of the identified target genes by direct ChIP-seq. In addition, it would be of interest to further investigate the regulatory network of BCORL1. Luciferase assays could potentially bring up new insights on direct or indirect interactions of BCORL1 with certain target gene promoters. Furthermore, re-ChIP could determine which gene is regulated in association with CtBP1/2 or PRC1.1. Additional knockout studies of CtBP1/2 and/or inhibition of PRC1.1 and PRC1.2 members might also determine which other proteins are actually needed for BCORL1 regulation of target genes and how it would

## DISCUSSION

affect for example the HUH6 cell line if PRC1.2 would not compensate BCORL1 and thus result in PRC1.1 function loss.

Another aspect to be investigated is the observed tumorigenic effects. It is crucial to know if the identified target genes are actually responsible for the induction of the stem cell-like morphology, the decreased proliferation, and the increased clonogenicity. Hence, these target genes should be used for siRNA/CRISPR-Cas9 mediated knockdown/knockout to discover evidence on which target genes are responsible for these effects. In general, the newly identified as well as additional target genes of the ChIP-seq have to be investigated for their tumorigenic effects in hepatoblastoma.

We showed that BCORL1 regulates the expression of stemness related target genes. It is known that cancer stem cells respond worse to chemotherapy or are even resistant to it. We presume that BCORL1 mutations can actually lead to cancer cells with stem cell properties. The two patients with truncating BCORL1 mutations were both identified as high-risk hepatoblastoma, due to metastases and the C2 subtype of the 16-gene signature. Thus, these patients suffer from intense chemotherapeutical treatment. Restoration of BCORL1<sup>WT</sup> expression could have beneficial effects for these patients by lessening the intensity of the chemotherapy. BCORL1 is also known to be mutated in other cancers, like AML or intracranial germ cell tumors. If BCORL1 induces stem cell-like behavior in these cancers as well, restoring BCORL1<sup>WT</sup> expression could also show perspectives for other patients.

## 6. SUMMARY/ZUSAMMENFASSUNG

---

### 6.1. Summary

---

With an incidence rate of one in a million children, hepatoblastoma is the most common pediatric liver tumor. The surgical resection indeed promises a cure, but is often not possible. In lots of cases, the tumor is identified in late stages and therefore only treatable in combination with chemotherapy. Due to the unknown origin of hepatoblastoma, targeted therapy is not possible. However, certain factors were identified, which influence development and tumor progression. Besides genetic syndromes and variations in cancer-associated signaling pathways like WNT, IGF2, or Hedgehog, these factors include sporadic mutations in *CTNNB1*, *NFE2L2*, and *TERT*.

Exome sequencing of hepatoblastoma samples revealed one previously unknown mutation in the *BCORL1* gene. *BCORL1* is a transcriptional corepressor, which is associated with the PRC1.1 complex. Sanger sequencing of additional hepatoblastoma samples, TLCTs, and cell lines led to the identification of further mutations of the *BCORL1* gene. For functional analysis, HEK293 cells were transfected with a plasmid containing an EGFP-tagged version of the mutated *BCORL1*. In turn, this revealed a complete loss of function in case of one mutation due to the inability to translocate to the nucleus and therefore emphasized the need for further investigation of the role of *BCORL1* in hepatoblastoma.

Hence, hepatoblastoma cell lines were used for targeted mutagenesis of the *BCORL1* gene by the CRISPR-Cas9 system in order to generate a loss-of-function model. Two clones of each cell line with mutations in different loci of *BCORL1* were selected to exclude target-dependent effects. In order to detect the truncated version of *BCORL1*, a custom-made antibody was established due to the insufficiency of commercially available antibodies in hepatoblastoma cells. After successful establishment of the new antibody, the truncated *BCORL1* and the missing translocation to the nucleus were detected. The mutagenesis had serious effects on tumor biology. Four out of eight clones showed induction of a stem cell-like morphology instead of a flat growth pattern. Furthermore, six of the clones demonstrated strong decreases in proliferation. Clonogenicity on the other hand strongly increased in comparison to the parental cell lines.

To uncover the molecular context of these effects, the effects of *BCORL1* knockout on gene regulation were examined by global RNA and ChIP sequencing. This led to the identification of the candidate target genes *CDH24*, *ESAM*, *EPCAM*, *TDGF1*, *NANOG*, and *KRT19*, which are associated with adhesion and/or stemness. *KRT19* was also investigated on protein level in comparison to the wildtype cell lines and found to be increased.

Furthermore, we investigated the reversibility of the effects on tumor biology and gene regulation. Thus, restoration of the wildtype *BCORL1* expression was performed by transfection of the knockout

## SUMMARY/ZUSAMMENFASSUNG

clones. The investigation of morphology, proliferation and clonogenicity not only demonstrated to be reversible, but also the examination of target genes.

In summary, we demonstrated the role of BCORL1 in regulation of adhesion and stemness-related genes and identified associated target genes. Regarding tumor biology, functional loss of BCORL1 was associated with serious consequences, which proved to be reversible and thus might aid future anti-tumor therapies.

### 6.2. Zusammenfassung

---

Das Hepatoblastom ist mit einer Häufigkeit von einem aus 1 Million Kindern der häufigste pädiatrische Lebertumor. Die vollständige chirurgische Resektion verspricht zwar Heilung, jedoch ist dies oft nicht direkt möglich. In vielen Fällen werden diese Tumore erst in späten Stadien erkannt und sind daher nur in Kombination mit einer Chemotherapie behandelbar. Da der Ursprung des Hepatoblastoms größtenteils unbekannt ist, kann leider keine gezielte Ursachenbekämpfung erfolgen. Allerdings sind Faktoren bekannt, die Entwicklung und Fortschreiten des Tumorwachstums beeinflussen. Zu diesen gehören neben genetischen Syndromen und Veränderungen bekannter Krebs-assozierter Signalwege wie WNT-/IGF2-/Hedgehog-Signalweg, sporadische Mutationen in den Genen *CTNNB1*, *NFE2L2* und *TERT*.

Ein Exom-Sequenzierprojekt von Hepatoblastomproben ergab neben den bereits bekannten Genen auch eine Mutation in dem *BCORL1* Gen. *BCORL1* ist ein transkriptioneller Ko-Repressor, der mit dem Polycomb Repressiven Komplex PRC1.1 assoziiert ist. Durch Sanger-Sequenzierung von weiteren Hepatoblastomproben, transitionellen Lebertumoren und Zelllinien konnten weitere *BCORL1*-Mutationen identifiziert werden. Um diese Mutationen funktionell zu untersuchen, wurden HEK293 Zellen mit Plasmiden transfiziert, die die mutierten Varianten von *BCORL1* gekoppelt an ein GFP exprimieren. Dies zeigte den kompletten Funktionsverlust einer Mutation an, da diese Variante nicht mehr befähigt war, in den Nukleus zu translozieren und betonte die Dringlichkeit weiterer Forschung in Bezug auf die Rolle von *BCORL1* in Hepatoblastomen.

Daher wurden Hepatoblastomzelllinien mit Hilfe des CRISPR-Cas9 Systems einer Mutagenese unterzogen, um ein *loss-of-function* Modell zu kreieren. Für jede der vier Zelllinien wurden zwei Klone ausgewählt, welche an unterschiedlichen *BCORL1*-Loci mutiert waren, um Lokus-abhängige Effekte auszuschließen. Um die verkürzte Form von *BCORL1* nachzuweisen, musste ein eigens generierter Antikörper etabliert werden, da die kommerziell verfügbaren Varianten für die Detektion in Hepatoblastomzellen leider unzureichend waren. Nach erfolgreicher Etablierung des neuen Antikörpers konnte die verkürzte Variante von *BCORL1* und deren fehlende Translokation in den Nukleus gezeigt werden. Die Mutagenese bewirkte ebenfalls gravierende Effekte bezüglich des tumorbiologischen Verhaltens. Vier der acht Klone zeigten eine stark veränderte Morphologie. Anstatt

## SUMMARY/ZUSAMMENFASSUNG

des normalen, einschichtigen Wachstums zeigten diese Klone die Induktion einer Stammzell-ähnlichen Morphologie. Darüber hinaus war in sechs von acht Klonen eine starke Reduktion der Proliferationsrate ersichtlich. Zudem stieg auch der prozentuale Anteil neu gebildeter Kolonien in allen Klonen stark an gegenüber den Wildtypzelllinien.

Um die molekularen Zusammenhänge dieser Effekte nachvollziehen zu können, wurden die Folgen der BCORL1 Mutagenese auf Genregulation mittels globaler RNA und ChIP Sequenzierung untersucht. Hierbei wurden die möglichen Zielgene *CDH24*, *ESAM*, *EPCAM*, *TDGF1*, *NANOG* und *KRT19* identifiziert, die mit Adhäsion und/oder *stemness* zusammenhängen. Als wahrscheinlichstes Zielgen wurde *KRT19* zusätzlich auf Proteinebene in den Knockout-Klonen im Verhältnis zur jeweiligen Wildtypzelllinie untersucht und erhöhte Mengen festgestellt.

Des Weiteren wurde die Reversibilität dieser Effekte untersucht. Dafür wurde die Expression von Wildtyp-BCORL1 durch Transfektion der knockout Klonen wiederhergestellt. Sowohl die Untersuchung von Morphologie, Proliferation und klonogenem Wachstum als auch die Untersuchung der Zielgene bestätigte die Reversibilität der beobachteten Effekte.

Zusammenfassend wurde BCORL1 eine Rolle in der Regulation von Adhäsion- und *stemness*-assoziierten Genen zugeschrieben und dazu gehörige Zielgene identifiziert. Ein Funktionsverlust von BCORL1 wurde assoziiert mit dramatischen Folgen bezüglich Tumobiologie, welche jedoch reversibel sind und daher die Möglichkeit einer zukünftigen Tumortherapie anbieten.

## 7. APPENDIX

Table 4: List of BCORL1 supernatants

#	Supernatant	Reactivity	Secondary antibody
1	4B2	R2A	IgG2a
2	5B1	R2A	IgG2a
3	5C3	R2A	IgG2a
4	5F10	R2A	IgG2a
5	6C11	R2A	IgG2a
6	6D4	R2A	IgG2a
7	6E4	R2A	IgG2a
8	6G1	R2A	IgG2a
9	7G6	R2A	IgG2a
10	8A8	R2A	IgG2a
11	8B12	R2A	IgG2a
12	8C9	R2A	IgG2a
13	8D11	R2A	IgG2a
14	8H11	R2A	IgG2a
15	9D7	R2A	IgG2a
16	10B8	R2A	IgG2a
17	10C10	R2A	IgG2a
18	1D1	R2A	IgG2a
19	12A5	R2A	IgG2a
20	12G8	R2A	IgG2a
21	13E10	R2A	IgG2a
22	14F7	R2A	IgG2a
23	16A4	R2A	IgG2a
24	16A11	R2A	IgG2a
25	18E10	R2A	IgG2a
26	19A4	R2A	IgG2a
27	20G1	R2B	IgG2b
28	3E6	R2A	IgG2a
29	1H3	R2C	IgG2c
30	1H2	R2C	IgG2c
31	17H7	R2C	IgG2c
32	19H7	R2C	IgG2c
33	1H1	R2C	IgG2c
34	1B11	RG1	IgG1
35	1C8	RG1	IgG1
36	3G11	RG1	IgG1
37	4F9	RG1	IgG1
38	9H11	RG1	IgG1
39	13B11	RG1	IgG1
40	15A5	RG1	IgG1
41	1F11	R2C	IgG2c
42	2F4	R2C	IgG2c
43	4G1	R2C	IgG2c
44	5D9	R2C	IgG2c
45	5E11	R2C	IgG2c
46	8G9	R2C	IgG2c
47	11G10	R2C	IgG2c
48	18G2	R2C	IgG2c
49	19F3	R2C	IgG2c
50	19H9	R2C	IgG2c
51	1D8	R2C	IgG2c
52	2B5	R2C	IgG2c

53	2D2	R2C	IgG2c
54	3D10	R2C	IgG2c
55	9B3	R2C	IgG2c
56	9D1	R2C	IgG2c
57	13C2	R2C	IgG2c
58	17F12	R2C	IgG2c
59	19E11	R2C	IgG2c
60	20E2	R2C	IgG2c
61	3A8	R2C	IgG2c
62	3C9	R2C	IgG2c
63	4C8	R2C	IgG2c
64	5C5	R2C	IgG2c
65	7A5	R2C	IgG2c
66	11C10	R2C	IgG2c
67	12C11	R2C	IgG2c
68	16C8	R2C	IgG2c
69	18C8	R2C	IgG2c
70	20H3	R2C	IgG2c
71	2A5	R2C	IgG2c
72	3A9	R2C	IgG2c
73	5A8	R2C	IgG2c
74	9B12	R2C	IgG2c
75	10A8	R2C	IgG2c
76	10C5	R2C	IgG2c
77	13A7	R2C	IgG2c
78	15A4	R2C	IgG2c
79	18A12	R2C	IgG2c
80	23A11	R2C	IgG2c
81	20C2	R2C	IgG2c
82	5D1	R2B	IgG2b
83	12B3	R2A	IgG2a
84	22F3	R2A2C	IgG2a, IgG2c
85	9C3	R2A2C	IgG2a, IgG2c
86	5E2	R2A	IgG2a
87	11B3	R2A2C	IgG2a, IgG2c
88	17F2	R2A2C	IgG2a, IgG2c
89	23F6	R2A2C	IgG2a, IgG2c
90	20C9	R2A2C	IgG2a, IgG2c
91	14A8	R2C	IgG2c
92	13B7	R2A2C	IgG2a, IgG2c
93	5E4	R2A2C	IgG2a, IgG2c
94	20E11	R2B	IgG2b
95	2H10	R2A2C	IgG2a, IgG2c
96	13B5	R2A2C	IgG2a, IgG2c
97	8E6	R2C	IgG2c
98	1D8	R2B	IgG2b
99	18H9	R2C	IgG2c
100	11C11	R2A2C	IgG2a, IgG2c
101	12A3	R2A2C	IgG2a, IgG2c
102	18C6	R2A2C	IgG2a, IgG2c
103	14A6	R2A2C	IgG2a, IgG2c
104	19D5	R2B	IgG2b
105	13H7	R2A2C	IgG2a, IgG2c

## APPENDIX

Table 5: GO terms of DAVID analysis of reactivated genes after BCORL1 knockout in HepG2 and HUH7 clone O1.1.

Term	Genes
cell division	ITGB3BP, SEPT3, CDC14A, CUZD1, FAM83D, ATAD3B, OIP5, MIS18A, CCSAP, KLHL21, TPR, CDCA5, CCNO, CCNA2, CDCA4, CDCA3, CDC7, CDC6, ARHGEF2, KIF11, DSN1, LIG1, CCNF, DYNLT3, LIG4, HEPACAM2, TACC3, MCM5, NCAPD3, TACC1, MAD2L1, SPAG5, ZWINT, CDK11B, ARL8A, FBXL7, MAD2L2, CKS1B, BRSK2, CDC73, CHEK2, RCC1, SPC24, SPC25, NCAPH, MAP10, PMF1-BGLAP, APITD1-CORT, NCAPG2, FIGN, BUB1, SKA3, SKA1, HELLS, NUDC, SEPT14, CENPF, CDC20, CDC25C, MISP, SMC2, CDC25B, CCNB1, FAM64A, CCNB2, PHF13, USP44
positive regulation of GTPase activity	RAB3GAP2, FGF9, FGF17, PREX1, RGL3, ARHGAP19, RASGEF1C, MCF2L, ARHGAP4, ARHGAP6, GRIN2B, GRIN2C, STARD8, RAPGEF6, SHC1, ARHGAP11A, EIF2B3, ERF1, EGFR, F11R, ARHGEF2, ARHGEF19, SIPA1L2, PSD3, ARTN, ACTN2, CCL4L2, FGF22, DEPDC1, ARHGEF9, CD40, FGF20, ARHGEF12, ARHGAP23, CDKL5, ELMO1, ARHGEF11, ACAP3, SBF2, JUN, PDGFRB, SRGAP1, FGD2, CCL3, CCL2, RAP1GAP, ERBB4, ASAP3, RCC1, GCG, MYO9A, DENND2C, ADCYAP1, CCL25, DOCK2, CCL23, PLEKHG1, PLEKHG7, RASGRP4, RASGRP1, TEK, RASGRP2, PLEKHG5, CAMK2B, IL2RG, AGRN, RAP1GAP2, RASA3, INPP5B, FGD6, CAMK2A, CDC42EP3, ARHGEF10L, ARHGDIB, LAMTOR5, OBSCN, GNAO1, ARHGEF38, ARHGEF37, SRGAP2C, DOCK9, S100A10, DOCK8, VAV1, DOCK3, DENND1B, FZD10, RGS5, RGS6, HBEGF, RAP1A, RGS7, RGS9, ARHGAP10, BCAR3
cell proliferation	RETNLB, TSPAN1, CDC14A, E2F8, CUZD1, AURKB, FER, TXLNA, MCM10, PRDX1, TGFB2, FAM83D, KDM1A, GFI1B, FAM83A, INSIG1, TGFA, GNG2, ROS1, IL1A, OCA2, CYR61, EGFR, NANOG, KIF15, CD160, LIG4, TACC3, TACC1, GLUL, CHRM3, CDK11B, FBXL7, MDM4, EMP2, MELK, MIA, CKS1B, ACHE, ERBB4, CSF1, MAP4K1, TYMS, RASGRP4, BCL2, ENTPD5, BUB1, LHX9, NUDC, CSF1R, GNAT1, CRIP1, MKI67, NASP, CENPF, SKI, DACH1, CDC25C, EPS15, PPP1R8, H3F3A, MPL, LRP2
cell adhesion	ITGB3BP, NRP2, ATP1B1, MYBPC2, CLSTN1, PCDHA1, FER, MMRN1, KIAA1462, CD44, CSF3R, IZUMO1, KIRREL2, CYR61, F11R, ADGRE1, CLCA2, PTPRF, IZUMO1R, EFNB2, ACTN2, PTPRU, SIGLEC14, SSPO, SIRPA, CD36, HEPACAM, LSAMP, CX3CR1, CNTN3, CD226, EMP2, PARVB, ACHE, CCL2, CYP1B1, ITGB4, ITGA11, DSCAML1, ITGA10, CLDN10, SPOCK1, CDH4, VCAM1, SEMA5A, IGSF11, LAMB3, LGALS3BP, ITGB8, ITGB7, COMP, COL6A2, CD2, CD4, SSX2IP, COL8A1, SELPLG, APBA1, THBS3, HAPLN1, LPP, HCK, STAB2, COL16A1, TINAGL1, TINAG, ADGRG1, COL5A1, LAMA1, CASS4, EPHA8, CD58, TROAP, PDZD2, FEZ1
basolateral plasma membrane	KCNC2, FXYD2, ATP1B1, NKD2, CLDN19, ERBB4, LEPR, RHBG, DSTYK, EPCAM, P2RY6, NOD2, ATP2B4, DISP1, CD46, P2RY1, TEK, TGFA, DLG3, CEACAM5, MSN, DLG2, EGFR, MYO1A, LPO, SLCO4C1, SLC8A2, SLC22A7, SLC22A8, ANXA1, FRMPD2, STXBP3, ATP1A1, IL6R, ATP7A, KCNJ4, CA9, CHRM3, OTOF, SLCO1B1, ST14, SLC41A1, ANXA13, MAP7, SLC9A1
apical plasma membrane	KCNC2, ATP1B1, OCLN, LZTS1, DUOX2, DUOX1, DSTYK, AMOTL1, SLC52A3, EPCAM, SLC2A5, SLC2A2, TDGF1, TRPV5, RAPGEF6, ATP8B1, MSN, RAB27B, CHRFAM7A, DPEP1, USH2A, MUC13, KCNMA1, EGFR, PLD1, STXBP3, IL6R, ADRB2, CD36, PDGFRB, VAMP3, EMP2, CPO, SHROOM2, PKHD1, OXTR, NAALADL1, P2RY6, AKR1A1, TEK, P2RY1, SCNN1B, MUC1, GNAT1, MYO1A, SLC12A3, SI, ANXA1, ATP1A1, UPK3A, SLCO2B1, EPS15, TMEM114, ANXA13, AHCYL1, LRP2, SLC14A2, SLC9A1
plasma membrane	SLC9A9, SGMS2, CROCC, SLC9A2, GRIN3B, MYLIP, KIAA0319L, SLC52A3, GNG8, ADTRP, GRIN2B, GRIN2C, GNG2, ADAM8, GNG4, CDCA5, GNG5, ROS1, CDH24, CLCA2, PTPRF, PIK3CD, F8, CDHR4, COLEC12, LIG4, PTPRU, HLA-DQA2, SIRPA, MARK1, HLA-DQA1, ERMAP, SSTR5, SSTR3, SSTR1, F3, KIAA1524, ST14, ROR1, RYR2, MST1R, SLC30A10, PMP22, DOC2B, CD226, HLA-DRA, ADSS, LY6G6F, ERBB4, LY6G6C, KCNJ3, OR52N2, OR56B4, RAC2, KLB1, AHNAK2, CDC42EP3, SLC28A1, TECTA, EPM2A, ATP11A, PCDH19, DVL1, KCNJ5, BTBD17, KCNJ4, ARF1, CD207, RGS5, RGS6, RGS7, SYTL2, RGS9, SYTL1, SLC9A1, GPR84, KCNAB3, ATP10B, KCNAB2, GLRA1, MARCKSL1, USH1G, GLRA3, GLRA2, UNC93A, NOD2, KISS1R, SMPDL3B, MAPT, TRPV5, GUCY1A2, SNAP47, DPEP1, STX6, CLMP, PIK3C2A, SLC22A7, PIK3C2B, SDK2, SLC22A8, IL6R, ELMO1, EPB41L3, MAST2, CLIC4, PLXDC1, CLIC6, KCNH6, GRIP2, KCNH8, TNFSF12-TNFSF13, THEM4, PARVB, KCNH4, RASD2, KCNH5, EXOC8, GPR63, FFAR2, CSF1, FPR1, IGSF11, PLEKHG5, PCSK9, SLC4A9, HTR3A, HTR3B, PHLDA3, HSD17B7, ACSL6, ABCA12, FLRT2, SLC8A1, CNST, SLC8A2, DGKK, STAB2, CAPN2, TMPRSS6, PLG, SDHB, WNT7B, PTP4A2, PRSS27, HBEGF, LRP8, LRP2, KCNC2, GNA14, KCNC1, ENAH, SLCO1B7, TSPAN1, PRC1, SLC44A3, SLC44A5, GRIK4, JAG2, SLC2A7, PACSIN1, SLC2A5, UNC5A, SLC2A2, TDGF1, SLCO1C1, FLVCR1, EGFR, KCND3, ACTN2, C1ORF210, ANKRD13B, C2CD4C, VAMP3, C2CD4A, PTGFRN, EDA, FLAD1, COBL, ACHE, ME3, FGR, FOLH1B, NKAIN1, CDC42SE1, ABCA3, RABGGTB, P2RY6, ECE1, P2RY1, TEK, HCN4, PRIMA1, SDF4, HCN3, EPB41, SYT12, TNFRSF13C, BFSP2, CACNA2D3, SLC02B1, VAV1, CACNA2D2, CACNA2D4, EPS15, ATP7A, P2RX7, P2RX6, COA6, CACNA1G, SLC13A2, RHBDL2, TM4SF20, CACNA1C, DNAJB4, CACNA1D, SLC5A11, CACNA1B, MTNR1A, RHOJ, IGDCC4, CYB5R1, LEPR, PREX1, LRRK8D, DUOX2, GABBR1, DUOX1, MFSD2A, RHOV, RHOU, GPC5, PCDH1, FRMD6, SPINT2, SLC1A7, ANO3, ANO2, DLG3, ANO5, TREH, AHNAK, ANO9, DLG2, PTGER2, TRPM5, IZUMO1R, SLA2, SPINT1, STXBP3, EDAR, SIGLEC14, SLC7A11, LYPD6B, SIGLEC1, ADRB2, RIF1, CA9, CHRM3, STXBP6, LCK, SLC41A1, CNTN3, JAM2, PTAFR, DCC, CD101, APH1A, CLCNKA, C2CD4D, CLCNKB, OXTR, CDH4, ALDH3A1, VCAM1, NDC1, CDH9, HRH4, CD2, CD4, SCNN1B, SELPLG, INPP5B, SCNN1D, SECTM1, GNAO1, SLC12A3, ANXA1, TSPAN13, C4BPB, ASIC1, ANXA3, GDPD2, CYBB, SLC01B1, MEP1B, SMPD3, FEZ1, SLC14A2, SLC36A1, RAB3GAP2, ATP1B1, EFNA1, LYPD8, EFNA3, S100A9, SYT6, CCT3, ATP2B4, CD44, CD46, RAB29, RAPGEF6, IZUMO1, NPSR1, HCAR1, F11R, CD3E, EFNB2, POLE, CD40, KRT19, CCR7, CD36, RAB19, SERBP1, CX3CR1, FER1L5, CCR2, HTR6, PLA2G2A, PDGFRB, EFNA4, RAB13,

## APPENDIX

	ADD2, CLCN1, CATSPERD, ITGA11, STK17B, ITGA10, BDKRB2, GPR142, EPHB2, SEMA5A, EPHB6, ACE, AGRN, EMB, STX11, RAP1GAP2, FCHO1, GNAT1, CNKS1, S100A16, GPR157, TRPC5, CELSR2, EPHA2, ABCG1, GPR153, NOTCH2, EPHA8, CD58, RIT1, NRP2, JPH4, STEAP4, ACVRL1, SUSD2, CDCP1, PCDHA1, KCNJ11, MCF2L, KCNIP4, SLC24A3, TGFA, FANCG, CAP1, CHRFAM7A, IFNLR1, KCNMA1, RXFP4, ADAM11, ATP4A, LY96, CD160, NFAM1, SLIT2, GRM4, GRM2, SEMA4A, PLA2G5, CLDN16, DHH, PRF1, SHROOM2, CA14, PRTN3, SLC39A10, CLDN10, SLC19A3, CLDN11, SLC19A2, GCGR, PLCL1, FAT3, CLEC2A, UGT8, FZD9, SI, CD1C, HSPG2, ATP1A1, GRIA4, FZD2, PTGFR, ITPR3, RAPH1, ITPR1, IYD, KREMEN2, GRIA1, TENM1, DRP2, TJP3, CIT, ABCC8, FAM126B, SLC22A17, OCLN, TUSC3, SLC6A1, HFE2, CNGB1, TLR5, ILDR1, VIPR1, TLR7, GHRHR, WNT1, SLC16A1, GP6, ZNF185, CSF3R, ORC1, SLC04A1, PLXNB3, BASP1, RALGAPA2, LSAMP, LRP11, SLC38A1, EMP2, C1ORF186, SLC38A4, FXYD2, FXYD3, SNAP91, SSH1, HAX1, PAQR6, ITGB4, DSCAML1, PAQR7, EPHA10, TRH, PAQR5, KCNS3, PPP1R16B, SLC30A1, ITGB8, ITGB7, ENTPD3, MFAP3L, TBC1D30, CSF1R, SETDB1, SLC04C1, LPP, CPNE7, ADGRG6, MISP, RAB33A, ADGRG3, CORO1A, RAP1A, CD79A, DIO1, FAM84B, PHEX, IFI6, RSC1A1, ARHGAP10, SLC5A5, TACR2, CXCR1, LGR6, ACVR1C, EPCAM, KCNQ4, VN1R2, TMEM59, PAK3, VN1R5, ATP8B1, ATP8B2, ESAM, SHC1, MSN, KCNQ2, KIRREL2, LTB, AKT3, ATP8B4, RAMP3, LAIR1, PARM1, COL23A1, RAB39B, PRKCG, CD83, BVES, CD82, CEMIP, MELK, PPP1R12B, RHBG, LINGO1, KRT5, RASGRP4, RASGRP1, RASGRP2, SLC39A8, IL2RG, CAMK2B, CAMK2A, ENO1, EDA2R, SPARC, GPRC6A, PARK7, KCNN4, KCNN3, KCNN2, SLC5A9, ANXA13, MPL, ATP8A1
integral component of plasma membrane	SGMS2, EFNA1, EFNA3, SLC52A3, ATP2B4, GRIN2B, CD44, GRIN2C, CD46, NPSR1, ADAM8, CLCA2, PTPRF, CD3E, PTPRG, TRABD2B, EFNB2, PTPRU, CD40, HLA-DQA2, HLA-DQA1, SSTR5, SSTR3, CD36, SSTR1, CCR2, CX3CR1, ST14, HTR6, ROR1, MST1R, EFNA4, CD226, HLA-DRA, CLCN1, BDKRB2, EPHB2, EPHB6, XG, EMB, SLC28A1, TRPC5, ATP13A2, ABCG1, EPHA2, NOTCH2, SEMA6C, EPHA8, CD58, TGFBR3, SLC9A1, GPR84, STEAP4, ACVRL1, GLRA1, GLRA3, GLRA2, PCDHA1, KCNJ11, KISS1R, SLC24A3, TRPV5, TGFA, CEACAM5, RXFP4, ATP4A, SLC22A7, SLC22A8, GRM4, GRM2, KCNH6, KCNH8, TNFSF12-TNFSF13, DEGS1, KCNH5, SLC39A10, FFAR2, FPR1, SLC19A3, GCGR, SLC19A2, BEST4, BEST2, FUT1, SLC4A9, HTR3B, FLRT2, SLC8A1, SLC8A2, LRRN4, TMPRSS9, CD1C, NLGN3, STAB2, ITPR3, PTGFR, OPN5, TENM1, TENM3, HBEGF, OPN3, KCNC2, SLC22A17, TUSC3, TSPAN1, SLC6A1, GRIK4, JAG2, KIAA1324, CNGB1, TLR5, VIPR1, IL17RD, TLR7, SLC16A1, SLC2A5, GP6, SLC2A2, SLC01C1, CSF3R, FLVCR1, SLC04A1, SLC22A25, PLXNB3, SLC38A1, EDA, SLC38A4, FXYD3, EPHA10, ABCA4, P2RY6, LAPTMS, TEK, P2RY1, B3GNT3, SLC30A3, HCN4, HCN3, CSF1R, MUC1, SLC04C1, GPR137B, SLC02B1, ADGRG1, MUC4, ATP7A, P2RX7, P2RX6, SLC13A2, CD79A, PHEX, SLC5A11, MTNR1A, SLC5A5, TACR2, LRRC8D, GABBR1, MFSD2A, LGR6, EPCAM, GPC5, PCDH1, ATP8B1, TIE1, RAMP3, PTGER2, ADGRE1, SLC7A11, CD83, ADRB2, CHRM3, CD82, JAM2, PTAFR, APH1A, CLCNKA, RHBG, CLCNKB, OXTR, TNFRSF8, CDH4, GPR3, PRRG2, C1QTNF1, SLC39A8, CD2, IL2RG, SCNN1B, SELPLG, FAM26D, AMHR2, SLC12A3, EDA2R, TSPAN13, ASIC1, SLC10A5, CYBB, FZD10, SLC01B1, MEP1B, SLC5A9, MPL, SLC14A2
cell surface	KCNC1, ACVRL1, HFE2, SLC6A1, STRC, CLSTN1, GHRHR, EPCAM, WNT1, NOD2, KISS1R, GP6, CD44, GRIN2B, CD46, TDGF1, TGFA, ADAM8, ROS1, EGFR, RAMP3, CIITA, TMEM206, CLMP, SCUBE1, PLXNB3, FGF22, NFAM1, CD40, IL6R, HNRNPU, SLC7A11, SLT2, ADAMTS7, CCR7, CD36, CLIC4, F3, PDGFRB, VAMP4, VAMP3, PTGFRN, MST1R, CD226, EMP2, HLA-DRA, KCNH5, ACHE, TSPEAR, ITGB4, DSCAML1, TIMP2, VCAM1, EPHB6, FOLR2, ITGB8, ITGB7, TEK, P2RY1, CD2, PCSK9, FUT4, TNN, HTR3B, CSF1R, FZD9, PLAT, BMP2, ANXA1, NLGN3, MXRA8, SPARC, ASIC1, GPRC6A, EPHA2, PLG, NOTCH2, FZD10, SRPX2, GRIA1, CD58, KCNN2, SFRP4, HBEGF, TGFBR3, MPL, SLC9A1
cytoplasm	KIFC2, CTHRC1, FHIT, XRCC3, CROCC, AIF1, AMOTL1, CCDC141, PPP1R1B, WDR77, PHTF1, PLS1, RPL11, ZNF664-FAM101A, ADAM8, CCNA2, SDR9C7, CDCA5, LRRK7, YARS, BCL2L14, MYLK3, SPAG1, ESPL1, SCYL3, LIG4, MARK1, ERMAP, BTBD8, GLUL, SSTR3, MSX1, WDR87, SSTR1, SPAG5, KIAA1524, ZWINT, ROR1, ARL8A, GRAP2, DOC2B, TRAPPC3, UNC13A, TP53TG3, RTP3, CPSF3L, CRTC2, DNAH10, ADSS, KIF4A, DNAH12, DNAH14, ACP6, PABPC4, DUSP10, FAM19A2, WARS2, DUSP12, RCC1, SH3BP5L, RAC2, CASZ1, AHNAK2, CDC42EP3, ARHGEF10L, NUDC, FH, SEPT14, MKI67, ARHGEF38, ARHGEF37, EPM2A, MYADML2, TINAGL1, GAS7, EMILIN3, RPS8, BTBD17, AIDA, AKNAD1, RGS5, MAP2, CDC42BPA, TGFBR3, RWDD3, SYTL2, MAP7, RGS9, BTBD11, SLC9A1, APOL5, GAS2L3, BACH2, LZTS1, KCNAB3, ELF3, KCNAB2, NUAK2, MARCKSL1, FGF9, TP63, RNF187, LRRK15, EIF2D, YBX2, DDI2, NOD2, MAPT, SPIB, ERRFI1, USH2A, CCDC28B, CDC7, CDC6, ARHGEF2, PIK3C2A, GMEB1, TNMD, KLHDC1, ARHGEF9, PI4KB, ARHGEF12, TTF2, LRRK26, ARHGEF11, ELMO1, EPB41L3, MAST2, KSR2, CLIC3, CLIC4, FANCD2, HIST2H2BF, CKAP2L, PLXDC1, CLIC5, RRM2, CLIC6, RRM1, C1QL1, TXK, USP24, CLOCK, SRGAP1, REPS2, EXOC8, FGGY, EEA1, TRIM10, ZNF175, TRIM11, NECAB1, TEKT1, PLEKHG5, BUB1, PCSK9, TEKT4, PER3, LYPLAL1, RASA3, ACSL4, HTR3A, PHLDA3, HPGDS, ABCA12, FLRT2, NBPF15, LRRK41, CAPN8, TRIM29, NBPF11, CAPN9, SRGAP2C, LMNA, DGKK, STAB2, CAPN2, MID1, LRRK49, KANK4, MT1X, CCNB1, WDR26, PTP4A2, TUBA3, NLRP12, HSPA4L, MYCBPAP, DPYD, NR5A2, DUSP8, BARD1, CGB1, ENAH, TSPAN1, PRC1, TXLNA, ZIC1, TXLNB, IL11, PACSIN1, OIP5, MIER1, CDKN2C, SLC2A2, LIX1L, BPNT1, ASPM, MTUS2, EGFR, DFFA, SIX4, TACC3, TACC1, ANKRD13B, MIB2, SPATA17, HSPB3, FLAD1, SSC5D, ZNF438, ZNF436, ACTBL2, FGD2, CAMTA1, MEAF6, HMGB2, CCL3, FOLH1B, CDC42SE1, ARPC5, SESN2, ARNT, SESN3, OAZ3, PTK6, DDX3Y, TEK, TFDP3, FGD6, SDF4, ARHGDIB, MUC1, GINS1, MYO1A, LURAP1, EPB41, FDPS, NR4A2, ARMC4, BFSP2, BRIP1, DOCK3, EPS15, IKBKE, HDAC4, P2RX7, CASS4, PLK3, P2RX6, HDAC1, PLK2, BEX5, DDX59, CACNA1G, HIVEP3, FABP4, CACNA1C, PDZD2, HDAC9, DNAJB4, KIF22, CDC14A, REG4, PREX1, DEDD, LRRK8D, ARID4B, GABBR1, IFI44L, MFSD2A, FER, PRDX1, SPRY3, FRMD3, ACOT7, FRMD5, TRIM2, FRMD6, SPINT2, NBPF1, TRIM7, HEY2, NBPF3, DLG3, NBPF4, KDM5B, AHNAK, OCA2, NBPF8, PPIAL4C, KIF11, PPIAL4G, PPIAL4F, SLA2, SARS, PPIAL4E, PPIAL4D, TBCE, PADI2, TP53TG3B, IRF2BP2,

## APPENDIX

	PRPF3, MBNL1, HUNK, RIF1, CAPN11, ATG4C, CA8, INPP4A, CA1, FHOD1, KMT2A, BRSK2, FPGT-TNNI3K, CDC73, EGLN1, IVNS1ABP, ALDH3A1, ESPN, NDC1, FIGN, SAPCD2, DCLK3, PLEKHO1, GPSM2, NFATC4, CALML6, INPP5B, NFATC1, EXO1, RSG1, TMC8, ANXA1, DACH1, SMC2, FUCA1, ANXA3, CDC25B, ACTL8, GDPD2, FZD10, PPP1R9A, CCDC110, CCDC116, ID4, KDM4A, ID3, FEZ1, FAM110A, CTTNBP2NL, ITGB3BP, RAB3GAP2, TARS2, ALOXE3, S100A7, NELL1, DZIP1, PRR11, BBX, KPRP, DNAJB13, IARS2, CCT3, KDF1, CD44, RAVER2, RBM8A, MIS18A, RAB29, NPSR1, RARB, EIF2B3, RNF220, EMX1, UNC5CL, UBR4, WNK3, CD40, RSPH9, VASH1, TMEM27, TXNDC2, HEPACAM, CAMK4, PIAS3, SERBP1, PGM1, CCR2, PDGFRB, PDE4DIP, FBXL7, RAB13, PRDM1, EPS8L3, MAD2L2, KIF26B, NEK7, TADA1, ASAP3, MYT1, POMC, GPR142, CAPZB, TIPRL, TEX40, FAM65B, FAM65C, DNAAF3, CEP170, FBXO6, SKA3, AGRN, RAP1GAP2, WDHD1, PLAT, GNAT1, CRIP1, MSTO1, S100A16, TRPC5, TP53BP2, NOTCH2NL, SMYD3, CHI3L1, EPRS, CDC20, CELSR2, SKI, CRYZ, S100A13, TULP2, OASL, DESI2, FAM64A, SRPX2, SFRP4, PLA2G4F, CHAF1B, SASH3, ADAR, CPEB4, TTL6, DMAP1, GLI3, MCF2L, KCNIP4, CKB, AP3B2, FANCG, CCNO, IP6K3, ZCCHC11, LPGAT1, DSN1, ZNF354C, IQCJ-SCHIP1, HERC6, SLT2, CHRDL2, CDK11A, CDK11B, SNRNP40, FCRLB, RAB11FIP1, GADD45A, SGCA, SHROOM2, CLDN19, CLDN10, SFN, PLCL1, PEX19, STRIP1, MEFV, TOE1, AGT, BCL2, AGO1, AGO3, AGO4, STPG1, FZD9, BCAS1, NOS1, IPO13, NASP, BIRC7, FZD2, PTGFR, ITPR3, RAPH1, SNAI1, AFP, SPANXB1, TEX15, ILF2, PPP1R8, TENM1, PBX1, SEPT3, ALDH1L1, APOBEC1, CRABP1, TRIM50, DSTYK, APOBEC3H, MCM10, TLR7, CALB2, FOXO6, APOBEC3C, GHRHR, APOBEC3D, GSTM2, WNT1, GSTM3, GSTM4, ZNF185, TRIM45, ATOH8, C1ORF198, ORC1, CEP85, UBIAD1, BASP1, CDKL5, RALGAPA2, CDKL1, FAM72A, FAM72B, LYST, CELF3, AKAP6, RAD18, MAP7D1, EMP2, CEP97, SSH1, PKHD1, SSH2, MAP4K1, LIN28A, SOX8, CMPK1, RRAGC, KCNS3, PEF1, PSMB4, GCKR, TRIM67, SLC30A1, PSMB2, HECTD3, UBAP2L, SLC30A3, MFAP3L, RUNX3, SLC30A7, SETDB1, LPO, LPP, EEF1A2, CPNE7, DMP1, LCE2C, MUL1, BRCA2, AK5, TRIM62, AK9, RIMKLA, CORO1A, PPIH, LCE1E, LCE1F, TROAP, MTR, GLMN, RAP1A, AHCYL1, CD79A, FAM84B, PPP1R14D, SULT2B1, FAM83D, ARHGAP4, ARHGAP6, FAM83A, PAK3, CAMSAP2, ACOT11, KLHL21, PSMD4, YRDC, MSN, TPR, AKT3, KLHL20, PARM1, DYNLT3, MCM2, NLRP3, EML6, PANK4, CTH, HIPK1, TPPP, HIPK2, PERM1, CEMIP, KLHL11, NANOS3, MOB1B, CNN3, PPP1R12B, FOXM1, KIAA0101, TNFRSF8, SPOCK1, PALMD, EXOSC10, TYMS, KRT5, HJURP, SH3GLB1, KRT7, POU2F3, POU2F2, PYCARD, TGM3, MAGEA11, H1FOO, ZC3H12D, ENO1, TXNIP, ICA1, UBE4B, FRMPD2, CENPF, SPARC, BAALC, GORAB, PARK7, SH3BGRL, MICALCL, SYDE2, IRF5, KCNN3, SP4, SP7
--	--

## **8. ACKNOWLEDGEMENTS**

---

I want to thank Prof. Dr. med. Dietrich von Schweinitz for the opportunity to conduct my PhD project in the department of pediatric surgery of the Dr. von Hauner children's hospital. My gratitude goes to Prof. Dr. rer. nat. Roland Kappler for supervising my PhD project and contributing to my better understanding of the complex project with new ideas and discussions. Furthermore, I want to thank the other lab members for a nice working environment and atmosphere. My special thanks goes out to Corinna Eberherr and Fatemeh Promoli for introducing me to the lab protocols and Sebastian Sigl, without whom this project would not have been possible. Moreover, I want to thank Susanna Kinting and Steffeni Mountford for their trouble-shooting assistance and encouraging talks whenever needed. Thanks to all the people working in the Kubus for their advice, helping hand and equipment. I also want to express my deep gratitude to my proof readers (Thorsten, Markus and Latoya) and last but not least I want to thank my significant other and my family for supporting me.

## 9. REFERENCES

---

1. Bray, F., et al., *Global cancer statistics 2018: GLOBOCAN estimates of incidence and mortality worldwide for 36 cancers in 185 countries*. CA: A Cancer Journal for Clinicians, 2018. **68**(6): p. 394-424.
2. NIH. *What is Cancer?* 2007 September 28 March 2018]; Available from: [cancer.gov/about-cancer/understanding/what-is-cancer](http://cancer.gov/about-cancer/understanding/what-is-cancer).
3. Gatta, G., et al., *Childhood cancer survival in Europe 1999-2007: results of EUROCARE-5--a population-based study*. The Lancet Oncology, 2014. **15**(1): p. 35-47.
4. Steliarova-Foucher, E., et al., *Geographical patterns and time trends of cancer incidence and survival among children and adolescents in Europe since the 1970s (the ACCIS project): an epidemiological study*. The Lancet, 2004. **364**(9451): p. 2097-2105.
5. Stiller, C.A., *Epidemiology and genetics of childhood cancer*. Oncogene, 2004. **23**: p. 6429.
6. Weinberg, A.G. and M.J. Finegold, *Primary hepatic tumors of childhood*. Hum Pathol, 1983. **14**(6): p. 512-537.
7. Perilongo, G. and E.A. Shafford, *Liver tumours*. Vol. 35. 1999. 953-8; discussion 958.
8. Meyers, R.L., *Tumors of the liver in children*. Surgical Oncology, 2007. **16**(3): p. 195-203.
9. Ortega, J.A., et al., *Randomized comparison of cisplatin/vincristine/fluorouracil and cisplatin/continuous infusion doxorubicin for treatment of pediatric hepatoblastoma: A report from the Children's Cancer Group and the Pediatric Oncology Group*. J Clin Oncol, 2000. **18**(14): p. 2665-75.
10. Pritchard, J., et al., *Cisplatin, doxorubicin, and delayed surgery for childhood hepatoblastoma: a successful approach--results of the first prospective study of the International Society of Pediatric Oncology*. J Clin Oncol, 2000. **18**(22): p. 3819-28.
11. Perilongo, G., et al., *Risk-adapted treatment for childhood hepatoblastoma: final report of the second study of the International Society of Paediatric Oncology&#x2014;SIOPEL 2*. European Journal of Cancer, 2004. **40**(3): p. 411-421.
12. Spector, L.G., J.H. Feusner, and J.A. Ross, *Hepatoblastoma and low birth weight*. Pediatr Blood Cancer, 2004. **43**(6): p. 706-706.
13. Kaur, G. and S.S. Mutum, *Hepatoblastoma in a low birth weight infant : a case report and review of the literature*. The Malaysian journal of medical sciences : MJMS, 2001. **8**(1): p. 69-72.
14. Stocker, J.T., *Hepatoblastoma*. Semin Diagn Pathol, 1994. **11**(2): p. 136-43.
15. Haas, J.E., J.H. Feusner, and M.J. Finegold, *Small cell undifferentiated histology in hepatoblastoma may be unfavorable*. Cancer, 2001. **92**(12): p. 3130-4.
16. Herzog, C.E., R.J. Andrassy, and F. Eftekhari, *Childhood cancers: hepatoblastoma*. Oncologist, 2000. **5**(6): p. 445-53.
17. Haas, J.E., et al., *Histopathology and prognosis in childhood hepatoblastoma and hepatocarcinoma*. Cancer, 1989. **64**(5): p. 1082-95.
18. Koh, K.N., et al., *Prognostic implications of serum alpha-fetoprotein response during treatment of hepatoblastoma*. Pediatr Blood Cancer, 2011. **57**(4): p. 554-60.
19. De Ioris, M., et al., *Hepatoblastoma with a low serum alpha-fetoprotein level at diagnosis: the SIOPEL group experience*. Eur J Cancer, 2008. **44**(4): p. 545-50.
20. Tsuchida, Y., et al., *Evaluation of alpha-fetoprotein in early infancy*. J Pediatr Surg, 1978. **13**(2): p. 155-62.
21. Wu, J.T., L. Book, and K. Sudar, *Serum alpha-fetoprotein (AFP) levels in normal infants*. Pediatric Research, 1981. **15**(1): p. 50-2.
22. Perilongo, G., et al., *Hepatoblastoma presenting with lung metastases: treatment results of the first cooperative, prospective study of the International Society of Paediatric Oncology on childhood liver tumors*. Cancer, 2000. **89**(8): p. 1845-53.
23. Roebuck, D.J., et al., *2005 PRETEXT: a revised staging system for primary malignant liver tumors of childhood developed by the SIOPEL group*. Pediatr Radiol, 2007. **37**(2): p. 123-32; quiz 249-50.
24. Towbin, A.J., et al., *Another point of view on 2017 PRETEXT: reply to Pariente et al*. Pediatr Radiol, 2018. **48**(12): p. 1820-1822.
25. Emre, S., V. Ummar, and M. Rodriguez-Davalos, *Current concepts in pediatric liver tumors*. Pediatric Transplantation, 2012. **16**(6): p. 549-563.
26. Maibach, R., et al., *Prognostic stratification for children with hepatoblastoma: the SIOPEL experience*. Eur J Cancer, 2012. **48**(10): p. 1543-9.
27. Zsiros, J., et al., *Dose-dense cisplatin-based chemotherapy and surgery for children with high-risk hepatoblastoma (SIOPEL-4): a prospective, single-arm, feasibility study*. Lancet Oncol, 2013. **14**(9): p. 834-42.
28. Perilongo, G., et al., *Cisplatin versus cisplatin plus doxorubicin for standard-risk hepatoblastoma*. N Engl J Med, 2009. **361**(17): p. 1662-70.
29. Aronson, D.C., et al., *Predictive value of the pretreatment extent of disease system in hepatoblastoma: results from the International Society of Pediatric Oncology Liver Tumor Study Group SIOPEL-1 study*. J Clin Oncol, 2005. **23**(6): p. 1245-52.
30. SIOPEL. *Childhood Liver Tumours Strategy Group*. 2018; Available from: [www.siopal.org](http://www.siopal.org).

31. Zsiros, J., et al., *Successful treatment of childhood high-risk hepatoblastoma with dose-intensive multiagent chemotherapy and surgery: final results of the SIOPEL-3HR study*. J Clin Oncol 2010. **28**(15): p. 2584-90. doi: 10.1200/JCO.2009.22.4857. Epub 2010 Apr 20.

32. Schweinitz, D.v. and K. Becker, *Hepatoblastom*. 2016, GPOH: AWMF online - Das Portal der wissenschaftlichen Medizin.

33. Cairo, S., et al., *Hepatic stem-like phenotype and interplay of Wnt/beta-catenin and Myc signaling in aggressive childhood liver cancer*. Cancer Cell, 2008. **14**(6): p. 471-84.

34. Sivaprakasam, P., et al., *Survival and long-term outcomes in children with hepatoblastoma treated with continuous infusion of cisplatin and doxorubicin*. J Pediatr Hematol Oncol, 2011. **33**(6): p. e226-30.

35. Howlader N, N.A., Krapcho M, Garschell J, Miller D, Altekruse SF, Kosary CL, Yu M, Ruhl J, Tatalovich Z, Mariotto A, Lewis DR, Chen HS, Feuer EJ, Cronin KA (eds). *SEER Cancer Statistics Review*. 2014 [cited 1975-2011; Available from: [seer.cancer.gov/archive/csr/1975\\_2011/#contents](http://seer.cancer.gov/archive/csr/1975_2011/#contents).

36. Knight, K.R., D.F. Kraemer, and E.A. Neuweit, *Ototoxicity in children receiving platinum chemotherapy: underestimating a commonly occurring toxicity that may influence academic and social development*. J Clin Oncol, 2005. **23**(34): p. 8588-96.

37. Schultz, K.A.P., et al., *Behavioral and Social Outcomes in Adolescent Survivors of Childhood Cancer: A Report From the Childhood Cancer Survivor Study*. Journal of Clinical Oncology, 2007. **25**(24): p. 3649-3656.

38. Tomlinson, G.E. and R. Kappler, *Genetics and epigenetics of hepatoblastoma*. Pediatr Blood Cancer, 2012. **59**(5): p. 785-92.

39. Kingston, J.E., G.J. Draper, and J.R. Mann, *Hepatoblastoma and polyposis coli*. Lancet, 1982. **1**(8269): p. 457.

40. Hughes, L.J. and V.V. Michels, *Risk of hepatoblastoma in familial adenomatous polyposis*. Am J Med Genet, 1992. **43**(6): p. 1023-5.

41. Buckley, J.D., et al., *A case-control study of risk factors for hepatoblastoma. A report from the Childrens Cancer Study Group*. Cancer, 1989. **64**(5): p. 1169-76.

42. DeBaun, M.R. and M.A. Tucker, *Risk of cancer during the first four years of life in children from The Beckwith-Wiedemann Syndrome Registry*. J Pediatr, 1998. **132**(3 Pt 1): p. 398-400.

43. Fukuzawa, R., et al., *Beckwith-Wiedemann syndrome-associated hepatoblastoma: wnt signal activation occurs later in tumorigenesis in patients with 11p15.5 uniparental disomy*. Pediatr Dev Pathol, 2003. **6**(4): p. 299-306.

44. Kato, M., et al., *Hepatoblastoma in a patient with sotos syndrome*. J Pediatr, 2009. **155**(6): p. 937-9.

45. Mussa, A., et al., *The overlap between Sotos and Beckwith-Wiedemann syndromes*. Vol. 156. 2010. 1035-6; author reply 1036.

46. Mateos, M.E., et al., *Simpson-Golabi-Behmel syndrome type 1 and hepatoblastoma in a patient with a novel exon 2-4 duplication of the GPC3 gene*. Am J Med Genet A, 2013. **161a**(5): p. 1091-5.

47. Swarts, S., J. Wisecarver, and J.A. Bridge, *Significance of extra copies of chromosome 20 and the long arm of chromosome 2 in hepatoblastoma*. Cancer Genet Cytogenet, 1996. **91**(1): p. 65-7.

48. Schneider, N.R., et al., *The first recurring chromosome translocation in hepatoblastoma: der(4)t(1;4)(q12;q34)*. Genes Chromosomes Cancer, 1997. **19**(4): p. 291-4.

49. Weber, R.G., et al., *Characterization of genomic alterations in hepatoblastomas. A role for gains on chromosomes 8q and 20 as predictors of poor outcome*. Am J Pathol, 2000. **157**(2): p. 571-578.

50. Tomlinson, G.E., et al., *Cytogenetic evaluation of a large series of hepatoblastomas: numerical abnormalities with recurring aberrations involving 1q12-q21*. Genes Chromosomes Cancer, 2005. **44**(2): p. 177-84.

51. Grobner, S.N., et al., *The landscape of genomic alterations across childhood cancers*. Nature, 2018. **555**(7696): p. 321-327.

52. Eichenmuller, M., et al., *The genomic landscape of hepatoblastoma and their progenies with HCC-like features*. J Hepatol, 2014. **61**(6): p. 1312-20.

53. Koch, A., et al., *Childhood hepatoblastomas frequently carry a mutated degradation targeting box of the beta-catenin gene*. Cancer Res, 1999. **59**(2): p. 269-73.

54. Klaus, A. and W. Birchmeier, *Wnt signalling and its impact on development and cancer*. Nat Rev Cancer, 2008. **8**(5): p. 387-98.

55. Turashvili, G., et al., *Wnt signaling pathway in mammary gland development and carcinogenesis*. Pathobiology, 2006. **73**(5): p. 213-23.

56. Rijsewijk, F., et al., *The Drosophila homolog of the mouse mammary oncogene int-1 is identical to the segment polarity gene wingless*. Cell, 1987. **50**(4): p. 649-57.

57. Nusse, R. and H.E. Varmus, *Many tumors induced by the mouse mammary tumor virus contain a provirus integrated in the same region of the host genome*. Cell, 1982. **31**(1): p. 99-109.

58. Nusse, R., et al., *A new nomenclature for int-1 and related genes: the Wnt gene family*. Cell, 1991. **64**(2): p. 231.

59. Barker, N. and H. Clevers, *Mining the Wnt pathway for cancer therapeutics*. Nat Rev Drug Discov, 2006. **5**(12): p. 997-1014.

60. Morin, P.J., et al., *Activation of beta-catenin-Tcf signaling in colon cancer by mutations in beta-catenin or APC*. Science, 1997. **275**(5307): p. 1787-90.

61. Rubinfeld, B., et al., *Stabilization of beta-catenin by genetic defects in melanoma cell lines*. Science, 1997. **275**(5307): p. 1790-2.

62. Sakanaka, C., J.B. Weiss, and L.T. Williams, *Bridging of beta-catenin and glycogen synthase kinase-3beta by axin and inhibition of beta-catenin-mediated transcription*. Proc Natl Acad Sci U S A, 1998. **95**(6): p. 3020-3.

63. Bilic, J., et al., *Wnt induces LRP6 signalosomes and promotes dishevelled-dependent LRP6 phosphorylation*. Science, 2007. **316**(5831): p. 1619-22.

64. Behrens, J., et al., *Functional interaction of beta-catenin with the transcription factor LEF-1*. Nature, 1996. **382**(6592): p. 638-42.

65. Huber, O., et al., *Nuclear localization of beta-catenin by interaction with transcription factor LEF-1*. Mech Dev, 1996. **59**(1): p. 3-10.

66. Shtutman, M., et al., *The cyclin D1 gene is a target of the beta-catenin/LEF-1 pathway*. Proc Natl Acad Sci U S A, 1999. **96**(10): p. 5522-7.

67. He, T.C., et al., *Identification of c-MYC as a target of the APC pathway*. Science, 1998. **281**(5382): p. 1509-12.

68. Kioussi, C., et al., *Identification of a Wnt/Dvl/beta-Catenin --> Pitx2 pathway mediating cell-type-specific proliferation during development*. Cell, 2002. **111**(5): p. 673-85.

69. Huelsken, J. and J. Behrens, *The Wnt signalling pathway*. J Cell Sci, 2002. **115**(Pt 21): p. 3977-8.

70. Leyns, L., et al., *Frzb-1 is a secreted antagonist of Wnt signaling expressed in the Spemann organizer*. Cell, 1997. **88**(6): p. 747-56.

71. Glinka, A., et al., *Dickkopf-1 is a member of a new family of secreted proteins and functions in head induction*. Nature, 1998. **391**(6665): p. 357-62.

72. Kawano, Y. and R. Kypta, *Secreted antagonists of the Wnt signalling pathway*. J Cell Sci, 2003. **116**(Pt 13): p. 2627-34.

73. Oda, H., et al., *Somatic mutations of the APC gene in sporadic hepatoblastomas*. Cancer Res, 1996. **56**(14): p. 3320-3.

74. Taniguchi, K., et al., *Mutational spectrum of beta-catenin, AXIN1, and AXIN2 in hepatocellular carcinomas and hepatoblastomas*. Oncogene, 2002. **21**(31): p. 4863-71.

75. Koch, A., et al., *Mutations and elevated transcriptional activity of conductin (AXIN2) in hepatoblastomas*. J Pathol, 2004. **204**(5): p. 546-54.

76. de La Coste, A., et al., *Somatic mutations of the beta-catenin gene are frequent in mouse and human hepatocellular carcinomas*. Proc Natl Acad Sci U S A, 1998. **95**(15): p. 8847-51.

77. Buendia, M.A., *Genetic alterations in hepatoblastoma and hepatocellular carcinoma: common and distinctive aspects*. Med Pediatr Oncol, 2002. **39**(5): p. 530-5.

78. Mokkapati, S., et al., *beta-catenin activation in a novel liver progenitor cell type is sufficient to cause hepatocellular carcinoma and hepatoblastoma*. Cancer Res, 2014. **74**(16): p. 4515-25.

79. Hirotsu, Y., et al., *Nrf2-MafG heterodimers contribute globally to antioxidant and metabolic networks*. Nucleic Acids Res, 2012. **40**(20): p. 10228-39.

80. Itoh, K., et al., *An Nrf2/small Maf heterodimer mediates the induction of phase II detoxifying enzyme genes through antioxidant response elements*. Biochem Biophys Res Commun, 1997. **236**(2): p. 313-22.

81. Nguyen, T., H.C. Huang, and C.B. Pickett, *Transcriptional regulation of the antioxidant response element. Activation by Nrf2 and repression by MafK*. J Biol Chem, 2000. **275**(20): p. 15466-73.

82. Lau, A., et al., *Dual roles of Nrf2 in cancer*. Pharmacol Res, 2008. **58**(5-6): p. 262-70.

83. Sporn, M.B. and K.T. Liby, *NRF2 and cancer: the good, the bad and the importance of context*. Nat Rev Cancer, 2012. **12**(8): p. 564-71.

84. Homma, S., et al., *Nrf2 enhances cell proliferation and resistance to anticancer drugs in human lung cancer*. Clin Cancer Res, 2009. **15**(10): p. 3423-32.

85. Abazeed, M.E., et al., *Integrative radiogenomic profiling of squamous cell lung cancer*. Cancer Res, 2013. **73**(20): p. 6289-98.

86. Kirkpatrick, K.L. and K. Mokbel, *The significance of human telomerase reverse transcriptase (hTERT) in cancer*. Eur J Surg Oncol, 2001. **27**(8): p. 754-60.

87. Sundin, T. and P. Hentosh, *InTERTesting association between telomerase, mTOR and phytochemicals*. Expert Rev Mol Med, 2012. **14**: p. e8.

88. Flores, I. and M.A. Blasco, *The role of telomeres and telomerase in stem cell aging*. FEBS Lett, 2010. **584**(17): p. 3826-30.

89. Flores, I., R. Benetti, and M.A. Blasco, *Telomerase regulation and stem cell behaviour*. Curr Opin Cell Biol, 2006. **18**(3): p. 254-60.

90. Zhang, X., et al., *Telomere shortening and apoptosis in telomerase-inhibited human tumor cells*. Genes & development, 1999. **13**(18): p. 2388-2399.

91. Calado, R. and N. Young, *Telomeres in disease*. F1000 Med Rep, 2012. **4**: p. 8.

92. Cukusic, A., et al., *Telomerase regulation at the crossroads of cell fate*. Cytogenet Genome Res, 2008. **122**(3-4): p. 263-72.

93. Kyo, S., et al., *Understanding and exploiting hTERT promoter regulation for diagnosis and treatment of human cancers*. *Cancer Sci*, 2008. **99**(8): p. 1528-38.

94. Poole, J.C., L.G. Andrews, and T.O. Tollefsbol, *Activity, function, and gene regulation of the catalytic subunit of telomerase (hTERT)*. *Gene*, 2001. **269**(1-2): p. 1-12.

95. Beachy, P.A., S.S. Karhadkar, and D.M. Berman, *Tissue repair and stem cell renewal in carcinogenesis*. *Nature*, 2004. **432**(7015): p. 324-31.

96. Omenetti, A., et al., *Hedgehog-mediated mesenchymal-epithelial interactions modulate hepatic response to bile duct ligation*. *Lab Invest*, 2007. **87**(5): p. 499-514.

97. Sicklick, J.K., et al., *Role for hedgehog signaling in hepatic stellate cell activation and viability*. *Lab Invest*, 2005. **85**(11): p. 1368-80.

98. Sicklick, J.K., et al., *Hedgehog signaling maintains resident hepatic progenitors throughout life*. *Am J Physiol Gastrointest Liver Physiol*, 2006. **290**(5): p. G859-70.

99. Bellusci, S., et al., *Involvement of Sonic hedgehog (Shh) in mouse embryonic lung growth and morphogenesis*. *Development*, 1997. **124**(1): p. 53-63.

100. Hardcastle, Z., et al., *The Shh signalling pathway in tooth development: defects in Gli2 and Gli3 mutants*. *Development*, 1998. **125**(15): p. 2803-11.

101. Marigo, V. and C.J. Tabin, *Regulation of patched by sonic hedgehog in the developing neural tube*. *Proc Natl Acad Sci U S A*, 1996. **93**(18): p. 9346-51.

102. Riddle, R.D., et al., *Sonic hedgehog mediates the polarizing activity of the ZPA*. *Cell*, 1993. **75**(7): p. 1401-16.

103. St-Jacques, B., et al., *Sonic hedgehog signaling is essential for hair development*. *Curr Biol*, 1998. **8**(19): p. 1058-68.

104. Litingtung, Y., et al., *Sonic hedgehog is essential to foregut development*. *Nat Genet*, 1998. **20**(1): p. 58-61.

105. Bitgood, M.J., L. Shen, and A.P. McMahon, *Sertoli cell signaling by Desert hedgehog regulates the male germline*. *Curr Biol*, 1996. **6**(3): p. 298-304.

106. St-Jacques, B., M. Hammerschmidt, and A.P. McMahon, *Indian hedgehog signaling regulates proliferation and differentiation of chondrocytes and is essential for bone formation*. *Genes Dev*, 1999. **13**(16): p. 2072-86.

107. Vortkamp, A., et al., *Regulation of rate of cartilage differentiation by Indian hedgehog and PTH-related protein*. *Science*, 1996. **273**(5275): p. 613-22.

108. Lee, J.J., et al., *Autoproteolysis in hedgehog protein biogenesis*. *Science*, 1994. **266**(5190): p. 1528-37.

109. Marigo, V., et al., *Biochemical evidence that patched is the Hedgehog receptor*. *Nature*, 1996. **384**(6605): p. 176-9.

110. Stone, D.M., et al., *The tumour-suppressor gene patched encodes a candidate receptor for Sonic hedgehog*. *Nature*, 1996. **384**(6605): p. 129-34.

111. Nakano, Y., et al., *A protein with several possible membrane-spanning domains encoded by the Drosophila segment polarity gene patched*. *Nature*, 1989. **341**(6242): p. 508-13.

112. Alcedo, J. and M. Noll, *Hedgehog and its patched-smoothened receptor complex: a novel signalling mechanism at the cell surface*. *Biological Chemistry*, 1997. **378**(7): p. 583-590.

113. Chen, Y. and G. Struhl, *In vivo evidence that Patched and Smoothened constitute distinct binding and transducing components of a Hedgehog receptor complex*. *Development*, 1998. **125**(24): p. 4943-8.

114. Corcoran, R.B. and M.P. Scott, *Oxysterols stimulate Sonic hedgehog signal transduction and proliferation of medulloblastoma cells*. *Proc Natl Acad Sci U S A*, 2006. **103**(22): p. 8408-13.

115. Dwyer, J.R., et al., *Oxysterols are novel activators of the hedgehog signaling pathway in pluripotent mesenchymal cells*. *J Biol Chem*, 2007. **282**(12): p. 8959-68.

116. Kenney, A.M., M.D. Cole, and D.H. Rowitch, *Nmyc upregulation by sonic hedgehog signaling promotes proliferation in developing cerebellar granule neuron precursors*. *Development*, 2003. **130**(1): p. 15-28.

117. Kenney, A.M. and D.H. Rowitch, *Sonic hedgehog promotes G(1) cyclin expression and sustained cell cycle progression in mammalian neuronal precursors*. *Mol Cell Biol*, 2000. **20**(23): p. 9055-67.

118. Hahn, H., et al., *Patched target Igf2 is indispensable for the formation of medulloblastoma and rhabdomyosarcoma*. *J Biol Chem*, 2000. **275**(37): p. 28341-4.

119. Katoh, Y. and M. Katoh, *Hedgehog target genes: mechanisms of carcinogenesis induced by aberrant hedgehog signaling activation*. *Curr Mol Med*, 2009. **9**(7): p. 873-86.

120. Huang, S., et al., *Activation of the hedgehog pathway in human hepatocellular carcinomas*. *Carcinogenesis*, 2006. **27**(7): p. 1334-40.

121. Jung, Y., et al., *Bile ductules and stromal cells express hedgehog ligands and/or hedgehog target genes in primary biliary cirrhosis*. *Hepatology*, 2007. **45**(5): p. 1091-6.

122. Regel, I., et al., *IGFBP3 impedes aggressive growth of pediatric liver cancer and is epigenetically silenced in vascular invasive and metastatic tumors*. *Mol Cancer*, 2012. **11**: p. 9.

123. Grimberg, A. and P. Cohen, *Role of insulin-like growth factors and their binding proteins in growth control and carcinogenesis*. *J Cell Physiol*, 2000. **183**(1): p. 1-9.

124. Li, X., et al., *Expression, promoter usage and parental imprinting status of insulin-like growth factor II (IGF2) in human hepatoblastoma: uncoupling of IGF2 and H19 imprinting*. *Oncogene*, 1995. **11**(2): p. 221-229.

125. Hartmann, W., et al., *p57(KIP2) is not mutated in hepatoblastoma but shows increased transcriptional activity in a comparative analysis of the three imprinted genes p57(KIP2), IGF2, and H19*. The American journal of pathology, 2000. **157**(4): p. 1393-1403.

126. Foulstone, E., et al., *Insulin-like growth factor ligands, receptors, and binding proteins in cancer*. J Pathol, 2005. **205**(2): p. 145-53.

127. Zatkova, A., et al., *Amplification and overexpression of the IGF2 regulator PLAG1 in hepatoblastoma*. Genes Chromosomes Cancer, 2004. **39**(2): p. 126-37.

128. Hartmann, W., et al., *Activation of phosphatidylinositol-3'-kinase/AKT signaling is essential in hepatoblastoma survival*. Clin Cancer Res, 2009. **15**(14): p. 4538-45.

129. Rumbajan, J.M., et al., *Comprehensive analyses of imprinted differentially methylated regions reveal epigenetic and genetic characteristics in hepatoblastoma*. BMC Cancer, 2013. **13**: p. 608.

130. Yuan, T.L. and L.C. Cantley, *PI3K pathway alterations in cancer: variations on a theme*. Oncogene, 2008. **27**(41): p. 5497-510.

131. Bonasio, R., S. Tu, and D. Reinberg, *Molecular signals of epigenetic states*. Science, 2010. **330**(6004): p. 612-6.

132. Nicodemi, M. and A. Pombo, *Models of chromosome structure*. Current Opinion in Cell Biology, 2014. **28**: p. 90-95.

133. Perissi, V., et al., *Deconstructing repression: evolving models of co-repressor action*. Nature Reviews Genetics, 2010. **11**(2): p. 109-123.

134. Bolden, J.E., M.J. Peart, and R.W. Johnstone, *Anticancer activities of histone deacetylase inhibitors*. Nat Rev Drug Discov, 2006. **5**(9): p. 769-84.

135. Grozinger, C.M. and S.L. Schreiber, *Deacetylase enzymes: biological functions and the use of small-molecule inhibitors*. Chem Biol, 2002. **9**(1): p. 3-16.

136. Kouzarides, T., *Chromatin modifications and their function*. Cell, 2007. **128**(4): p. 693-705.

137. Zhou, W., et al., *Histone H2A monoubiquitination represses transcription by inhibiting RNA polymerase II transcriptional elongation*. Mol Cell, 2008. **29**(1): p. 69-80.

138. Sergi Aranda, G.M., Luciano Di Croce, *Regulation of gene transcription by Polycomb proteins*.

139. Beck, A., et al., *Overexpression of UHRF1 promotes silencing of tumor suppressor genes and predicts outcome in hepatoblastoma*. Clinical epigenetics, 2018. **10**: p. 27-27.

140. Pagan, J.K., et al., *A novel corepressor, BCOR-L1, represses transcription through an interaction with CtBP*. J Biol Chem, 2007. **282**(20): p. 15248-57.

141. Huynh, K.D., et al., *BCOR, a novel corepressor involved in BCL-6 repression*. Genes Dev, 2000. **14**(14): p. 1810-23.

142. Farcas, A.M., et al., *KDM2B links the Polycomb Repressive Complex 1 (PRC1) to recognition of CpG islands*. Elife, 2012. **1**: p. e00205.

143. Gao, Z., et al., *PCGF homologs, CBX proteins, and RYBP define functionally distinct PRC1 family complexes*. Mol Cell, 2012. **45**(3): p. 344-56.

144. Gearhart, M.D., et al., *Polycomb Group and SCF Ubiquitin Ligases Are Found in a Novel BCOR Complex That Is Recruited to BCL6 Targets*. Mol Cell Biol, 2006. **26**(18): p. 6880-6889.

145. Yamamoto, Y., A. Abe, and N. Emi, *Clarifying the impact of polycomb complex component disruption in human cancers*. Mol Cancer Res, 2014. **12**(4): p. 479-84.

146. Wang, H., et al., *Role of histone H2A ubiquitination in Polycomb silencing*. Nature, 2004. **431**(7010): p. 873-8.

147. Tavares, L., et al., *RYBP-PRC1 complexes mediate H2A ubiquitylation at polycomb target sites independently of PRC2 and H3K27me3*. Cell, 2012. **148**(4): p. 664-78.

148. Cao, R., Y. Tsukada, and Y. Zhang, *Role of Bmi-1 and Ring1A in H2A ubiquitylation and Hox gene silencing*. Mol Cell, 2005. **20**(6): p. 845-54.

149. Sanchez, C., et al., *Proteomics analysis of Ring1B/Rnf2 interactors identifies a novel complex with the Fbxl10/Jhdm1B histone demethylase and the Bcl6 interacting corepressor*. Mol Cell Proteomics, 2007. **6**(5): p. 820-34.

150. Wu, X., J.V. Johansen, and K. Helin, *Fbxl10/Kdm2b recruits polycomb repressive complex 1 to CpG islands and regulates H2A ubiquitylation*. Mol Cell, 2013. **49**(6): p. 1134-46.

151. He, J., et al., *Kdm2b maintains murine embryonic stem cell status by recruiting PRC1 complex to CpG islands of developmental genes*. Nat Cell Biol, 2013. **15**(4): p. 373-84.

152. Junco, S.E., et al., *Structure of the polycomb group protein PCGF1 in complex with BCOR reveals basis for binding selectivity of PCGF homologs*. Structure, 2013. **21**(4): p. 665-71.

153. Ross, K., et al., *Polycomb group ring finger 1 cooperates with Runx1 in regulating differentiation and self-renewal of hematopoietic cells*. Blood, 2012. **119**(18): p. 4152-61.

154. Grootelaes, M., et al., *C-terminal-binding protein corepresses epithelial and proapoptotic gene expression programs*. Proc Natl Acad Sci U S A, 2003. **100**(8): p. 4568-73.

155. Grootelaes, M.L. and S.M. Frisch, *Evidence for a function of CtBP in epithelial gene regulation and anoikis*. Oncogene, 2000. **19**(33): p. 3823-8.

156. Kovi, R.C., et al., *An ARF/CtBP2 complex regulates BH3-only gene expression and p53-independent apoptosis*. Cell Death Differ, 2010. **17**(3): p. 513-21.

157. Kim, J.H. and H.D. Youn, *C-terminal binding protein maintains mitochondrial activities*. Cell Death Differ, 2009. **16**(4): p. 584-92.

158. Guadamillas, M.C., A. Cerezo, and M.A. Del Pozo, *Overcoming anoikis--pathways to anchorage-independent growth in cancer*. J Cell Sci, 2011. **124**(Pt 19): p. 3189-97.

159. Di, L.J., et al., *Transcriptional regulation of BRCA1 expression by a metabolic switch*. Nat Struct Mol Biol, 2010. **17**(12): p. 1406-13.

160. Deng, H., et al., *CtBP1 is expressed in melanoma and represses the transcription of p16INK4a and Brca1*. J Invest Dermatol, 2013. **133**(5): p. 1294-301.

161. Katsanis, N. and E.M. Fisher, *A novel C-terminal binding protein (CTBP2) is closely related to CTBP1, an adenovirus E1A-binding protein, and maps to human chromosome 21q21.3*. Genomics, 1998. **47**(2): p. 294-9.

162. Furusawa, T., et al., *Identification of CtBP1 and CtBP2 as corepressors of zinc finger-homeodomain factor deltaEF1*. Mol Cell Biol, 1999. **19**(12): p. 8581-90.

163. Li, S., et al., *Binding of CtIP to the BRCT repeats of BRCA1 involved in the transcription regulation of p21 is disrupted upon DNA damage*. J Biol Chem, 1999. **274**(16): p. 11334-8.

164. Dahiya, A., et al., *Linking the Rb and polycomb pathways*. Mol Cell, 2001. **8**(3): p. 557-69.

165. Meloni, A.R., E.J. Smith, and J.R. Nevins, *A mechanism for Rb/p130-mediated transcription repression involving recruitment of the CtBP corepressor*. Proc Natl Acad Sci U S A, 1999. **96**(17): p. 9574-9.

166. Sewalt, R.G., et al., *C-Terminal binding protein is a transcriptional repressor that interacts with a specific class of vertebrate Polycomb proteins*. Mol Cell Biol, 1999. **19**(1): p. 777-87.

167. Chinnadurai, G., *CtBP family proteins: more than transcriptional corepressors*. Bioessays, 2003. **25**(1): p. 9-12.

168. Lose, F., et al., *BCoR-L1 variation and breast cancer*. Breast Cancer Res, 2007. **9**(4): p. R54.

169. Tacci, E., et al., *The corepressors BCOR and BCORL1: two novel players in acute myeloid leukemia*. Haematologica, 2012. **97**(1): p. 3-5.

170. Wang, L., et al., *Novel somatic and germline mutations in intracranial germ cell tumours*. Nature, 2014. **511**(7508): p. 241-5.

171. Chang, M.H., *Hepatocellular carcinoma in children*. Zhonghua Min Guo Xiao Er Ke Yi Xue Hui Za Zhi, 1998. **39**(6): p. 366-70.

172. Yu, S.B., et al., *Clinical characteristics and prognosis of pediatric hepatocellular carcinoma*. World J Surg, 2006. **30**(1): p. 43-50.

173. Czauderna, P., et al., *Hepatocellular carcinoma in children: results of the first prospective study of the International Society of Pediatric Oncology group*. J Clin Oncol, 2002. **20**(12): p. 2798-804.

174. Prokurat, A., et al., *Transitional liver cell tumors (TLCT) in older children and adolescents: A novel group of aggressive hepatic tumors expressing beta-catenin*. Vol. 39. 2002. 510-8.

175. Pietsch, T., et al., *Characterization of the continuous cell line HepT1 derived from a human hepatoblastoma*. Lab Invest, 1996. **74**(4): p. 809-18.

176. Pfaffl, M.W., *A new mathematical model for relative quantification in real-time RT-PCR*. Nucleic Acids Res, 2001. **29**(9): p. e45.

177. Zhang, F. *CRISPR design tool*. Available from: tools.genome-engineering.org.

178. Stoehard, P. *Protein Molecular Weight*. 2000; Available from: bioinformatics.org/sms/prot\_mw.html.

179. Pagan, J.K., et al., *A Novel Corepressor, BCoR-L1, Represses Transcription through an Interaction with CtBP*. Journal of Biological Chemistry, 2007. **282**(20): p. 15248-15257.

180. Wegmann, F., et al., *Endothelial adhesion molecule ESAM binds directly to the multidomain adaptor MAGI-1 and recruits it to cell contacts*. Exp Cell Res, 2004. **300**(1): p. 121-33.

181. Litvinov, S.V., et al., *Ep-CAM: a human epithelial antigen is a homophilic cell-cell adhesion molecule*. The Journal of cell biology, 1994. **125**(2): p. 437-446.

182. Ju, J.-h., et al., *Regulation of Cell Proliferation and Migration by Keratin19-Induced Nuclear Import of Early Growth Response-1 in Breast Cancer Cells*. Clinical Cancer Research, 2013. **19**(16): p. 4335-4346.

183. Kim, H., et al., *Human hepatocellular carcinomas with "Stemness"-related marker expression: keratin 19 expression and a poor prognosis*. Hepatology, 2011. **54**(5): p. 1707-17.

184. Yamashita, T., et al., *EpCAM-positive hepatocellular carcinoma cells are tumor-initiating cells with stem/progenitor cell features*. Gastroenterology, 2009. **136**(3): p. 1012-24.

185. Choi, Y., et al., *PROVEAN*.

186. Plevin, M.J., M.M. Mills, and M. Ikura, *The LxxLL motif: a multifunctional binding sequence in transcriptional regulation*. Trends Biochem Sci, 2005. **30**(2): p. 66-9.

187. Eckert, M., S.E. Meek, and K.L. Ball, *A novel repressor domain is required for maximal growth inhibition by the IRF-1 tumor suppressor*. J Biol Chem, 2006. **281**(32): p. 23092-102.

188. Yan, Y., et al., *Loss of Polycomb Group Protein Pcgf1 Severely Compromises Proper Differentiation of Embryonic Stem Cells*. Sci Rep, 2017. **7**: p. 46276.

189. Scelfo, A., et al., *Functional Landscape of PCGF Proteins Reveals Both RING1A/B-Dependent-and RING1A/B-Independent-Specific Activities*. Mol Cell, 2019. **74**(5): p. 1037-1052.e7.

190. Mroz, E.A., et al., *COOH-terminal binding protein regulates expression of the p16INK4A tumor suppressor and senescence in primary human cells*. *Cancer Res*, 2008. **68**(15): p. 6049-53.

191. Kim, T.W., et al., *Ctbp2 Modulates NuRD-Mediated Deacetylation of H3K27 and Facilitates PRC2-Mediated H3K27me3 in Active Embryonic Stem Cell Genes During Exit from Pluripotency*. *Stem Cells*, 2015. **33**(8): p. 2442-55.

192. Kim, T.W., et al., *Ctbp2-mediated beta-catenin regulation is required for exit from pluripotency*. *Exp Mol Med*, 2017. **49**(10): p. e385.

193. Razi, E., et al., *Cancer stem cells as therapeutic targets of pancreatic cancer*. *Fundam Clin Pharmacol*, 2019.

194. Bhatt, T., et al., *Signaling and Mechanical Roles of E-cadherin*. *Cell Communication & Adhesion*, 2013. **20**(6): p. 189-199.

195. Arthur, S.A., J.P. Blaydes, and F.D. Houghton, *Glycolysis Regulates Human Embryonic Stem Cell Self-Renewal under Hypoxia through HIF-2alpha and the Glycolytic Sensors CTBPs*. *Stem Cell Reports*, 2019. **12**(4): p. 728-742.

196. Dragoi, A.M., et al., *Novel strategies to enforce an epithelial phenotype in mesenchymal cells*. *Cancer Res*, 2014. **74**(14): p. 3659-72.

197. Katafiasz, B.J., et al., *Characterization of cadherin-24, a novel alternatively spliced type II cadherin*. *J Biol Chem*, 2003. **278**(30): p. 27513-9.

198. An, C.H., et al., *Frameshift mutations of cadherin genes DCHS2, CDH10 and CDH24 genes in gastric and colorectal cancers with high microsatellite instability*. *Pathol Oncol Res*, 2015. **21**(1): p. 181-5.

199. Cangara, H.M., et al., *Role of endothelial cell-selective adhesion molecule in hematogeneous metastasis*. *Microvasc Res*, 2010. **80**(1): p. 133-41.

200. Ishibashi, T., et al., *ESAM is a novel human hematopoietic stem cell marker associated with a subset of human leukemias*. *Exp Hematol*, 2016. **44**(4): p. 269-81.e1.

201. Clasper, S., et al., *A Novel Gene Expression Profile in Lymphatics Associated with Tumor Growth and Nodal Metastasis*. *Cancer Research*, 2008. **68**(18): p. 7293-7303.

202. Lee, J.S., et al., *A novel prognostic subtype of human hepatocellular carcinoma derived from hepatic progenitor cells*. *Nat Med*, 2006. **12**(4): p. 410-6.

203. Munz, M., et al., *The carcinoma-associated antigen EpCAM upregulates c-myc and induces cell proliferation*. *Oncogene*, 2004. **23**(34): p. 5748-58.

204. Yahyazadeh Mashhadi, S.M., et al., *Shedding light on the EpCAM: An overview*. *Journal of Cellular Physiology*, 2019. **234**(8): p. 12569-12580.

205. Marquardt, J.U., et al., *Human hepatic cancer stem cells are characterized by common stemness traits and diverse oncogenic pathways*. *Hepatology*, 2011. **54**(3): p. 1031-42.

206. Munz, M., P.A. Baeuerle, and O. Gires, *The emerging role of EpCAM in cancer and stem cell signaling*. *Cancer Res*, 2009. **69**(14): p. 5627-9.

207. Azizi, H., B. Asgari, and T. Skutella, *Pluripotency Potential of Embryonic Stem Cell-Like Cells Derived from Mouse Testis*. *Cell J*, 2019. **21**(3): p. 281-289.

208. Brandt, R., et al., *Identification and biological characterization of an epidermal growth factor-related protein: cripto-1*. *J Biol Chem*, 1994. **269**(25): p. 17320-8.

209. Strizzi, L., et al., *Potential for cripto-1 in defining stem cell-like characteristics in human malignant melanoma*. *Cell Cycle*, 2008. **7**(13): p. 1931-5.

210. de Castro, N.P., et al., *Cripto-1: an embryonic gene that promotes tumorigenesis*. *Future Oncol*, 2010. **6**(7): p. 1127-42.

211. Karkampouna, S., et al., *CRYPTO promotes an aggressive tumour phenotype and resistance to treatment in hepatocellular carcinoma*. *J Pathol*, 2018. **245**(3): p. 297-310.

212. Wang, J.H., et al., *Elevated expression of Cripto-1 correlates with poor prognosis in hepatocellular carcinoma*. *Oncotarget*, 2015. **6**(33): p. 35116-28.

213. Ilmer, M., et al., *Targeting the Neurokinin-1 Receptor Compromises Canonical Wnt Signaling in Hepatoblastoma*. *Mol Cancer Ther*, 2015. **14**(12): p. 2712-21.

214. Roskams, T.A., L. Libbrecht, and V.J. Desmet, *Progenitor Cells in Diseased Human Liver*. *Semin Liver Dis*, 2003. **23**(04): p. 385-396.

215. Blevins, M.A., M. Huang, and R. Zhao, *The Role of CtBP1 in Oncogenic Processes and Its Potential as a Therapeutic Target*. *Mol Cancer Ther*, 2017. **16**(6): p. 981-990.

216. Hu, P.S., et al., *NSPc1 promotes cancer stem cell self-renewal by repressing the synthesis of all-trans retinoic acid via targeting RDH16 in malignant glioma*. *Oncogene*, 2017. **36**(33): p. 4706-4718.

217. van der Stoop, P., et al., *Ubiquitin E3 ligase Ring1b/Rnf2 of polycomb repressive complex 1 contributes to stable maintenance of mouse embryonic stem cells*. *PLoS One*, 2008. **3**(5): p. e2235.

218. Lee, J.Y., et al., *Loss of the polycomb protein Mel-18 enhances the epithelial-mesenchymal transition by ZEB1 and ZEB2 expression through the downregulation of miR-205 in breast cancer*. *Oncogene*, 2014. **33**(10): p. 1325-35.